國立臺灣師範大學生命科學系博士論文

Rh 蛋白在斑馬魚胚胎皮膚的功能

The Function of Rh Proteins in the Skin of Zebrafish (*Danio rerio*) Larvae

研 究 生：施廷翰

Tin-Han Shih

指導教授：林豐益 博士

Li-Yih Lin

中華民國 102 年七月

Contents

摘要

Rh 蛋白是在脊椎動物中發現的氣體通道蛋白，被認為具有運輸氨以及二氧化碳的能力。在魚類中，鰓(成魚)以及皮膚(胚胎仔魚)都是主要用來呼吸的器官，但是目前仍不確定是由何種特定細胞來執行排氨以及二氧化碳的功能，也尚未清楚 Rh 蛋白在其中扮演的角色。在我的研究中，我將利用斑馬魚胚胎，證明 Rh 蛋白參與皮膚氨以及二氧化碳運輸的功能。

在第一章的研究中，我以螢光免疫染色證明 Rhcg1 表現在富含氫幫浦細胞(HR cell)的頂端細胞膜上。利用 SIET 分析仔魚體表細胞的排氨功能後發現，HR cell 比它型表皮細胞具有更強的排氨能力，而此排氨能力也隨抑制 Rhcg1 的表現而顯著降低。我也發現 HR cell 在高氨下仍可維持排氨作用，但若是抑制氫幫浦(H^+-ATPase)或 Rhcg1 的表現則會使得 HR cell 失去高氨下的排氨能力，顯示 H^+-ATPase 以及 Rhcg1 是 HR cell 執行主動排氨的關鍵分子。

我在第二章要探討排氨以及鈉離子吸收的運輸機制。透過高氨環境抑制排氨將使得鈉離子吸收能力降低。而增加鈉離子的吸收後則使排氨量增加，顯示氨與鈉離子的運輸息息相關。抑制了 Rhcg1 以及鈉氫交換蛋白(Na^+/H^+ exchanger, NHE3b)的表現後發現排氨與吸鈉量皆降低。抑制這兩蛋白也影響了體內鈉離子的含量，顯示 Rhcg1 以及 NHE3b 是魚類進行排氨依賴性的鈉離子吸收機制的重要蛋白。

於第三章我將分析另一 Rh 蛋白 Rhbg 在仔魚皮膚上的分布與功能。利用原位雜交以及免疫螢光染色我證明 Rhbg 表現在皮膚 keratinocyte 頂端與底側端的細胞膜上。與抑制 Rhcg1 相比，抑制了 Rhbg 的表現會造成更嚴重的排氨能力失調，顯示 Rhbg 對於排氨的影響更大。然而，Rhbg 的抑制將造成 Rhcg1 的表現增加以及 HR cell 排氨能力的提升，這些現象說明補償性的排氨機制是藉由 HR cell 來調節。

在最後的章節中，我分析了仔魚皮膚 Rh 蛋白與二氧化碳運輸的相關性。研究發現利用高氨環境會抑制二氧化碳的排放，而高碳酸水也會降低氨的排放量，顯

示二氧化碳與氨可能透過同一路徑排放。抑制了 Rhbg 蛋白會顯著降低二氧化碳排放量，但抑制 Rhcg1 則不會造成此現象。本實驗也利用 H^+探針測量表皮二氧化碳的水合(產生 H^+)與碳酸的水解(減少 H^+)，藉以分析細胞膜對於二氧化碳的通透性。在高碳酸水的浸泡實驗中，抑制 Rhbg 將減少體表鹼化的程度，說明較少的二氧化碳通過表皮。這些數據證實 Rhbg 是魚類排放二氧化碳的重要路徑。

關鍵字：斑馬魚、氨、Rh 蛋白、二氧化碳、皮膚、氫幫浦蛋白

Abstract

Rhesus glycoproteins (Rh proteins) are the gas channels in vertebrates, and were suggested to conduct ammonia and CO_2. In fish, adult gill and larva skin are the organs responsible for gas transport, but the specific cell types for ammonia or CO_2 excretion were not identified yet. It is also unclear whether Rh proteins are involved in fish gas excretion? In present study, I use zebrafish larval as animal model to demonstrate the gas excretion function of Rh proteins in skin epithelium.

In chapter 1, I used SIET to examine the ammonia excretion ability of skin epithelial cells. The subcellular localization of Rhcg1 was also demonstrated by immunohistochemistry. Results showed that Rhcg1 was distributed in the apical membrane of HR cell. The HR cells exhibited a stronger ammonia efflux than other cell types (keratinocytes and non-HR ionocytes) and the efflux was significant reduced after transcriptional knockdown of Rhcg1 by Rhcg1-antisense morpholino (MO). Under high ammonia environment, HR cell was able to exhibit ammonia efflux, suggesting that HR cell actively excrete ammonia.

In chapter 2, an ammonium-dependant Na^+ uptake mechanism was demonstrated. The inhibition of ammonia excretion caused a significant decrease of Na^+ uptake. Induce of Na^+ uptake by high Na^+ environment increase ammonia excretion, indicating a linkage of Na^+ uptake to ammonia. Knockdown of Rhcg1 or Na^+/H^+ exchanger (NHE3b) impaired both ammonia excretion and Na^+ uptake. The larvae Na^+ content was also reduced in the MO-injected larvae. These results suggested that Rhcg1 and NHE3b are the key molecules in this Na^+ uptake mechanism.

In chapter 3, I analyzed the expression and function of Rhbg in the skin of zebrafish larvae. The results of *in situ* hybridization and immunohistochemistry showed that Rhbg were expressed at the apical and basolateral membrane of keratinocytes. Knockdown of Rhbg inhibited the ammonia efflux in keratinocytes and caused a severe

deficient in total ammonia excretion. On the other hand, Rhbg MO induced the expression of Rhcg1 and elevated the NH_4^+ efflux in HR cells, suggesting a compensatory effect was occurred.

The involvement of Rh proteins in CO_2 excretion was showed in chapter 4. In this chapter, CO_2 excretion was inhibited in the larvae treated with high ammonia environment. On the other hand, environmental hypercapnia inhibit ammonia excretion as well, suggesting that CO_2 shared common pathway of ammonia. The knockdown of Rhbg but not Rhcg1 impaired the CO_2 excretion, revealing that Rhbg is important for CO_2 transport. I used H^+ probe to analyze the hydration/dehydration of surface CO_2/HCO_3^- and determined the membrane permeability to CO_2. While exposing to hypercapnia, the change of surface pH was reduced in Rhbg MO-injected larvae, indicating that Rhbg regulated the CO_2 permeability.

Keywords: Zebrafish, ammonia, Rh protein, CO_2, skin, H^+-ATPase

Background

Rhesus glycoproteins (Rh proteins)

Rh proteins were first identified as the antigen for blood types but were recently found out to be the channel proteins responsible for gas transport (Boron, 2010; Huang and Ye, 2010). Rh proteins were determined in mammals in early 1990s and several major isoforms were subsequently identified: erythroid RhAG, RhCE and RhD; and non-erythroid RhBG and RhCG (Huang and Peng, 2005; Huang and Ye, 2010). The sequences of Rh proteins showed highly relativities to the ammonia transporter (Amt) in *E coli* and methylammonium permeases (Mep) in yeast (Marini et al., 1997; Marini et al., 1994), giving a hint of Rh proteins in ammonia transport function.

Using X-ray crystal structure to analyze bacterial AmtB, researchers strongly suggested that AmtB proteins conduct NH_3 but not NH_4^+ (Khademi et al., 2004). The following study on erythroid RhAG functionally identified RhAG as a conduit for NH_3 (Bakouh et al., 2006; Musa-Aziz et al., 2009a; Ripoche et al., 2004). The permeation of CO_2 by Rh proteins was also demonstrated in the RhAG-expressed *Xenopus* oocyte (Musa-Aziz et al., 2009a), indicating that Rh proteins are dual channel for NH_3 and CO_2. The non-erythroid RhBG and RhCG were found in variety of tissues including liver, lung, and kidney (Han et al., 2009a; Handlogten et al., 2005; Nakhoul and Hamm, 2004). In kidney, RhBG and RhCG are present in the α-intercalated cells and the principle cells of collecting duct. The apical (RhCG) and basolateral (RhBG or RhCG) expression of Rh proteins provide an efficient ammonia excretion pathway (Weiner and Verlander, 2011).

Ammonia excretion in fish

Ammonia (NH_3 and NH_4^+) is the nitrogen waste in teleost fish (Wilkie, 2002; Wright and Wood, 2009). Gill is the primary organ for ammonia elimination, directly transport ammonia into ambient water. Early studies on ammonia excretory

mechanisms indicated a passive NH_3 transport down a blood-to-water gradient through membrane. After diffusion, NH_3 was trapped by the unstirred acid layer in the apical surface to form NH_4^+, thus maintain the favorable NH_3 diffusion gradient. However, it was argued that NH_4^+ is the molecule which being transported via an electroneutral Na^+/NH_4^+ exchange pathway (by Na^+/H^+ exchanger, NHE)

Since the discovery of Rh proteins, the ammonia excretion mechanisms in fish were reexamined in various studies. Fish Rh proteins were first identified in pufferfish (*Takifugu tetraodon*)(Nakada et al., 2007b), and were subsequently found in other species including rainbow trout (*Oncorhynchus mykiss*), killifish (*Kryptolebias marmoratus*), Japanese medaka (*Oryzias latipes*) , zebrafish (*Danio rerio*) and shark (*Triakis scyllium*)(Hung et al., 2007; Nakada et al., 2007a; Nakada et al., 2010; Nawata et al., 2007; Wu et al., 2010). In pufferfish, Rhag, Rhbg, and Rhcg2 were found in gill pavement cell (PVC), whereas Rhcg1 were predominantly expressed in the apical membrane of ionocytes (Nakada et al., 2007b). These distributions of Rh on epithelium enable gill to perform ammonia excretion efficiently.

CO_2 excretion in fish

The metabolic product CO_2 is transported by red blood cell (RBC) toward the respiratory organ, and is eliminated by passive diffusion into water. The diffusion of CO_2 through biological membrane is so rapid that only the enzymatic reaction (CO_2 + $H_2O \leftrightarrow HCO_3^-$) in RBC was stated to be the major restriction in CO_2 excretion (Boron et al., 2011; Missner et al., 2008b). However, it was recently found that some epithelium in mammalian tissue have lower permeability to CO_2 (Endeward and Gros, 2005; Itel et al., 2012; Kikeri et al., 1989; Waisbren et al., 1994). On the other hand, the expression of AQP and Rh proteins in *Xenopus* oocytes or artificial membrane elevated the permeability of CO_2 across membrane (Endeward et al., 2006b; Itel et al., 2012; Musa-Aziz et al., 2009a), suggesting that gas channel mediate membrane permeability

to CO_2

Gill is the primary organ for fish to excrete CO_2, relying on the countercurrent model which allows the gas exchanges more efficiently (Evans et al., 2005). In the gill epithelium, CO_2 is excreted mainly via the thin layer pavement cell (PVC) on gill lamellae, where also the Rh proteins were found. In the analysis of Rh proteins in pufferfish, Rhbg and Rhcg2 were identified at the basolateral and apical membrane, respectively, in the PVC (Nakada et al., 2007b). Another study on zebrafish found that Rhbg was localized at the outer membrane of gill, suggesting that a PVC-expressed Rhbg (Braun et al., 2009b). However, whether Rh protein contribute to CO_2 excretion needs more investigations.

Na^+ uptake mechanism

To maintain osmolarity of body fluids, freshwater (FW) fish need to absorb ions from water. Most of FW fish actively uptake ion via specialized cells named ionocytes in gill epithelium (Hwang and Lee, 2007). To uptake Na^+, current models proposed indicates three pathways: (1) Na^+/H^+ exchanger (NHE), (2) Na^+ channel (ENaC) and H^+-ATPase, and (3) Na^+/Cl^- cotransporter (NCC). In the NHE model, Na^+ was exchanged electroneutrally with H^+ by the secondary active transport driven by Na^+-K^+-ATPase, which pump Na^+ out and create favorable water-to-cell Na^+ gradient (Hwang et al., 2011; Yan et al., 2007). In the ENaC/H^+-ATPase pathway, although it was proposed by the observation that the inhibition of H^+-ATPase resulted in the impaired Na^+ uptake and body Na^+ content, the lack of ENaC in fish genome keep this model under debate (Parks et al., 2008). In the NCC model, Na^+ is co-transported with the uptake of Cl^-. However, it was found that deficiency of NCC in zebrafish resulted in the body Cl^- loss but not Na^+, suggesting that NCC is not the predominant Na^+ uptake pathway in fish (Wang et al., 2009).

The association of Na^+-uptake to ammonia excretion was first observed by Krogh

(Krogh, 1938) and were consolidated by the following studies. NHE is the molecule involved in this ammonia-dependent Na^+ uptake mechanisms since the NHE inhibitor significantly blocked both Na^+ and ammonia transport (Hirata et al., 2003). In the zebrafish acclimated to diluted freshwater, expression of Rhcg1 was significantly induced. The analysis of medaka ionocytes, where NHE and Rh proteins (Rhbg and Rhcg1) are expressed, showed a significant Na^+ uptake (Wu et al., 2010). These evidences support the important role of Rh proteins in Na^+ uptake mechanisms.

Purpose

Since its first discovery in mammal, Rh proteins received *in vitro* analytical processes and showed the characteristic of NH_3 and CO_2 transport. In fish, Rh genes were recently identified and became the key factors for understanding fish gas transport. To date, however, only few studies have showed the function of Rh proteins in fish. In the present research, I examined the distributions and the physiological contribution of Rh proteins in fish. With the background of molecular database, I use zebrafish as the model for studying fish gas transport. In chapter 1, the localization of Rhcg1 was identified in HR cell, and the significant function of HR cell in ammonia excretion was demonstrated. In chapter 2, I examined the long controversial question: "is ammonia excretion link to Na^+ uptake?" at the molecular level. This chapter showed the involvement of both Rhcg1 and NHE3 in Na^+ uptake. In chapter 3, I investigated the expression and the ammonia transport function of Rhbg. I also want to know if Rh proteins transport CO_2 in fish. In chapter 4, I examined the contribution or Rh proteins to CO_2 excretion. I also used surface pH measurement to determine the CO_2 permeability in the epithelium.

Chapter 1

Rhcg1 regulates ammonia excretion in the skin of zebrfish larvae: evidence of active ammonia excretion by HR cell

Introduction

Ammonia (including both NH_3 and NH_4^+) is the primary nitrogenous waste in most teleost and is eliminated via the gills. The model indicates that branchial ammonia is excreted down favorable blood-to-water (transbranchial) NH_3 diffusion gradients (Wilkie, 2002). The NH_3 diffusion model is based on the observation that ammonia flow is inhibited when the gradient is reduced by high ambient ammonia (Avella and Bornancin, 1989; Wilson et al., 1994). It was suggested that maintenance of the transbranchial ammonia gradient relies on acidification of unstirred layers at the apical surface (Wright et al., 1989). This is especially advantageous during exposure to high ammonia (H-Amm), which reverses the normally positive ammonia gradient. Abolishing this layer with HEPES buffer during H-Amm reduced the flux of total ammonia (Wilson et al., 1994). On the other hand, the H^+ arising from CO_2 hydration traps NH_3 as NH_4^+ as it enters the unstirred layers on the surfaces of gills (Nawata et al., 2007; Wilson et al., 1994; Wright et al., 1989). Despite CO_2 hydration, evidence has shown that the branchial surface might also be acidified by H^+ secreted from an apical vacuolar H^+-ATPase (Horng et al., 2007; Lin et al., 2006).

Recently, several isoforms of the Rh glycoprotein (Rhag, Rhbg, Rhcg1, and Rhcg2) have been identified in the gill epithelium of pufferfish (*Takifugu rubripes*) (Nakada et al., 2007b), killifish (*Kryptolebias marmoratus*) (Hung et al., 2007), and zebrafish (Nakada et al., 2007a). This putative ammonia channel provides the new direction for studying ammonia transport mechanism. Nawata et al. (Nawata et al., 2007) found that the mRNA of Rhcg2, Rhbg, and H^+-ATPase (the β-subunit) were upregulated in pavement cell (PVC) fractions during H-Amm. Moreover, increases in Rhcg1 and H^+-ATPase transcripts were reported in zebrafish acclimated to high external ammonia, suggesting that HR cell mediated ammonia excretion was induced (Braun et al., 2009a). However, direct evidence of functional study has not yet reported.

In present study, I attempted to measure NH_4^+ excretion in specific skin cells with scanning ion-selective electrode technique (SIET), and provide direct evidence for the contributions of Rhcg1 in ammonia excretion. I also attempted to answer whether the skin cells can excrete ammonia actively and how high the gradient it can excrete ammonia against?

Results

Ammonia excretion in the skin epithelial cells of zebrafish larvae

The skin in the larval stage is functionally analog to the gill in adult, expressing same types of cell on the epithelium responsible for osmoregulation and respiration. In the present study I use zebrafish larvae for investigating the function of epithelial cell in ammonia excretion. By using vital fluorescent dye concanavalin A, HR cells are able to be identified (Lin et al., 2006) and subsequently being probed by microelectrode. Using the NH_4^+-selective microelectrode, NH_4^+ flux at specific cells was measured by probing NH_4^+ activity at 10-μm intervals. Under a microscope, ionocytes and keratinocytes can easily be identified by their morphology. Microelectrode detected weaker outward flux of NH_4^+ in keratinocytes and non-HR ionocytes (Fig. 1-1). In contrast, the flux from HR cells was about threefold higher than that from other cell types.

Immunohistochemistry of Rhcg1 in the skin of zebrafish larvae

Previous study showed that Rhcg1 in zebrafish were colocalized to the Con-A positive cell, suggesting the expression of Rhcg1 in HR cell (Nakada et al., 2007a). To demonstrate the subcellular expression of Rhcg1, I used zebrafish Rhcg1-specific antibody and examine the fluorescence by confocal microscope. As showed in Fig. 1-2A, immunoreactivity of Rhcg1 was found in the membrane of yolk sac surface, and was not colocalized with ionocyte expressed NKA (Fig. 1-2B). In the z-plane analysis, the immunoreactivity of Rhcg1 appeared to be located at the apical region (Fig. 1-2C).

Ammonia excretion in the larvae with Rhcg1 MO knockdown

To study the contribution of Rhcg1 in ammonia excretion, a loss-of-function method was introduced. By applying with Rhcg1-antisense morpholino oligonucleotides (MO), a translational knockdown was induced. In the larvae injected with Rhcg1-specific morpholino (Rhcg1 MO), no immunoreactivity of Rhcg1 was found (Fig. 1-2D). This result suggested a high efficiency of MO on *Rhcg1* knockdown. I used NH_4^+ probe to measure the whole larval ammonia excretion and the result showed that ammonia excretion was impaired (~35% decrease) in the *Rhcg1* MO (Fig. 1-3A). I further examine the function of HR cell in Rhcg1 MO and found the cellular NH_4^+ efflux was significantly reduced (~50%)(Fig. 1-3B).

NH_4^+ flux of keratinocytes and HR cells in larvae subjected to high external ammonia

To compare the capability of keratinocytes and HR cells in ammonia excretion, NH_4^+ fluxes were measured in larvae exposed to a series of external ammonia concentrations (0.1-5 mM NH_4^+). In addition, three groups of larva which had been pre-acclimated to Normal water (NW), 1 mM NH_4^+ water (1 mM-HA), and 5 mM NH_4^+ water (5 mM-HA) for 4 days were compared. Results showed that the NH_4^+ flux gradually declined from positive values (efflux) to negative values (influx) in keratinocytes and revealed the "reverse concentration (RC)" as the flux declined to zero (Fig. 1-4A). Apparently, HA acclimation shifted the curve upward and increased the RC of keratinocytes.

Similar phenomenon was also found in HR cells of NW group, the NH_4^+ flux declined to negative values as external NH_4^+ increased and the RC was revealed (Fig. 1-4B). However, the curves of the two HA groups were quite different. The NH_4^+ fluxes seem to be relatively independent on external NH_4^+ levels and the RC was not presented within the scale. Apparently, the RC of the same group is higher in HR cells

than in keratinocytes.

Reverse concentration (RC) of keratinocytes and HR cells

The RCs were further derived from the regression line of the curves obtained from each keratinocytes (dash lines are regression lines, Fig. 1-5A). To determine the RCs of HR cells, the external NH_4^+ concentrations were increased to 10 mM. The curves of keratinocytes and HR cells from the three groups were respectively shown in Fig. 1-5A and 1-5B and the RCs from each cell were compared in Fig. 1-5C. The RC of keratinocytes was 0.7 ± 0.1 mM in NW group, and it increased to 1.2 ± 0.3 mM in 1 mM-HA group, and 4.2 ± 0.5 mM in 5 mM-HA group. The RC of HR cells was 2.9 ± 0.5 mM in NW group, and it increased to 5.5 ± 0.3 mM in 1 mM-HA group, and 8.5 ± 0.5 mM in 5 mM-HA group. The RC was remarkably higher in HR cells than in keratinocytes in all three groups.

Reverse concentration (RC) of HR cells in Rhcg1 or atp6v1a morphant

To test if Rhcg1 and H^+-ATPase were involved in the high capability of HR cells in ammonia excretion, the RC was determined in *Rhcg1* or *atp6v1a* (a subunit of H^+-ATPase) morphants. The *atp6v1a* MO was previously shown to effectively suppress the expression of H^+-ATPase in HR cells (Horng et al., 2007). Results showed that knockdown of either *Rhcg1* or *atp6v1a* decreased the NH_4^+ flux of HR cells (shifted the curve downward; Fig. 1-6A), and significantly decreased the RC of HR cells from ~3 mM to the level less than 1 mM (Fig. 1-6B).

Discussion

In previous reports on fish ammonia transport, the net flux of total ammonia (including NH_3 and NH_4^+) was determined by calculating changes in total ammonia in the water during the experiment (Wilson et al., 1994). However, that method provides the ammonia flux from the entire animal but not specific organs or cell types. In the

present study, SIET was used to measure the NH_4^+ activity and flux at specific locations on the surface of larval skin. The application of SIET to probing NH_4^+ has been reported in studies of *Xenopus* oocyte membrane permeability (Musa-Aziz et al., 2009a; Musa-Aziz et al., 2009b), plant root absorption (Henriksen et al., 1990) and mosquito ammonia excretion (Donini and O'Donnell, 2005). For the first time, the present study used SIET to detect cellular NH_4^+ transport in an intact vertebrate model zebrafish and provides direct evidence for the cellular location and molecular mechanism of ammonia transport. In a study on the air-breathing mudskipper (Periophthalmodon schlosseri), mitochondria rich cells (MRCs) were suggested to be the location of branchial ammonia transport (Wilson et al., 2000). In zebrafish, vH-MRCs (which refer to HR cells in this study) were also suggested to be involved in ammonia transport based on evidence of Rhcg1 in the apical membrane (Nakada et al., 2007a). Furthermore, pavement cells were also suggested to be involved in ammonia transport of zebrafish (Nakada et al., 2007a), pufferfish (Nakada et al., 2007b), and rainbow trout (Nawata et al., 2007). However, those studies provide molecular evidence for the localization of the ammonia transporter, but functional evidence on these cells has not been reported. Present study use SIET detect outward NH_4^+ fluxes and showed about threefold higher in HR cells than in adjacent keratinocytes or other ionocytes. This finding coincides with the previous finding that HR cells are acid-secreting cells (Lin et al., 2006) and consequently drive a significant amount of NH_3 transport by the mechanism of "acid-trapping." Although the NH_4^+ flux in HR cells is relatively high, keratinocytes should greatly contribute to overall NH_4^+ transport due to their large number and surface area.

Four isoforms of the Rh protein (Rhag, Rhbg, Rhcg1, and Rhcg2) have been identified in the gill epithelium of zebrafish (Nakada et al., 2007a). Among them, Rhcg1 expression has been located in the apical membrane of HR cells in the yolk sac

and gills. In this study, I use zebrafish-specific antibody to examine the subcellular localization of Rhcg1 and demonstrated that Rhcg1 was expressed at the apical membrane (Fig. 1-2). I further conducted a loss-of-function study (Rhcg1 gene knockdown) to demonstrate the function of Rhcg1 in ammonia transport. In Rhcg1 morphants, about 50% of cellular NH_4^+ efflux and a 35% decrease in total ammonia secretion were revealed (Fig. 1-3). Taking this evidence together, I proposed a model that H^+-ATPase in HR cells generates an extracellular H^+ gradient to drive facilitative NH_3 diffusion through Rhcg1 in HR cells and possibly through other Rh glycoproteins in keratinocytes. The knockdown of Rhcg1 in my study provided the first functional evidence of Rhcg1 in ammonia transport. The following study of Braun et al in zebrafish further consisted with our finding (Braun et al., 2009a). In the mammalian studies, knockout of Rhcg showed that the acidosis in distal renal tubule was impaired (Biver et al., 2008; Lee et al., 2009). The role of fish ammonia in acid-base balance had been reported in the air-breathing fish, which use ammonia to eliminate body H^+ (Randall and Ip, 2006; Randall and Tsui, 2006). It is also possible of the fish live in extremely acid environment (pH 3.5) use ammonia as H^+ regulator although the authors suggested that NHE play the acid-base regulation role (Hirata et al., 2003). Despite the fact that H^+-ATPase is dominant in acid secretion, it is interesting to examine the contribution of Rhcg in the acid-base homeostasis of freshwater fish.

Another major finding was a comparison of the ammonia transporting capabilities between keratinocytes and HR cells. The RC of ammonia excretion was used as a criterion to compare the capability of cells. I showed for the first time that ionocytes (HR cells) are able to secrete ammonia against a higher external ammonia level compared to keratinocytes (Fig. 1-4). In larvae acclimated to NW (without the addition of ammonia), the RC of HR cells was ~3 mM, over 2 mM higher than that of keratinocytes. High-ammonia water (1 and 5 mM NH_4^+) acclimation increased the RCs

of both HR cells and keratinocytes, but RCs of HR cells were always higher than those of keratinocytes (Fig. 1-5). Accordingly, I suggest that HR cells are able to secrete ammonia by a H^+-ATPase-linked secondarily active pathway. Since the ammonia concentration in the body fluid of larvae was not available in this study, I cannot conclude if ammonia was passively or actively excreted by keratinocytes. However, the linear relationship between external NH_4^+ concentrations and NH_4^+ fluxes shown in keratinocytes (Figs. 1-4, 1-5) implies that ammonia moves across keratinocytes by passive diffusion. If this is true, the RC would be close to the internal ammonia level. The RC in keratinocyte of zebrafish larva was ~0.7 mM, slightly higher than the common blood ammonia level observed in adult fishes (usually < 0.5 mM; (Evans et al., 2005)). This might have been due to the higher metabolic rate in the larval stage than in adult fish (Barrionuevo and Burggren, 1999). Alternatively, it is possible that the internal ammonia of larvae is < 0.7 mM and keratinocytes can excrete ammonia against the gradient.

Since keratinocytes cover almost the entire larval surface, passive diffusion through keratinocytes is supposedly a highly efficient way to excrete ammonia into water. However, this pathway would be blocked if the external ammonia level is raised. After 1 or 5 mM NH_4^+ acclimation, it was found that the RCs of keratinocytes turned out to be close (1 mM group) or lower (5 mM group) than the NH_4^+ concentration of the acclimation water, indicating that ammonia excretion from keratinocytes was difficult in high-ammonia water. In this situation, the role of HR cells is magnified by their capability to pump out ammonia against a high external ammonia level.

The knockdown of either Rhcg1 or H^+-ATPase decreased the RC of HR cells to a level close to that of keratinocytes (Fig. 1-6), suggesting that both of these molecules are required for active ammonia transport by HR cells. The coupling of Rhcg1 and H^+-ATPase in the apical membrane probably functions as an “ammonia pump”, even

though Rhcg1 alone is a passive NH_3 channel. With H^+-ATPase in the apical membrane, the H^+ gradient across the apical membrane probably provides the driving force to pump NH_3 out of cells. Acid-tapping ammonia excretion was proposed for a long time in a variety of animals from invertebrates to mammals (Weihrauch et al., 2012a; Weihrauch et al., 2012b; Weiner and Hamm, 2007; Wilkie, 2002). However, to my knowledge, no convincing evidence has been proposed to demonstrate this mechanism to be effective for active ammonia transport.

In addition to H^+-ATPase, the Na^+/H^+ exchanger (NHE) was also suggested to be involved in ammonia excretion in mammalian kidneys and fish gills/skin (Nagami, 1988; Shih et al., 2012; Wu et al., 2010). In seawater pufferfish, the expression of NHE3 was induced during high-ammonia exposure, indicating that the NHE is involved in ammonia excretion in seawater (Nawata et al., 2010). However, in freshwater rainbow trout, expression of the NHE (NHE2 and NHE3) was unchanged after acclimation to high-ammonia water (Wood and Nawata, 2011). My unpublished data also showed that NHE3 transcripts did not change in zebrafish acclimated to high-ammonia water. However, some species do not have H^+-ATPase on the apical side of ionocytes such as medaka (Lin et al., 2012) and killifish (Katoh et al., 2003). Whether NHE in these species can directly transport NH_4^+ or indirectly transport H^+ for NH_3 trapping needs to be further investigated.

In some seawater species or euryhaline species in seawater, ionocytes were suggested to actively excrete ammonia through transporting NH_4^+ with K^+ transporters such as Na^+/K^+-ATPase (NKA) and the Na^+-K^+-$2Cl^-$ cotransporter (NKCC). For example, the addition of an NKA inhibitor (ouabain) reduced the ammonia excretion by the mudskipper (*Periophthalmodon schlosseri*) (Randall et al., 1999). Recent studies on pufferfish and climbing perch (*Anabas testudineus*) showed that gene/protein expressions of NKCC and NKA were induced after high-ammonia exposure (Ip et al.,

2012; Nawata et al., 2010). It is likely that NKA in the basolateral membranes of HR cells (Liao et al., 2009) is also involved in the active ammonia transport of zebrafish. Whether a specific isoform of NKA in HR cells is involved in ammonia transport needs to be tested.

Chapter 2

Rhcg1 and NHE3b are involved in ammonium-dependent sodium uptake by zebrafish larvae acclimated to low-sodium water

Introduction

Na^+ uptake by gills of freshwater (FW) fish being linked to NH_4^+ excretion was first proposed by August Krogh in the 1930s. Since then, many studies have been carried out to test Na^+/NH_4^+ exchange in fish gills, and a number of studies produced conflicting conclusions (Evans et al., 2005). For example, several studies reported that the amount of NH_4^+ excreted is close to the amount of Na^+ taken up by fish gills (McDonald and Millsgan, 1988; Payan, 1978; Salama et al., 1999; Wright and Wood, 1985), and NH_4^+ loading may stimulate Na^+ uptake (Salama et al., 1999; Wilson et al., 1994). On the other hand, several studies reported that non-ionic diffusion of NH_3 plays a major role in branchial ammonia excretion (Kirschner et al., 1973; Wilkie and Wood, 1994; Wilson et al., 1994; Wright et al., 1989).

In the 1970s, several landmark studies proposed that Na^+ was in fact exchanged for H^+ instead of NH_4^+, and suggested that an amiloride-sensitive Na^+/H^+ exchanger (NHE) is involved in Na^+ uptake by fish gills (Kerstetter et al., 1970; Kirschner et al., 1973). Avella and Bornancin (Avella and Bornancin, 1989) also reported that Na^+ is exchanged for H^+, but they questioned the thermodynamics of NHE in Na^+ uptake in fish living in FW. Alternatively, an apical V-type H^+-ATPase electrochemically linked to a Na^+ channel that drives Na^+ uptake was suggested. Since then, the two pathways through an NHE- or H^+-ATPase-coupled Na^+ channel have become dominant models for Na^+ uptake in FW fish.

Use zebrafish as animal model, sodium green labeling showed that HR cells are sites of Na^+ uptake by zebrafish larvae (Esaki et al., 2007; Horng et al., 2007). Yan et al. (Yan et al., 2007) cloned and identified an NHE3b (*slc9a3b*) in HR cells of zebrafish gills, and found that *nhe3b* mRNA expression was induced by low-Na^+ (L-Na) water, suggesting that Na^+ uptake in HR cells is via NHE3b. In other species, including the Osorezan dace (*Tribolodon hakonensis*) (Hirata et al., 2003), rainbow trout (Ivanis et al., 2008), and

tilapia (*Oreochromis mossambicus*) (Hiroi et al., 2008), NHE2/3 were identified in their MR cells and were also suggested to be involved in Na^+ uptake. Although those molecular identifications support the role of NHE isoforms in branchial Na^+ uptake, the driving force of NHE remains an unresolved question. As Avella and Bornancin (Avella and Bornancin, 1989) previously questioned, Parks et al. (Parks et al., 2008) also emphasized the thermodynamic constraints that might prevent the electroneutral NHE from functioning in FW environments. However, recent studies on the Rh proteins may provide a potential solution for the driving force of NHE in fish gills.

In chapter 1, I provided strong loss-of-function evidence for the function of Rhcg1 in ammonia excretion by HR cells. The presence of Na^+ uptake and NH_4^+ excretion in HR cells of zebrafish led me to reconsider if Krogh's Na^+/NH_4^+ exchange is conducted by a coupling function of NHE3b and Rhcg1. Recently, the Na^+/NH_4^+ exchange mechanism was also investigated in cultured gill cells of trout, and it was suggested that Na^+/NH_4^+ exchange is mediated by a putative protein complex including an Rh protein, the NHE, H^+-ATPase, and an unidentified Na^+ channel (Wright and Wood, 2009). Using medaka larvae as a new model, it was demonstrated that Na^+ uptake and NH_4^+ excretion in medaka larvae were accomplished by the same MR cells, and there is a tight linkage between Na^+ uptake and NH_4^+ excretion by those cells (Wu et al., 2010).

However, to provide more-solid evidence of the involvement of NHE3 and Rhcg1 in the NH_4^+-dependent Na^+ uptake mechanism, a loss-of-function approach is required. In this chapter, I attempted to examine if the Na^+ uptake by zebrafish is NH_4^+ dependent, and more specifically to test if NHE3b and Rhcg1 are involved in the Na^+ uptake mechanism with emphasis on low-Na^+ situation, which was previously reported to stimulate NHE3b expression and function (Yan et al., 2007).

Results

Na^+, H^+, and NH_4^+ gradients at the yolk-sac surface of larvae acclimated to different waters

Surface ionic gradients of zebrafish larvae acclimated to Normal water (NW), low Na^+ water (L-Na), 5 mM NH_4^+ water (H-Amm), and low Na^+ and 5 mM NH_4^+ water (L-Na-H-Amm) for 4 days were measured with the SIET to determine ionic excretion and uptake by larval skin. The yolk sac showed notable gradients of H^+, NH_4^+, and Na^+; therefore I chose this location to compare ionic gradients (Fig. 2-1A shows the location of probing). Positive gradient values indicate secretion of ions by the yolk sac membrane; in contrast, negative values indicate uptake of ions. Results showed that H^+ and NH_4^+ were secreted by NW larvae; however, a Na^+ gradient was almost absent (Fig. 2-1B-D). L-Na acclimation remarkably increased Na^+ gradients but not NH_4^+ gradients (Fig. 2-1B, C). H-Amm acclimation increased NH_4^+ gradients but not Na^+ gradients (Fig. 2-1B, C). There seemed to be no correlation between NH_4^+ excretion and Na^+ uptake. However, comparing the L-Na and L-Na-H-Amm groups, both NH_4^+ gradients and Na^+ gradients were induced by high NH_4^+ acclimation (Fig. 2-1B, C). In this experiment, no significant differences were found in mortality or hatching rates among the four groups.

Acute effects of external medium on Na^+ and NH_4^+ gradients

To further test the linkage between Na^+ uptake and NH_4^+ excretion, larvae were subjected to acute changes in external media with H-MOPS (5 mM MOPS), H-Amm (5 mM NH_4^+), or H-Na (10 mM Na^+), and changes in Na^+ and NH_4^+ gradients were then determined by the SIET. L-Na-acclimated larvae were used because NH_4^+-dependent Na^+ uptake was found (Fig. 2-1C). In my previous study, the MOPS buffer was shown to effectively suppress H^+ accumulation and NH_4^+ excretion at the surface of larval skin (Shih et al., 2008). In this experiment, both the Na^+ and NH_4^+ gradients were suppressed by the H-MOPS buffer (Fig. 2-2A, B). H-Amm water reversed the NH_4^+ gradient (values dropped from positive to negative; Fig. 2-2D) at the surface of larvae and almost

completely eliminated the Na^+ gradient (Fig. 2-2C). In contrast, raising the external Na^+ level (H-Na water) increased the Na^+ gradient (Fig. 2-2E) and also increased the NH_4^+ gradient (Fig. 2-2F). Once again, this experiment revealed a tight linkage between the Na^+/NH_4^+ transport of zebrafish larvae.

Real-time qPCR of nhe3b, Rhcg1, and atp6v1a in NW and L-Na zebrafish

To examine the expressions of genes involved in Na^+/NH_4^+ transport, a qPCR was applied to analyze transcripts of *nhe3b, Rhcg1,* and *atp6v1a* in larvae and gills of adult zebrafish acclimated to NW or L-Na for 4 days (larvae) and 7 days (adult fish) . Results showed that *nhe3b* was significantly induced in L-Na larvae (Fig. 2-3A), whereas *atp6v1a* was significantly downregulated (Fig. 2-3C). No significant change was found in *Rhcg1* of whole larvae acclimated to L-Na water (Fig. 2-3B). In the gill of adult fish, both of *nhe3b* and *Rhcg1* was upregulated (Fig. 2-3D-E), whereas *atp6v1a* was significantly downregulated (Fig. 2-3F).

Na^+ and NH_4^+ transport in larvae with Rhcg1 gene knockdown

The effect of *Rhcg1* knockdown on NH_4^+ excretion of zebrafish was reported in chapter 1. In this experiment, I further used the same approach to investigate if Na^+ uptake was also affected by *Rhcg1* MOs. After being microinjected with *Rhcg1* MOs, embryos were transferred to L-Na water and measured with SIET at 4 dpf. Dose-dependent decreases in the NH_4^+ (Fig. 2-4A) and Na^+ (Fig. 2-4B) gradients were found in larvae with an *Rhcg1* MO injection. A dose of 4 ng effectively decreased both the Na^+ and NH_4^+ gradients to significant levels (about 50% decreases). However, no significant change was found in H^+ gradient in *Rhcg1* morphants (Fig. 2-4C). Although morphological changes in morphants (MO-injected larvae) were not obvious, the whole-body Na^+ content of morphants was significantly lower than that of control larvae (Fig. 2-5A).

Na^+ and NH_4^+ transport in larvae with EIPA treatment and nhe3b gene knockdown

To test the role of NHE in ionic transport, 1mM EIPA was applied to L-Na larvae for 10 min before measurements. As shown in Fig. 2-6, Na^+ gradients (uptake), NH_4^+ gradients (secretion) and H^+ gradients (secretion) were significantly suppressed by EIPA treatment. In addition, *nhe3b* MO-injected embryos (4 dpf) were also examined. Results shows that Knockdown of *nhe3b* significantly decreased Na^+, NH_4^+, and H^+ gradients (Fig. 2-7) at the yolk-sac skin, and whole-body Na^+ content (Fig. 2-5B).

Discussion

The advantages of SIET in the examination of ion activity have been showed in many studies. Wu et al. (Wu et al., 2010) used the SIET to demonstrate a NH_4^+-dependent Na^+ uptake mechanism in MRCs of medaka larvae. Recently, Shen et al. (Shen et al., 2011) used it to demonstrate a functional plasticity of MRCs in medaka larvae. In this chapter, I further used the same approach to measure Na^+, NH_4^+, and H^+ transport by zebrafish larvae. However, the SIET and other similar techniques also have limitations and drawbacks. In zebrafish, I found that the Na^+ signals from individual ionocytes (including HR cells and other subtypes) were not high enough to reveal their function in Na^+ transport (signal-to-noise level is not good enough). Therefore, I only used SIET to measure ionic gradients at their yolk-sac surface but not individual ionocytes.

In the previous study on medaka larvae, a tight linkage between Na^+ uptake and NH_3/NH_4^+ excretion (NH_4^+-dependent Na^+ uptake) was found. L-Na acclimation induced compensatory Na^+ uptake and also induced NH_3/NH_4^+ excretion; H-Amm acclimation induced compensatory NH_3/NH_4^+ excretion and also induced Na^+ uptake (Wu et al., 2010). However, in the present study, L-Na acclimation induced compensatory Na^+ uptake but not NH_4^+ secretion (Fig. 2-1B, C); H-Amm acclimation increased NH_4^+ secretion but not Na^+ uptake (Fig. 2-1B, C). A linkage between NH_4^+

excretion and Na^+ uptake seemed to be absent or insignificant. However, both NH_4^+ secretion and Na^+ uptake were induced by H-Amm acclimation when the Na^+ level was low (compare L-Na and L-Na-H-Amm in Fig. 2-1B, C), suggesting that low-Na^+ water can induce NH_4^+-dependent Na^+ uptake. Since, more than one Na^+ uptake mechanism by zebrafish has been proposed (see below), the NH_4^+-dependent Na^+ uptake is probably not the dominant mechanism in normal Na^+ water. The purpose of this study is to examine the NH_4^+-dependent Na^+ uptake pathway; therefore, I did most experiments with L-Na induced larvae.

In addition to the above data, other data also support the NH_4^+-dependent Na^+ uptake in L-Na water. Acutely raising the external NH_4^+ level blocked NH_4^+ excretion and Na^+ uptake; in contrast, raising the external Na^+ level enhanced Na^+ uptake and NH_4^+ excretion. The addition of MOPS buffer to the medium which was previously shown to decrease H^+ accumulation and NH_4^+ excretion at the skin surface also suppressed Na^+ uptake. The result of MOPS addition is interesting. MOPS buffer is supposed to diminish extracellular H^+ and consequently increase Na^+ uptake via NHE due to the favorable H^+ gradient. However, the fact that MOPS decreased both Na^+ and NH_4^+ gradient supports the Na^+ uptake is dependent on NH_4^+ excretion.

As mentioned in the introduction, a coupling function of NHE3b and Rhcg1 in the NH_4^+- dependent Na^+ uptake was hypothesized and tested. I applied NHE inhibitor (EIPA) to the larvae and found that both Na^+ uptake and NH_4^+ excretion were suppressed. I knockdown *Rhcg1* translation and further found that *Rhcg1* MO suppressed both Na^+ uptake and NH_4^+ excretion (Fig. 2-4). In addition, *nhe3b* MO was also applied to the embryos and found that both Na^+ uptake and NH_4^+ excretion by larval skin were significantly suppressed, which is consistent with the effect of EIPA (Fig. 2-5). Taken together, the loss-of-function evidence supports that NHE3b and Rhcg1 in HR cells are involved in the NH_4^+-dependent Na^+ uptake.

I also examined the mRNA levels of related genes in whole larvae and gills from adult zebrafish acclimated to L-Na water. Results showed that *nhe3b* was upregulated whereas *atp6v1a* was downregulated in L-Na larva. This result consolidates previous report which showed that *nhe3b* was upregulated and *atp6v0c* (encodes another subunit of H^+-ATPase) was downregulated in gills of adult zebrafish acclimated to L-Na water (Yan et al., 2007). However, I found that the *Rhcg1* expression of larvae was not induced by L-Na acclimation (Fig. 2-3B). This result is inconsistent with a previous report, which showed that *Rhcg1* mRNA in zebrafish larvae was induced by diluted FW (Nakada et al., 2007a). This inconsistency might be due to differences in the ionic composition of water or developmental stage of larvae. Since the mRNA level in whole larvae cannot represent that in the target organ (larval skin), I also examined the mRNA level in gills from adult individuals. *Rhcg1* expression in gills was significantly induced after L-Na acclimation supporting that *Rhcg1* is involved in the NH_4^+-dependent Na^+ uptake mechanism.

In the previous study on medaka, a new model of Na^+/NH_4^+ exchange in the apical membrane of MR cells was proposed. Although the case of zebrafish is not totally identical to that of medaka, a similar model is suggested to elucidate Na^+/NH_4^+ exchange in HR cells of zebrafish. In this model (Fig. 2-8), Rhcg1 and NHE3 function together to achieve Na^+/NH_4^+ exchange as it was proposed in medaka. Rhcg1 deprotonates intracellular NH_4^+ and conducts non-ionic NH_3. The dissociated H^+ then provides a chemical gradient for the exchange of Na^+ via NHE3b. In addition to the association of Rhcg1 and NHE3b, H^+-ATPase is involved in pumping H^+ out of the apical membrane which facilitates non-ionic NH_3 diffusion (by an acid-trapping mechanism, (Shih et al., 2008)) and in turn facilitates the deprotonation of intracellular NH_4^+. However, the coupling of Rhcg1 and NHE3b seems to be more critical in terms of Na^+ uptake. When the external Na^+ level is low, the expression of NHE3b is upregulated to compensate the

Na^+ uptake; in contrast, the expression of H^+-ATPase is downregulated. Although the existence of H^+-ATPase promotes NH_4^+ excretion, it does not favor the accumulation of H^+ inside cells which is required to drive the NHE. Therefore, to compensate for Na^+ uptake in L-Na water, the expression of H^+-ATPase needs to be downregulated.

In a very recent study (Kumai and Perry, 2011), a similar mechanism of Rhcg1 and NHE3b coupling was also reported in zebrafish under an acidified situation. A similar acidic environment was previously reported to suppress the expression and function of NHE3b in zebrafish gills (Yan et al., 2007). In Kumai and Perry's study (Kumai and Perry, 2011), *Rhcg1* knockdown decreased zebrafish Na^+ uptake in acidic fresh water, but no effect was found in normal pH. EIPA was previously found to suppress Na^+ uptake in zebrafish embryos by either $^{22}Na^+$ radioisotope tracer or sodium green fluorescence (Esaki et al., 2007), but did not show an inhibitory effect in Kumai and Perry's study (Kumai and Perry, 2011). More experiments are needed to clarify Kumai and Perry's major claim that Rhcg1 facilitate zebrafish Na^+ uptake mechanism without upregulation of *nhe3b* expression in acidic water.

In addition to the coupling of NHE3b and Rhcg1 in HR cells, previous studies on zebrafish also suggested that the maintenance of transcellular pH gradient of HR cells is necessary for absorbing Na^+. Carbonic anhydrase (*CA15a*), anion exchanger (AE1, *slc4a1b*) and Na^+ pump (*atp1a1a.5*) were found to be induced by L-Na^+ acclimation in zebrafish (Lee et al., 2011; Lin et al., 2008). Knockdown of *CA15a* (Lin et al., 2008) and *AE1* (Lee et al., 2011) suppressed Na^+ uptake by zebrafish embryos. Taken together, a model for HR cells is proposed (Hwang, 2009; Hwang et al., 2011). In a very recent report, the tight association of the proteins mentioned above (Rhcg1, NHE3b, CA2a, CA15) were revealed, indicating a metabolon was formed to facilitate the Na^+ uptake (Ito et al., 2013).

In addition to the proposed NH_4^+-dependent Na^+ uptake pathway, I also agree with

the existence of other pathways for Na^+ uptake in zebrafish. A recent study on zebrafish with a double in situ hybridization indicated that Na^+-HCO_3^- cotransporter (NBC, *slc4A4b*) mRNA was co-expressed with the Na^+-Cl^- cotransporter (NCC, *slc12a10.2*) in another subtype of ionocytes (NCC cells), suggesting that a possible coordination of apical NCC and basolateral NBC in Na^+ uptake exists (Lee et al., 2011). In addition, a preliminary experiment on zebrafish demonstrated that knockdown of *gcm2*, a transcriptional factor involved in the differentiation of HR cells, resulted in the disappearance of HR cells, but also caused a compensatory increase in both the number of NCC cells and Na^+ uptake function in the skin of zebrafish embryos (Hwang et al., 2011). Therefore, both HR cells and NCC cells seem to be responsible for the Na^+ uptake of zebrafish. In my supplemental experiment, the result of increased *zncc* transcripts in *Rhcg1* MO supported this suggestion. However, the NH_4^+-dependent Na^+ uptake by HR cells is probably a dominant pathway when ambient Na^+ is low.

Chapter 3

Rhbg mediates ammonia excretion by keratinocytes in the skin of zebrafish larvae

Introduction

Ammonia excretion by renal tubules of mammals plays a critical role in eliminating metabolic acids and maintaining pH homeostasis (Weiner and Verlander, 2011). α-Type intercalated cells are thought to be responsible for acid/ammonia excretion in the collecting duct. With V-type H^+-ATPase and a RhCG in apical membranes of intercalated cells, H^+ is pumped out of cells and combines with non-ionic NH_3 to form NH_4^+. This reaction maintains a favorable partial pressure gradient across apical membranes for NH_3 diffusion through an NH_3 channel, the RhCG (Brown et al., 2009; Eladari et al., 2002). In basolateral membranes, RhBG was suggested to facilitate ammonia movement from the blood into intercalated cells (Seshadri et al., 2006; Verlander et al., 2003).

Unlike mammals which convert metabolic ammonia into urea, most teleost fishes are ammoniotelic animals and excrete over 80% of the ammonia produced directly into the ambient water through their skin and gills (Evans et al., 2005; Wilkie, 2002). Since the discovery of Rh proteins in skin and gill recently, delicate models were proposed for ammonia excretion by suggesting the cooperation of acid-secreting molecules and Rh proteins (Weihrauch et al., 2009; Wright and Wood, 2009). Four Rh protein isoforms (Rhag, Rhbg, Rhcg1, and Rhcg2) were identified in skin/gills of teleosts including pufferfish (Nakada et al., 2007b), zebrafish (Braun et al., 2009a; Nakada et al., 2007a), rainbow trout (Nawata et al., 2007), killifish (Hung et al., 2007), and Japanese medaka (Wu et al., 2010). In the gill epithelium of the pufferfish, Rhbg and Rhcg1 were respectively identified in pavement cells (PVCs) and ionocytes (also called mitochondrion-rich cells or MRCs), suggesting that both cell types are involved in ammonia excretion (Nakada et al., 2007b). It is generally believed that PVCs are the primary location for ammonia excretion since they cover over 90% of the gill surface (Evans et al., 2005; Laurent and Dunel, 1980). However, with the discovery of Rhcg1,

ionocytes were also suggested to play a critical role in ammonia excretion (Hwang et al., 2011).

Although Rh protein isoforms have been identified in gills of several fish species, their cellular and subcellular localizations are not very clear. In zebrafish, Rhcg1 was consistently localized to apical membranes of HR cells (Nakada et al., 2007a); however, localization of Rhbg was not convincing. In previous studies using immunohistochemistry, Rhbg was found in the outer membrane of gill epithelium in zebrafish and was suggested a PVC expressing pattern of Rhbg. However, the cellular localization of Rhbg in embryonic/larval skin is not clear (Braun et al., 2009a). Since zebrafish embryos/larvae are an important model for functional studies, it is necessary to clarify localization of Rhbg in their skin.

In the present study, immunohistochemistry and in situ hybridization were used to demonstrate the location of Rhbg in zebrafish skin. We attempted to compare the roles of Rhbg and Rhcg1 in ammonia excretion using morpholino oligonucleotides (MOs) to knock down specific genes and the non-invasive SIET to analyze NH_4^+ flux at specific skin cells.

Results

Localization of Rhbg in larval skin

The cellular localization of Rhbg was determined with *in situ* hybridization and immunohistochemistry. The *Rhbg* anti-sense probe labeled polygonal keratinocytes covering an entire larva (blue signals in Fig. 3-1A, B). No detectable signal was found in ionocytes in the larval skin. An image of a sense probe is shown in Fig. 3-1C as a negative control. In addition to mRNA localization, a specific Rhbg antibody was generated and used to label Rhbg protein localization. The specificity of antibody was assessed by Western blotting (Fig. 3-3A). Three major bands with molecular weights of 37, 51, and 58

kDa were revealed. The band of 51 kDa matches the predicted molecular weight of zebrafish Rhbg. The 58 kDa band may represent the glycosylated form of Rhbg as reported in previous studies (Liu et al., 2001; Quentin et al., 2003). The specificity of Rhbg antibody was also confirmed by *Rhbg* MO injection (see below). Immunohistochemical images showed that Rhbg was mainly located in both apical and basolateral membranes of keratinocytes (green signals in Fig. 3-2A, C, E) but not in ionocytes (red signals represent NKA-labeled NaR cells; an unlabeled apical surface indicates the location of other ionocytes). Apical and basolateral localization in keratinocytes was clearly revealed by the z-axis confocal images (Fig. 3-2E). Both of the apical and basolateral signals were remarkably attenuated by *Rhbg* MO (Fig. 3-2B, D, F).

Ammonia excretion in Rhcg1 and Rhbg knockdown larvae

MOs were injected into fertilized eggs to knock down the translation of *Rhbg* or *Rhcg1*. Survival rates of larvae injected with different dose of MOs are shown in Table 3. Injection with 1 or 2 ng *Rhbg* MO slightly decreased the survival rate, whereas 4 ng *Rhbg* MO remarkably decreased it. However, injection with the *Rhcg1* MO (1, 2, or 4 ng) did not decrease the survival rate. Therefore, 2 ng *Rhbg* MO and 4 ng *Rhcg1* MO were used for experiments and no significant defect was observed in those larvae injected with those MOs. In this chapter, the knockdown efficiency of the *Rhbg* MO was determined by Western blotting (Fig. 3-3A). With injection of 2 ng *Rhbg* MO, ~88% Rhbg protein abundance (the 51 and 58 kDa protein) was suppressed in 4 days post-fertilization (dpf) larvae (Fig. 2B). Using SIET to measure the NH_4^+ gradient at the yolk-sac surface of larvae, we found that the NH_4^+ gradient decreased by ~35% in *Rhcg1* morphants (MO-injected larvae), and by ~80% in *Rhbg* morphants (Fig. 3-4). NH_4^+ fluxes at the surface of HR cells and keratinocytes were also measured in *Rhbg* and *Rhcg1* morphants (Fig. 3-5). In *Rhbg* morphants, NH_4^+ flux was significantly suppressed at keratinocytes (Fig. 3-5C) but elevated at HR cells (Fig. 3-5A). In *Rhcg1* morphants, NH_4^+ flux was suppressed

at HR cells (Fig. 3-5B) but did not change at keratinocytes (Fig. 3-5D). Relative mRNA levels of *Rhbg* and *Rhcg1* in whole larvae were determined by a real-time PCR. Results showed that both *Rhbg* and *Rhcg1* levels were significantly elevated in *Rhbg* morphants (Fig. 3-6A), *Rhcg1,* but not *Rhbg,* was elevated in *Rhcg1* morphants (Fig. 3-6B).

Discussion

The apical localization of Rhcg1 in ionocytes of pufferfish and zebrafish was clearly shown in chapter 1 and previous studies (Nakada et al., 2007a; Nakada et al., 2007b). However, the localization of Rhbg in fish gills is not yet clear. In pufferfish, Rhbg was immunolocalized to the basolateral side of PVCs in gills (Nakada et al., 2007b). In rainbow trout, Nawata and colleagues (Nawata et al., 2007) also reported the localization of Rhbg in PVCs by analyzing separate gill cells; although apical or basolateral localization was not determined. In zebrafish, Braun et al. (Braun et al., 2009a) used immunohistochemistry to show the localization of Rhbg in gill PVCs, whereas Rhbg mRNA was detected in unidentified cells in yolk-sac skin of zebrafish larvae (Braun et al., 2009a). To further investigate the role of Rhbg in zebrafish, herein I used *in situ* hybridization and immunohistochemistry (with a zebrafish-specific antibody) to localize Rhbg and found that Rhbg mRNA/protein is expressed by keratinocytes (which are similar to PVCs in gills) but not in ionocytes of zebrafish larvae (Fig. 3-1). Confocal images revealed that Rhbg is expressed in both apical and basolateral membranes of keratinocytes (Fig. 3-2A, C, E). In pufferfish, Rhcg2 was found in the apical membranes of PVCs (Nakada et al., 2007b). In the case of zebrafish, however, expression levels of Rhcg2 in zebrafish gill and whole larvae were very low (data not shown), suggesting that Rhcg2 is not a major form and is unlikely to play a critical role in zebrafish.

The transcript level of Rhbg in zebrafish larvae was remarkably higher than that of

Rhcg1 (Braun et al., 2009a), implying that Rhbg plays a dominant function in ammonia excretion. In this study, we found that knockdown of Rhbg caused a remarkable decrease (~80%) in ammonia excretion (Fig. 3-4) and an increase in mortality (Table 3). However, knockdown of *Rhcg1* only decreased ammonia excretion by ~35%, and the survival rate was not affected when even twice the dose (4 ng) of the *Rhcg1* morpholino was injected. Using SIET to examine individual cells, I found that ammonia excretion by keratinocytes was suppressed in *Rhbg* morphants (Fig. 3-5C), demonstrating the localization and function of Rhbg in keratinocytes. Interestingly, ammonia excretion by HR cells increased in *Rhbg* morphants implying a compensatory upregulation of ammonia excretion (Fig. 3-5A). This notion was supported by the elevation of *Rhcg1* mRNA levels in tissue homogenates of *Rhbg* morphants (Fig. 3-6). In contrast, knockdown of *Rhcg1* only suppressed ammonia excretion by HR cells but did not increase ammonia excretion by keratinocytes (Fig. 3-5B, D). Taken together, the role of Rhbg in ammonia excretion seems to be dominant over Rhcg1 in zebrafish larvae.

In a previous study on zebrafish larvae, it was reported that knockdown of either *Rhbg* or *Rhcg1* caused similar impacts on ammonia excretion (Braun et al., 2009a). This inconsistency could have been due to different approaches used to measure ammonia excretion. In that study, they measured the excreted ammonia accumulation from pooled larvae in a limited amount of water for 3 h to calculate the ammonia excretion rate. That method probably increased the external ammonia level and reduced its excretion or even caused backflux. With the SIET in this study, the tiny ammonia gradient at the yolk-sac skin or specific type of cell was determined usually within 10 min, and the accumulation of ammonia in water was subtle.

In this study, 2 ng of Rhbg morpholino were applied. The morphologies of morphants we examined showed as the same as that in WT larvae. Compared to 2 ng *Rhbg* MO-injected larvae, however, larvae injected with 4 ng of *Rhbg* MO significantly

increased mortality (Table 3). This might be the result of Rhbg impairment in ammonia excretion, or be the consequences of *Rhbg* knockdown affected other life-depending factors. Although I am not able to determine the side effects of Rhbg MO, I suggested that Rhbg play a critical role in early developmental stage since I found that most fertilized embryos were dead before hatching.

Chapter 4

Rhbg transports CO_2 in the keratinocytes of zebrafish larvae

Introduction

It was generally accepted that cell membranes are highly permeable to respiratory gas CO_2 (Gutknecht et al., 1977; Missner et al., 2008a; Missner et al., 2008b). Although the CO_2 diffusivities and the diffusion distances have been reported as resistances (Boron et al., 2011; Itel et al., 2012), the diffusion of CO_2 through tissue is so rapid that no significant disturbances to this process were considered by researchers. Recently, however, the studies on mammalian epithelium cells and artificial lipid bilayer found that CO_2 permeability of cell membrane was interfered by the cholesterol amounts (Itel et al., 2012) and regulated by the gas channels (Boron, 2010; Nakhoul et al., 1998; Prasad et al., 1998). Thus, the mechanism of CO_2 transport needs to be re-evaluated.

In vertebrates, Rh proteins are ammonia channels homologous to the ammonia transporters in bacterial and plants (Huang and Peng, 2005; Huang and Ye, 2010). Three major isoforms (RhAG, RhBG and RhCG) were found to facilitate NH_3 transport in a variety of animal tissues. Despite NH_3, the emerging evidence revealed that Rh proteins are able to conduct CO_2. Previous work showed that the permeability of membrane to CO_2 were significantly reduced in the red blood cell (RBC) lacking RhAG (Endeward et al., 2008). Using H^+ microelectrode probe, Musa-Aziz and colleagues (Musa-Aziz et al., 2009a) demonstrated that surface pH of RhAG-expressing *Xenopus* oocytes was significant increased while exposed to hypercapnia, suggesting a greater CO_2 were introduced for permeation. Although these studies indicated that Rh proteins may serve as pathway for the CO_2 diffusion, *in vivo* evidences are still needed. Moreover, it is not known yet whether other Rh isoforms (RhBG and RhCG) participate in CO_2 transport.

The skin of zebrafish larvae is a good model for investigating ion regulation and gas transport (Chang and Hwang, 2011; Glover et al., 2013; Hwang, 2009). Skin gas exchange is performed in the squamous keratinocyte (KC) which is functional analog to

the gas permeating pavement cell (PVC) in gill (Laurent and Dunel, 1980; Wilson and Laurent, 2002). Studies in fish CO_2 excretory mechanism were predominantly addressed on the issue of carbonic anhydrase (CA) regulation. CA dehydrates HCO_3^- in red blood cell and plasma to form CO_2, therefore created a favorable gradient for excretion (Esbaugh and Tufts, 2006; Gilmour and Perry, 2010). However, the functional significance of gas channel in CO_2 excretion has yet been estimated. In chapter 3 I found that Rhbg expressed extensively at both apical and basolateral membrane of keratinocyte in zebrafish larvae. Is the route of CO_2 excretion provided by Rhbg needs further investigation.

In this chapter, the CO_2 excretion of larvae exposed to high ammonia was analyzed to determine if a common pathway was shared by CO_2 and ammonia. I used morpholino oligonucleotides (MO) to specifically knock down *Rhbg* and *Rhcg1* expression and demonstrated the contribution of Rh proteins in CO_2 excretion. I further measured the surface H^+ concentration (pH) of Rh-MO injected zebrafish exposed to hypercapnia. The change of surface pH (ΔpH) enabled me to reveal the effect of Rh proteins on membrane CO_2 permeability.

Results

CO_2 excretion of larvae exposed to high ammonia environment (H-Amm)

The first objective of present study was to demonstrate the pathway of CO_2 excretion in larval skin. In previous works I showed that ammonia was transported into larvae while exposing to high-ammonia environment (H-Amm)(Fig. 1-4); and was intensely excreted when body the ammonia was high (Shih et al., 2008). In this chapter, larvae also treated with high ammonia to test if CO_2 excretion was blocked when the bulk flow of NH_3 was occurred. During the measurement, larvae were incubated in a CO_2 probe-integrated water camber. The accumulation of water CO_2 content (CO_2

excretion) was continuously monitored by the CO_2 probe. Because the demand of O_2 is a critical factor that affects CO_2 production, the change of water O_2 (consumption) was also recorded. Results showed that the consumption of water O_2 (ΔO_2) were unchanged in Normal (NW), high environmental ammonia (External H-Amm, 5mM NH_4^+) and ammonia loaded (Internal H-Amm, pre-incubated in 5 mM NH_4^+ water) larvae (Fig. 4-1B), suggesting the metabolism among three group were the same. However, the water CO_2 level (ΔCO_2) of External H-Amm and Internal H-Amm larvae were significantly lower than that in WT (Fig. 4-1A). I calculated the respiratory exchange ratio (RER) to demonstrate the CO_2 excretion after the correction of metabolic rate. As shown in Fig. 4-1C, RER were significantly reduced in External H-Amm and Internal H-Amm larvae. These results indicated that ammonia transport blocked the CO_2 excretion pathway.

CO_2 excretion in the Rhbg and Rhcg1 morphants

To test if CO_2 were transported by Rh proteins, larvae injected with *Rhbg* or *Rhcg1* MO was underwent CO_2 excretion and O_2 uptake examination. Results showed that the consumption of O_2 in WT, *Rhbg* MO and *Rhcg1* MO were unchanged (Fig. 4-2B). In the CO_2 analysis, the ΔCO_2 had no difference between WT and *Rhcg1* MO (Fig. 4-2A). In the *Rhbg* MO, however, ΔCO_2 was lower than other two groups (Fig. 4-2A). The RER of *Rhbg* MO also showed a significant decreased (Fig. 4-2C). These results suggested that Rhbg but not Rhcg1 was involved in CO_2 transport,

Surface H^+ of Rhbg MO acute treated with hypercapnia

Since there was no effect of *Rhcg1* MO on CO_2 excretion, the following analysis was focus on the function of Rhbg. To analyze the skin CO_2 excretion in detail, a method was established by using H^+-selective probe to measure the surface H^+ concentration, which is the product of CO_2 hydration. In *Rhbg* MO, the surface H^+ gradient of skin and the H^+ efflux of keratinocyte were significantly decreased (Fig.

4-3A, B). On the other hand, neither the function nor the number of HR cell was altered (Fig. 4-3C, D), suggesting that the skin H^+ gradient was specifically affected by the loss CO_2 hydration in *Rhbg* MO. I further measured the change of pH (ΔpH) in larvae exposed to hypercapnia. While exposing to hypercapnia, the permeation of CO_2 from water into plasma induces a surface alkalinization (dehydration of HCO_3^-, (Endeward et al., 2006b; Musa-Aziz et al., 2009a)(Fig. 4-4A). The higher ΔpH represented a higher permeability of skin to CO_2. The pH at the surface of WT and *Rhbg* MO was initially raised but subsequently acidified by the H^+ actively secreted via H^+-ATPase (Fig. 4-4B). Notably, the maximum ΔpH in the *Rhbg* MO was lower than that in WT (Fig. 4-4C), suggesting a fewer CO_2 was permeated. Because the ionocytes (especially HR cell) also secrete H^+ (Lin et al., 2006), *foxi3* MO (co-injected with *foxi3a* and *foxi3b* morpholino) was applied to inhibit the differentiation of ionocytes in order to determine the contribution of keratinocyte and Rhbg in CO_2 permeation. During the exposure of hypercapnia, surface pH in the *foxi3* MO larvae also exhibited an alkalinization but lack of the subsequent acidification (Fig. 4-4B). Surface pH in the larvae co-injected with *Rhbg* and *foxi3* MO (*Rhbg*/*foxi3* MO) was also alkalized (Fig. 4-4B), but the ΔpH was remarkably lower than that in *foxi3* MO (Fig. 4-4C). These results showed that knockdown of Rhbg significantly increased the resistance of CO_2 (Fig. 4-4C).

NH_4^+ gradient in the larvae exposed to hypercapnia

Present study further examined the effects of CO_2 transport on ammonia excretion by applying the NH_4^+-selective probe. In the WT and *foxi3* MO larvae, $\Delta[NH_4^+]$ were reduced during the exposure to hypercapnia medium (bulk CO_2 inflow) and were not restored after the exposure (post-hypercapnia). In the *Rhbg* MO, no differences of $\Delta[NH_4^+]$ were found among the treatments (Fig. 4-5).

Discussion

Present study first provided the direct evidence to support that Rh protein regulate

membrane CO_2 permeability in an intact organism. Early studies on the permeation of CO_2 via gas channel focused on the function of aquaporins (Endeward et al., 2006b; Nakhoul et al., 1998). The investigations of CO_2 transport functions in Rh proteins only emerged in recent years (Boron, 2010). Since the expression of RhAG is predominantly at the membrane of red blood cell, RhAG is the only Rh proteins received attentions in studying CO_2 transport (Endeward et al., 2008). In the researches of other Rh proteins in mammals, it was suggested that RhBG coordinates with RhCG to transport ammonia for regulating renal acid-base homeostasis (Weiner and Hamm, 2007; Weiner and Verlander, 2011). However, the roles of RhBG and RhCG in mammalian CO_2 are not demonstrated yet. Interestingly, both RhBG and RhCG were found in the bronchiolar epithelium of murine lung, but it was concluded that neither RhBG nor RhCG contributed to pulmonary CO_2 transport (Han et al., 2009b).

Unlike mammals whose CO_2 is excreted directly into air, fish require more efficient pathway (i.e. through gas channel) for respiratory CO_2 excretion because the pCO_2 gradient in fish (plasma-to-water) is less than that in terrestrial animals (plasma-to-gas). In chapter 3 I found that zebrafish Rhbg was distributed in both apical and basolateral membrane of keratinocyte, which covered the skin (and gill) surface enormously (Laurent and Dunel, 1980). Therefore, I hypothesized that Rhbg is involved in CO_2 excretion. The fist evidence support this hypothesis is that a common pathway was shared by CO_2 and ammonia. In the larvae with bulk NH_3 flow (inflow and outflow), CO_2 excretion was significantly suppressed (Fig. 4-1). On the other hand, the ammonia excretion was also inhibited by the increased CO_2 excretion (Fig. 4-5). These results suggested the competition of CO_2 and NH_3 for permeation route. The function of Rhbg in CO_2 permeation was further confirmed by the application of morpholino knockdown. The analysis of water CO_2 showed that the CO_2 excretion in *Rhbg* MO was significantly reduced (Fig 4-2), indicating that the deficiency of Rhbg impaired the CO_2

excretion. The observation of surface pH consolidated this finding, showed a significant reduce of ΔpH in the Rhbg MO larvae exposed to hypercapnia (Fig. 4-4). Taking together, this research first provided *in vivo* evidence for CO_2-transport ability of Rhbg.

The quantitative index (ΔpH) is consisted between the work of Musa-Aziz and mine. By monitoring the membrane surface pH under hypercapnia, Endeward and Musa-Aziz developed an approach to examine the CO_2 permeability of biological membrane. Using *Xenopus* oocyte constructed with gas channels, they successfully demonstrated the CO_2 transport function of AQPs and RhAG (Endeward et al., 2006a; Musa-Aziz et al., 2009a; Musa-Aziz et al., 2009b). In the present work, hypercapnia induced an elevated surface pH as observed in oocytes, suggesting a reliable data interpretation in this study. One thing should be noticed is that the surface pH of larval skin is also affected by the secreted H^+ (via H^+-ATPase and other acid secreting proteins) and the effect of hypercapnia on surface ΔpH would be mask. Therefore, we inhibited the differentiation of HR cell (and other ionocytes) by knockdown the transcription factors foxi3a and foxi3b (Chang and Hwang, 2011; Esaki et al., 2009) to exclude the effects of ionocyte on surface pH. The *foxi3* MO-injected larvae treated with hypercapnia showed a higher alkalinization (ΔpH) and no instant acidification (Fig. 4-4B), thus revealed the response of keratinocyte during CO_2 transport.

The present research demonstrated that in keratinocyte, NH_3 and CO_2 were transported by Rhbg. However, other research suggested that CO_2 and NH_3 were diffused through different routes in the Rh protein. Musa-Aziz et al observed that DIDS, a non-specific inhibitor Rh protein inhibitor (Endeward et al., 2006a), completely blocked CO_2 transport but had no effect on NH_3 permeability in the RhAG-expressing oocytes (Musa-Aziz et al., 2007). The authors suggested that NH_3 and CO_2 were conducted via different conformation in Rh proteins, presumably by the Rh monomer and the central cavity of Rh homotrimer, respectively (Boron, 2010; Musa-Aziz et al.,

2007). Interestingly, the molecular simulation showed that the periplasmic vestibule (at inner region) of Amt monomer was able to recruit CO_2. This finding supported the movement of NH_3 and CO_2 through same Amt/Rh monomer (Akgun and Khademi, 2011).

Notably, no effect of Rhcg1 MO on larval CO_2 excretion was found in present study (Fig. 4-2), indicating that Rhcg1 may not participate in CO_2 excretion. In zebrafish, Rhcg1 was distributed in HR cell where the carbonic anhydrases (CA) were highly expressed (Gilmour and Perry, 2009; Gilmour et al., 2009; Lin et al., 2008). The role of cytosolic CA (CA2) in HR cell were suggested in facilitating the hydration of CO_2 to form bicarbonate (HCO_3^-), which is subsequently transported into plasma for maintaining acid-base homeostasis. Indeed, my preliminary experiment showed that H^+ secretion in HR cell was completely blocked by the CA inhibitor acetazolamide, suggesting the hydration of CO_2 was occurred in HR cell. These results indicated that HR cell is not the site for CO_2 excretion. Moreover, the expression of extracellular CA (CA15) in the outer membrane of HR cell may suggest that HR cell uptakes CO_2 (Hwang et al., 2011). A very recent study revealed that CA15 were distributed at the external cell surface of HR cell and was suggested to facilitate the dehydration of HCO_3^- and form CO_2 (Ito et al., 2013). The accumulating CO_2 may create a favorable water-to-plasma PCO_2 gradient at surface of HR cell. Although the evidence supporting the apical dehydration is still absent, it is interesting to examine if Rhcg1 is the route for HR cell uptake CO_2.

Perspectives and Significance

The results of this research provided molecular and physiological evidence to support the gas (NH_3 and CO_2) transport function of Rh proteins in zebrafish. The analysis of protein expression of Rhbg and Rhcg1 showed that Rhbg were distributed at both apical and basolateral membrane of keratinocyte, whereas Rhcg1 were distributed at the apical region of HR cell. Combining the anatomical fact that skin surface is massively covered by keratinocyte and the physiological evidence that high gas permeability provided by Rhbg, it is clearly that keratinocyte contributed to the majority of ammonia and CO_2 excretion in zebrafish. In HR cell, on the other hand, ammonia excretion was facilitated by the cooperation of Rhcg1 and H^+-ATPase. This cooperation enable HR cell to perform ammonia excretion against gradient. My results also suggested that HR cell played a regulatory role in ammonia excretion by adjusting the expression of Rhcg1. Despite ammonia excretion, Na^+ uptake was also enhanced by Rhcg1. The NH_4^+ was recruited by Rhcg1 and deprotonated to form NH_3 and H^+. The H^+ was subsequently provided the driving force of NHE to execute Na^+ absorption.

Although CO_2 is excreted via the lung in mammals, it is interesting to investigate if CO_2 is transported by Rh proteins in kidney. In the collecting duct of mammalian kidney, Rh proteins transporting NH_3 to trap luminal H^+ to prevent the bakcflux of H^+, thus regulate the acid excretion. It should be noted that the activity of carbonic anhydrase, which accelerates the hydration of CO_2, is high in the collecting duct (Purkerson and Schwartz, 2007), suggesting that CO_2 is continuously provided from the interstitium of collecting duct. To our knowledge so far, no research have been studied the CO_2 transport contribution of Rh proteins in the kidney.

As mentioned in Chapter 3, the mortality of Rhbg-MO injected larvae in pre-hatching stage (approximately before 48 h) was very high. This result indicated that Rhbg is critical in early embryonic development. However, it was suggested that in the

pre-hatching stage, urea but not ammonia is the major end product of nitrogen metabolism (Braun et al., 2009a; Chadwick and Wright, 1999; Wright et al., 1995). It would be interesting to study the effect of Rhbg in the embryogenesis.

The mainly toxicity of ammonia is that NH_3 substitutes K^+ to open the K^+-related channels or transporters, thus impairs the nervous system. To protect from brain damage caused by ammonia, astrocyte exhibited an ammonia-induced swelling resulting from the permeation of ammonia through the blood-brain barrier (Ip and Chew, 2010). In this swelling model, the absorbed ammonia elevates cellular nitrogen level and induced the oxidative/nitrosative stress (ONS). The occurrence of ONS results in astrocyte swelling and therefore eliminates excessive ammonia in the brain. The Rh proteins were found to express in the brain tissue in many species, but it is still unknown whether Rh proteins regulate ammonia transport in the brain?

Materials and methods

Experimental animals

Adult zebrafish (AB strain) were reared in circulating tap water at 28 °C with a photoperiod of 14 h of light/10 h of dark. Fertilized eggs were incubated in normal water (NW) or different artificial freshwaters for specific experiments (see below). During acclimation experiments, fish were starved, and the media were changed daily to guarantee optimal water quality. The experimental protocols were approved (no. 95013) by the National Taiwan Normal University Animal Care and Utilization Committee.

Preparation of water and acclimation

All of the incubating solutions were prepared with double-deionized water supplemented with various salts (Sigma-Aldrich, St. Louis, MO). Normal water (NW) contained (in mM) 0.5 NaCl, 0.2 $CaSO_4$, 0.2 $MgSO_4$, 0.16 KH_2PO_4, and 0.16 K_2HPO_4 (pH 7.0). In chapter 1, high ammonia water were prepared by adding $(NH_4)_2SO_4$ into NW to final concentration (1 mM and 5 mM NH_4^+). In chapter 2, L-Na water contained 0.005 NaCl, 0.25 $MgCl_2$, 0.2 $CaSO_4$, 0.16 KH_2PO4, and 0.16 K_2HPO_4 (pH 7.0); H-Amm and L-Na-H-Amm waters were prepared by adding 2.5 mM $(NH_4)_2SO_4$ to NW or L-Na water. Fertilized eggs were immediately transferred to the media after collection. The acclimated larvae were examined at 4-days post-fertilization (dpf) throughout present study. No significant increases in mortality or developmental abnormalities were found in larvae acclimated to L-Na, H-Amm, or L-Na-H-Amm for 4 days.

Scanning ion-selective electrode technique (SIET)

The SIET was used to measure NH_4^+, H^+, and Na^+ activities at the surface of zebrafish larvae. Glass capillary tubes (no. TW 150-4, World Precision Instruments, Sarasota, FL) were pulled on a Sutter P-97 Flaming Brown pipette puller (Sutter Instruments, San Rafael, CA) into micropipettes with tip diameters of 3~4 μm. These

were then baked at 120 °C overnight and coated with dimethyl chlorosilane (Sigma-Aldrich) for 30 min. The micropipettes were backfilled with a 1-cm column of electrolytes and frontloaded with a 20~30-μm column of liquid ion-exchange cocktail (Sigma-Aldrich) to create an ion-selective microelectrode (probe). The following ionophore cocktails (and electrolytes) were used: NH_4^+ ionophore I cocktail B (100 mM NH_4Cl); Na^+ ionophore II cocktail A (100 mM NaCl); and H^+ ionophore I cocktail B (40 mM KH_2PO_4 and 15 mM K_2HPO_4; pH 7). To calibrate the ion-selective probe, the Nernstian property of each microelectrode was measured by placing the microelectrode in a series of standard solutions (0.1, 1, and 10 mM NH_4Cl for the NH_4^+ probe; 0.1, 1, and 10 mM NaCl for the Na^+ probe; and pH 6, 7, and 8 for the H^+ probe). By plotting the voltage output of the probe against log [NH_4^+], [Na^+], and [H^+] values, a linear regression yielded a Nernstian slope of 58.5 ± 0.4 (n = 10) for NH_4^+, 56.7 ± 0.5 (n = 10) for Na^+, and 58.6 ± 0.8 (n = 10) for H^+.

According to technical documents published on the Sigma website (www.sigmaaldrich.com), the selectivity coefficients of the Fluka NH_4^+ ionophore I cocktail B is only four times more selective to NH_4^+ than to K^+. To prevent interference from K^+ in the medium, K^+-free recording medium (0.2 mM NaCl, 0.05 mM $(NH_4)_2SO_4$, 0.2 mM $CaSO_4$, 0.2 mM $MgSO_4$, 0.16 mM NaH_2PO_4, 0.16 mM Na_2HPO_4, 300 μM MOPS buffer, and 0.3 mg/l Tricaine) was used when probing NH_4^+. In addition, because the calibration (Nernstian) slope of NH_4^+ gradually decays at concentrations below 0.1 mM, the NH_4^+ concentration in the recording medium was raised by adding 0.05 mM $(NH_4)_2SO_4$ for a practical and precise calibration. In the preliminary test, the selectivity of the Fluka Na^+ ionophore II cocktail A was about 10-16 times more selective to Na^+ than to NH_4^+ (measured in 1-10 mM Na^+ solution).

Measurement of surface ion gradients

The SIET was performed at room temperature (26~28 °C) in a small plastic

recording chamber filled with 1 ml of recording medium that contained NW, 300 μM MOPS buffer, and 0.3 mg/l ethyl 3-aminobenzoate methanesulfonate (Tricaine, Sigma-Aldrich). The pH of the recording media was adjusted to 7.0 by adding a NaOH or HCl solution. Different recording medium (such as H-Amm, H-Na or hypercapnia) were also used for different purposes (see below). Before measurement, an anesthetized larva was positioned in the center of the chamber with its lateral side contacting the base of the chamber. After 3 min of waiting for signal stabilization, the ion-selective probe was moved to the target position (~10 μm away from the yolksac membrane) to record the ionic activities for 10 sec; then the probe was immediately moved away (~1000 μm) to record the background for another 10 sec. The averaged voltage (mV) from the serial recording in the 10 sec was used to calculate the ionic concentration at target or background. To calculate ionic gradients, the concentration at target was subtracted by the concentration at background. In this study, $\Delta[NH_4^+]$, $\Delta[Na^+]$, and $\Delta[H^+]$ were respectively used to represent the measured NH_4^+, Na^+, and H^+ gradients between the targets (at the surface of larval skin) and background.

Measurement of ion flux in skin cell

To record the NH_4^+ and H^+ flux at the surface of ionocytes and keratinocytes, the microelectrode was moved to a position ~1 μm above the surface of a cell. At every position, the voltage difference in microvolts was measured by probing orthogonally to the surface at 10-μm intervals. The recording was performed for 20~30 replicates, and the median of the repeats was used to calculate the ion flux of the cell. To calculate ionic flux, voltage differences were first converted into a concentration (activity) gradient ΔC ($\mu mol \cdot l^{-1} \cdot cm^{-3}$). ΔC was subsequently converted into ionic flux using Fick's law of diffusion in the following equation:

$$J = D(\Delta C) / \Delta X \qquad (1)$$

where J ($pmol \cdot cm^{-2} \cdot s^{-1}$) is the net flux of the ion, D is the diffusion coefficient of the

ion (2.09×10^{-5} cm^2/s for NH_4^+); and ΔX (cm) is the distance between the two points. The detailed calculation of ionic flux was shown in previous reports (Lin et al., 2006).

Surface pH measurement

In chapter 4, the H^+ activity (mV) recorded by SIET were converted into pH by fitting the mV into the regression line (see above). ΔpH was used to represent the H^+ concentration gradient between the yolk-sac surface and background. The positive value of ΔpH indicated an alkalization at skin and surface. The negative ΔpH represent the acidification.

Morpholino design and microinjection

MOs were obtained from Gene Tools (Philomath, OR). Sequences of MOs against specific genes are listed in Table. 1. A standard control MO was also used as the control. The control MO provided by Gene Tools had no target and no significant biological activity. An MO solution was prepared with sterile water and contained 0.1% phenol red as a visualizing indicator. The MO was microinjected into embryos at the 1~4-cell stage with an IM-300 microinjector system (Narishige Scientific Instrument Laboratory, Tokyo, Japan). In a preliminary test, embryos injected with 4 ng of control MO showed no significant differences in survival rates, morphology, or NH_4^+ gradients compared to wild-type (WT) embryos. To knockdown *foxi3a* and *foxi3b*, a *foxi3a/3b* MO solution was prepared by premixing two MOs into final concentration (see below). In present study, MO amount were injected as *Rhbg*: 2 ng; *Rhcg1*: 4 ng; *nhe3b*: 4 ng; *foxi3*: 2 ng (of *foxi3a* and *foxi3b* each); *Rhbg/foxi3*: 2ng/2ng.

Acute effects of artificial media on ionic gradient

In chapter 1, external high ammonia were prepared by adding $(NH_4)_2SO_4$ to final NH_4^+ concentration. In chapter 2, high-MOPS, high-NH_4^+, and high-Na^+ medium were applied to examine the association of Na^+ and NH_4^+ in Na^+ uptake mechanism. Ionic gradients (Na^+ and NH_4^+) of L-Na acclimated larvae were recorded in four different

recording media: Normal (control), high-MOPS (H-MOPS), high-ammonium (H-Amm), and high-Na^+ (H-Na) recording media. The H-Amm recording medium was prepared by adding 2.5 mM $(NH_4)_2SO_4$ to Normal recording medium. The H-MOPS recording medium was prepared by adding 5 mM MOPS buffer to Normal recording medium. The H-Na water was prepared by adding 5 mM Na_2SO_4 to Normal recording medium. The pH of the four media was adjusted to pH 7.0. When probing NH_4^+, K^+ in the 4 recording media was free (KH_2PO_4 and K_2HPO_4 in the recording media were replaced by NaH_2PO_4 and Na_2HPO_4) and 0.05 mM $(NH_4)_2SO_4$ was added as described above.

ΔCO2, ΔO_2, and respiratory exchange ratio (RER)

Water CO_2 or O_2 contents were continuous monitored by fiber optic CO_2 or O_2 transmitters (PreSens, Regensburg, Germany). In the measurement of O_2 uptake and CO_2 excretion, 20 larvae were incubated in the O_2 or CO_2 sensor-integrated 1.5 mL eppendorff fully filled with normal water. O_2 consumption (ΔO_2) and CO_2 excretion (ΔCO_2) were determined by the difference of content between 0 min and target time. To analyze the effect of high external ammonia on CO_2 excretion, larvae were incubated in the 5 mM [NH_4^+] water (H-Amm). The pH of medium were adjusted to 7.0. The ΔCO_2 and ΔO_2 in the tube without larvae were used for blank control. In order to correct the variations of metabolic rate, respiratory exchange ratio (RER, $\Delta CO_2/\Delta O_2$) was demonstrated.

Effects of 5-ethylisopropyl amiloride (EIPA) on ionic gradients

The EIPA (Sigma) stock solutions were prepared by dissolving EIPA in dimethyl sulfoxide (DMSO, Sigma). A final concentration of 1 mM EIPA was applied to larvae for 10 min according to a previous study (Shih et al., 2008; Wu et al., 2010). After treatment, the surface ionic gradients of larvae were immediately measured in recording medium.

Preparation of total RNA

Zebrafish larvae or adult gills were homogenized in TRIzol reagent (Invitrogen, Carlsbad, CA). Total RNA was purified following the manufacturer's protocol. The total amount of RNA was determined by spectrophotometry (ND-1000, NanoDrop Technologies, Wilmington, DE), and the RNA quality was checked by running electrophoresis in RNA-denatured gels. All RNA pellets were stored at -20 °C.

Real-time quantitative (q)PCR

Total RNA was extracted and reverse-transcribed from zebrafish larvae described above. The mRNA expression of target genes was measured by a qPCR with the Roche LightCycler 480 System (Roche Applied Science, Mannheim, Germany). Primers for all genes were designed using Primer Premier software (vers. 5.0; PREMIER Biosoft International, Palo Alto, CA). PCRs contained 5 ng of complementary (c)DNA, 50 nM of each primer, and the LightCycler 480 SYBR Green I Master (Roche) in a final volume of 10 μl. All qPCRs were performed as follows: one cycle of 50 °C for 2 min and 95 °C for 10 min, followed by 40 cycles of 95 °C for 15 s and 60 °C for 1 min (the standard annealing temperature of all primers). PCR products were subjected to a melting-curve analysis, and the samples were electrophoresed to verify that only a single product was present. Control reactions were conducted with sterile water to determine levels of background and genomic DNA contaminations. The standard curve of each gene was confirmed to be in a linear range with ribosomal protein L13a (*rpl13a*) as an internal control. All the primer sets used for qPCR were listed in Table. 2.

In situ hybridization

Rhbg probe fragments (nucleotides 1011~1433, accession no. NM_200071.2) were obtained by a PCR and inserted into a pGEM-T easy vector (Promega, Madison, WI). Digoxigenin (DIG)-labeled RNA probes were synthesized by in vitro transcription with T7 and SP6 RNA polymerase (Takara Bio, Tokyo, Japan), and the quality and concentration were examined with RNA gels. Zebrafish embryos fixed in a 4%

paraformaldehyde (PFA) phosphate-buffered saline (PBS; 1.4 mM NaCl, 0.2 mM KCl, 0.1 mM Na_2HPO_4, and 0.002 mM KH_2PO_4, at pH 7.4) solution at 4 °C overnight and then treated with methanol at 4 °C overnight again. Afterward, samples were treated with a methanol series at concentrations of 100% to 25% in diethylpyrocarbonate (DEPC)-PBST (PBS with 0.1% Tween 20) for 10 min each. Samples were then hybridized with the prepared probe in hybridization buffer (60% formamide, 5× SSC, 0.1% Tween 20, 500 μg/ml yeast tRNA, and 50 μg/ml heparin) overnight at 65 °C. The next day, samples were serially washed with 75% hybridization buffer in 25% 2× SSC at 65 °C up to 100% 2× SSC, and finally with 0.2× SSC for 5~10 min six times. Samples were blocked with 5% sheep serum in 2 mg/ml bovine serum albumin (BSA; Sigma, St. Louis, MO) at room temperature for 4 h and then incubated with an anti-DIG antibody (1: 5000, in blocking solution) at 4 °C overnight. After being washed with DEPC-PBST at room temperature for 15 min eight times, staining buffer (0.1 M Tris at pH 9.5, 50 mM $MgCl_2$, 0.1 M NaCl, and 0.1% Tween 20) was subsequently used for 5 min three times. Staining was conducted with a mixture of NBT and BCIP in 10 ml of staining buffer at room temperature from 10~30 min in the dark. The reaction was stopped by PFA and subsequently washed with methanol several times. Finally, samples were stored in PBS at 4 °C in the dark until further examination and analysis. Images were obtained with an upright microscope (BX51W1; Olympus, Tokyo, Japan) equipped with a digital camera (Canon 50D; Tokyo, Japan).

.Immunohistochemistry

Zebrafish embryos were fixed in 4% paraformaldehyde for 2 h at 4 °C. After washing in PBS, fixed embryos were treated with 100% ethanol for 10 min at -20 °C and subsequently subjected to blocking with 3% BSA at room temperature for 30 min. Embryos were then incubated with a polyclonal rabbit antibody (diluted 1: 500 in PBS) overnight. The Rhbg antibody were developed against zebrafish Rhbg (amino acids

33~51, accession no. NP_956365.2; Genomics BioSci&Tech, New Taipei City, Taiwan). The Rhcg1 antibody was provided by Dr. Hirose. The detail information of Rhcg1 antibody was showed in (Nakada et al., 2007a). The H^+-ATPase was identified by the antibody against atp6v0c (α-subunit of H^+-ATPase). After being washed with PBS, embryos were blocked again with 3% BSA for further double immunostaining of Na^+/K^+-ATPase (NKA). Embryos were incubated with an α5 monoclonal antibody against α-subunit of avian NKA (Hybridoma Bank, University of Iowa, Ames, IA; at a 1: 500 dilution) at room temperature for 2 h. Embryos were washed in PBS, and then incubated with 1: 200 PBS-diluted goat anti rabbit immunoglobulin G (IgG) (conjugated with Alexa Fluor 488, Molecular Probes, Carlsbad, CA) and goat anti-mouse IgG (conjugated with Alexa Fluor 568) for 2 h at room temperature. Embryos were finally stained with DAPI (Invitrogen, Carlsbad, CA) to identify nuclei. Images were acquired with a confocal laser scanning microscope (TCS-SP5, Leica Lasertechnik, Heidelberg, Germany). For z-plane images, 30 serial sections (0.5 μm/section; total thickness 15 μm) of images were acquired and subjected to image reconstruction and analysis.

Western blotting

Proteins of 20 μg/well were loaded onto a 10% sodium dodecyl sulfate-polyacrylamide gel electrophoresis (SDS-PAGE) at 100 V for 1.5 h. After separation, proteins were transferred onto polyvinylidene difluoride membranes (Merck Millipore, Darmstadt, Germany) at 30 V overnight. After being blocked for 3 h in 5% nonfat milk, blots were incubated with an anti-Rhbg antibody (overnight, 4 °C, diluted 1: 500) and with a horseradish peroxidase-conjugated goat anti-rabbit IgG antibody (dilute 1:5000; Millipore) at room temperature for another 2 h. Blots were visualized with an enhanced chemiluminescence system (Millipore). The image was captured using an ImageQuant LAS 4000 system (GE Healthcare, Buckinghamshire, UK). Intensities of the immunoreactive bands were quantified by densitometry (ChemiGenius, Syngene,

UK).

Measurement of whole-body Na^+ contents

Ten zebrafish larvae were briefly rinsed with deionized water and then pooled as one sample and weighed. HNO_3 (13.1 N) was added to samples for digestion at 60 °C overnight. Digested solutions were diluted with double-deionized water, and the total Na^+ content was measured with an atomic absorption spectrophotometer (model Z-8,000; Hitachi). Standard solutions of Na^+ measurements from Merck (Darmstadt, Germany) were used to make the standard curves.

Calculation of cell density

For the quantification of HR cell density, larvae were immunostained with H^+-ATPase antibody. A square (0.3×0.3 mm^2) on the yolk sac surface of an embryo were chosen for counting.

Statistical analysis

Data are expressed as the mean ± SE. Values from each condition were analyzed using one-way analysis of variance (ANOVA) followed by Tukey's pairwise comparisons. Student's unpaired *t*-test (two-tailed) was used for simple comparisons of two means. In all cases, significance was accepted at a level of 0.05.

References

Akgun, U. and Khademi, S. (2011). Periplasmic vestibule plays an important role for solute recruitment, selectivity, and gating in the Rh/Amt/MEP superfamily. *Proc Natl Acad Sci U S A* **108**, 3970-5.

Avella, M. and Bornancin, M. (1989). A new analysis of ammonia and sodium transport through the gills of the freshwater rainbow trout (*Salmo gairdneri*). *J Exp Biol* **142**, 155-175.

Bakouh, N., Benjelloun, F., Cherif-Zahar, B. and Planelles, G. (2006). The challenge of understanding ammonium homeostasis and the role of the Rh glycoproteins. *Transfus Clin Biol* **13**, 139-46.

Barrionuevo, W. R. and Burggren, W. W. (1999). O_2 consumption and heart rate in developing zebrafish (*Danio rerio*): influence of temperature and ambient O_2. *Am J Physiol* **276**, R505-13.

Biver, S., Belge, H., Bourgeois, S., Van Vooren, P., Nowik, M., Scohy, S., Houillier, P., Szpirer, J., Szpirer, C., Wagner, C. A. et al. (2008). A role for Rhesus factor Rhcg in renal ammonium excretion and male fertility. *Nature* **456**, 339-43.

Boron, W. F. (2010). Sharpey-Schafer lecture: gas channels. *Exp Physiol* **95**, 1107-30.

Boron, W. F., Endeward, V., Gros, G., Musa-Aziz, R. and Pohl, P. (2011). Intrinsic CO_2 permeability of cell membranes and potential biological relevance of CO_2 channels. *Chemphyschem* **12**, 1017-9.

Braun, M. H., Steele, S. L., Ekker, M. and Perry, S. F. (2009a). Nitrogen excretion in developing zebrafish (*Danio rerio*): a role for Rh proteins and urea transporters. *Am J Physiol Renal Physiol* **296**, F994-F1005.

Braun, M. H., Steele, S. L. and Perry, S. F. (2009b). The responses of zebrafish (*Danio rerio*) to high external ammonia and urea transporter inhibition: nitrogen excretion and expression of rhesus glycoproteins and urea transporter proteins. *J Exp Biol* **212**, 3846-56.

Brown, A. C., Hallouane, D., Mawby, W. J., Karet, F. E., Saleem, M. A., Howie, A. J. and Toye, A. M. (2009). RhCG is the major putative ammonia transporter expressed in the human kidney, and RhBG is not expressed at detectable levels. *Am J Physiol Renal Physiol* **296**, F1279-90.

Chadwick, T. D. and Wright, P. A. (1999). Nitrogen excretion and expression of urea cycle enzymes in the atlantic cod (*Gadus morhua l.*): a comparison of early life stages with adults. *J Exp Biol* **202 (Pt 19)**, 2653-62.

Chang, W. J. and Hwang, P. P. (2011). Development of zebrafish epidermis. *Birth Defects Res C Embryo Today* **93**, 205-14.

Donini, A. and O'Donnell, M. J. (2005). Analysis of Na^+, Cl^-, K^+, H^+ and NH_4^+

concentration gradients adjacent to the surface of anal papillae of the mosquito *Aedes aegypti*: application of self-referencing ion-selective microelectrodes. *J Exp Biol* **208**, 603-10.

Eladari, D., Cheval, L., Quentin, F., Bertrand, O., Mouro, I., Cherif-Zahar, B., Cartron, J. P., Paillard, M., Doucet, A. and Chambrey, R. (2002). Expression of RhCG, a new putative NH_3/NH_4^+ transporter, along the rat nephron. *J Am Soc Nephrol* **13**, 1999-2008.

Endeward, V., Cartron, J. P., Ripoche, P. and Gros, G. (2006a). Red cell membrane CO_2 permeability in normal human blood and in blood deficient in various blood groups, and effect of DIDS. *Transfus Clin Biol* **13**, 123-7.

Endeward, V., Cartron, J. P., Ripoche, P. and Gros, G. (2008). RhAG protein of the Rhesus complex is a CO_2 channel in the human red cell membrane. *FASEB J* **22**, 64-73.

Endeward, V. and Gros, G. (2005). Low carbon dioxide permeability of the apical epithelial membrane of guinea-pig colon. *J Physiol* **567**, 253-65.

Endeward, V., Musa-Aziz, R., Cooper, G. J., Chen, L. M., Pelletier, M. F., Virkki, L. V., Supuran, C. T., King, L. S., Boron, W. F. and Gros, G. (2006b). Evidence that aquaporin 1 is a major pathway for CO_2 transport across the human erythrocyte membrane. *FASEB J* **20**, 1974-81.

Esaki, M., Hoshijima, K., Kobayashi, S., Fukuda, H., Kawakami, K. and Hirose, S. (2007). Visualization in zebrafish larvae of Na^+ uptake in mitochondria-rich cells whose differentiation is dependent on foxi3a. *Am J Physiol Regul Integr Comp Physiol* **292**, R470-80.

Esaki, M., Hoshijima, K., Nakamura, N., Munakata, K., Tanaka, M., Ookata, K., Asakawa, K., Kawakami, K., Wang, W., Weinberg, E. S. et al. (2009). Mechanism of development of ionocytes rich in vacuolar-type H^+-ATPase in the skin of zebrafish larvae. *Dev Biol* **329**, 116-29.

Esbaugh, A. J. and Tufts, B. L. (2006). The structure and function of carbonic anhydrase isozymes in the respiratory system of vertebrates. *Respir Physiol Neurobiol* **154**, 185-98.

Evans, D. H., Piermarini, P. M. and Choe, K. P. (2005). The multifunctional fish gill: dominant site of gas exchange, osmoregulation, acid-base regulation, and excretion of nitrogenous waste. *Physiol Rev* **85**, 97-177.

Gilmour, K. M. and Perry, S. F. (2009). Carbonic anhydrase and acid-base regulation in fish. *J Exp Biol* **212**, 1647-61.

Gilmour, K. M. and Perry, S. F. (2010). Gas transfer in dogfish: a unique model of CO_2 excretion. *Comp Biochem Physiol A Mol Integr Physiol* **155**, 476-85.

Gilmour, K. M., Thomas, K., Esbaugh, A. J. and Perry, S. F. (2009). Carbonic

anhydrase expression and CO_2 excretion during early development in zebrafish Danio rerio. *J Exp Biol* **212**, 3837-45.

Glover, C. N., Bucking, C. and Wood, C. M. (2013). The skin of fish as a transport epithelium: a review. *J Comp Physiol B*.

Gutknecht, J., Bisson, M. A. and Tosteson, F. C. (1977). Diffusion of carbon dioxide through lipid bilayer membranes: effects of carbonic anhydrase, bicarbonate, and unstirred layers. *J Gen Physiol* **69**, 779-94.

Han, K. H., Kim, H. Y. and Weiner, I. D. (2009a). Expression of rh glycoproteins in the Mammalian kidney. *Electrolyte Blood Press* **7**, 14-9.

Han, K. H., Mekala, K., Babida, V., Kim, H. Y., Handlogten, M. E., Verlander, J. W. and Weiner, I. D. (2009b). Expression of the gas-transporting proteins, Rh B glycoprotein and Rh C glycoprotein, in the murine lung. *Am J Physiol Lung Cell Mol Physiol* **297**, L153-63.

Handlogten, M. E., Hong, S. P., Zhang, L., Vander, A. W., Steinbaum, M. L., Campbell-Thompson, M. and Weiner, I. D. (2005). Expression of the ammonia transporter proteins Rh B glycoprotein and Rh C glycoprotein in the intestinal tract. *Am J Physiol Gastrointest Liver Physiol* **288**, G1036-47.

Henriksen, G. H., Bloom, A. J. and Spanswick, R. M. (1990). Measurement of net fluxes of ammonium and nitrate at the surface of barley roots using ion-selective microelectrodes. *Plant Physiol* **93**, 271-80.

Hirata, T., Kaneko, T., Ono, T., Nakazato, T., Furukawa, N., Hasegawa, S., Wakabayashi, S., Shigekawa, M., Chang, M. H., Romero, M. F. et al. (2003). Mechanism of acid adaptation of a fish living in a pH 3.5 lake. *Am J Physiol Regul Integr Comp Physiol* **284**, R1199-212.

Hiroi, J., Yasumasu, S., McCormick, S. D., Hwang, P. P. and Kaneko, T. (2008). Evidence for an apical Na-Cl cotransporter involved in ion uptake in a teleost fish. *J Exp Biol* **211**, 2584-2599.

Horng, J. L., Lin, L. Y., Huang, C. J., Katoh, F., Kaneko, T. and Hwang, P. P. (2007). Knockdown of V-ATPase subunit A (*atp6v1a*) impairs acid secretion and ion balance in zebrafish (*Danio rerio*). *Am J Physiol Regul Integr Comp Physiol* **292**, R2068-76.

Huang, C. H. and Peng, J. (2005). Evolutionary conservation and diversification of Rh family genes and proteins. *Proc Natl Acad Sci U S A* **102**, 15512-7.

Huang, C. H. and Ye, M. (2010). The Rh protein family: gene evolution, membrane biology, and disease association. *Cell Mol Life Sci* **67**, 1203-18.

Hung, C. Y., Tsui, K. N., Wilson, J. M., Nawata, C. M., Wood, C. M. and Wright, P. A. (2007). Rhesus glycoprotein gene expression in the mangrove killifish *Kryptolebias marmoratus* exposed to elevated environmental ammonia levels and air. *J*

Exp Biol **210**, 2419-29.

Hwang, P. P. (2009). Ion uptake and acid secretion in zebrafish (*Danio rerio*). *J Exp Biol* **212**, 1745-52.

Hwang, P. P. and Lee, T. H. (2007). New insights into fish ion regulation and mitochondrion-rich cells. *Comp Biochem Physiol A Mol Integr Physiol* **148**, 479-97.

Hwang, P. P., Lee, T. H. and Lin, L. Y. (2011). Ion Regulation in Fish Gills: Recent Progress in the Cellular and Molecular Mechanisms. *Am J Physiol Regul Integr Comp Physiol*.

Ip, Y. K. and Chew, S. F. (2010). Ammonia production, excretion, toxicity, and defense in fish: a review. *Front Physiol* **1**, 134.

Ip, Y. K., Loong, A. M., Kuah, J. S., Sim, E. W., Chen, X. L., Wong, W. P., Lam, S. H., Delgado, I. L., Wilson, J. M. and Chew, S. F. (2012). Roles of three branchial Na^+-K^+-ATPase alpha-subunit isoforms in freshwater adaptation, seawater acclimation, and active ammonia excretion in Anabas testudineus. *Am J Physiol Regul Integr Comp Physiol* **303**, R112-25.

Itel, F., Al-Samir, S., Oberg, F., Chami, M., Kumar, M., Supuran, C. T., Deen, P. M., Meier, W., Hedfalk, K., Gros, G. et al. (2012). CO_2 permeability of cell membranes is regulated by membrane cholesterol and protein gas channels. *FASEB J* **26**, 5182-91.

Ito, Y., Kobayashi, S., Nakamura, N., Miyagi, H., Esaki, M., Hoshijima, K. and Hirose, S. (2013). Close Association of Carbonic Anhydrase (CA2a and CA15a), Na^+/H^+ Exchanger (Nhe3b), and Ammonia Transporter Rhcg1 in Zebrafish Ionocytes Responsible for Na^+ Uptake. *Front Physiol* **4**, 59.

Ivanis, G., Esbaugh, A. J. and Perry, S. F. (2008). Branchial expression an localization of SLC9A2 and SLC9A3 sodium/hydrogen exchangers and their possible role in acid-base regulation in freshwater rainbow trout (*Oncorhynchus mykiss*). *J Exp Biol* **211**, 2467-2477.

Katoh, F., Hyodo, S. and Kaneko, T. (2003). Vacuolar-type proton pump in the basolateral plasma membrane energizes ion uptake in branchial mitochondria-rich cells of killifish *Fundulus heteroclitus*, adapted to a low ion environment. *J Exp Biol* **206**, 793-803.

Kerstetter, T. H., Kirschner, L. B. and Rafuse, D. D. (1970). On the mechanisms of sodium ion transport by the irrigated gills of rainbow trout (*Salmo gairdneri*). *J Gen Physiol* **56**, 342-59.

Khademi, S., O'Connell, J., 3rd, Remis, J., Robles-Colmenares, Y., Miercke, L. J. and Stroud, R. M. (2004). Mechanism of ammonia transport by Amt/MEP/Rh: structure of AmtB at 1.35 A. *Science* **305**, 1587-94.

Kikeri, D., Sun, A., Zeidel, M. L. and Hebert, S. C. (1989). Cell membranes

impermeable to NH_3. *Nature* **339**, 478-80.

Kirschner, L. B., Greenwald, L. and Kerstetter, T. H. (1973). Effect of amiloride on sodium transport across body surfaces of freshwater animals. *Am J Physiol* **224**, 832-7.

Krogh, A. (1938). The active absorption of ions in some freshwater animals. *J comp physiol A* **25**, 335-350.

Kumai, Y. and Perry, S. F. (2011). Ammonia excretion via Rhcg1 facilitates Na^+ uptake in larval zebrafish, *Danio rerio*, in acidic water. *Am J Physiol Regul Integr Comp Physiol*.

Laurent, P. and Dunel, S. (1980). Morphology of gill epithelia in fish. *Am J Physiol* **238**, R147-59.

Lee, H. W., Verlander, J. W., Bishop, J. M., Igarashi, P., Handlogten, M. E. and Weiner, I. D. (2009). Collecting duct-specific Rh C glycoprotein deletion alters basal and acidosis-stimulated renal ammonia excretion. *Am J Physiol Renal Physiol* **296**, F1364-75.

Lee, Y. C., Yan, J. J., Cruz, S. A., Horng, J. L. and Hwang, P. P. (2011). Anion exchanger 1b, but not sodium-bicarbonate cotransporter 1b, plays a role in transport functions of zebrafish H^+-ATPase-rich cells. *Am J Physiol Cell Physiol* **300**, C295-307.

Liao, B. K., Chen, R. D. and Hwang, P. P. (2009). Expression regulation of Na^+-K^+-ATPase alpha1-subunit subtypes in zebrafish gill ionocytes. *Am J Physiol Regul Integr Comp Physiol* **296**, R1897-906.

Lin, C. C., Lin, L. Y., Hsu, H. H., Thermes, V., Prunet, P., Horng, J. L. and Hwang, P. P. (2012). Acid secretion by mitochondrion-rich cells of medaka (*Oryzias latipes*) acclimated to acidic freshwater. *Am J Physiol Regul Integr Comp Physiol* **302**, R283-91.

Lin, L. Y., Horng, J. L., Kunkel, J. G. and Hwang, P. P. (2006). Proton pump-rich cell secretes acid in skin of zebrafish larvae. *Am J Physiol Cell Physiol* **290**, C371-8.

Lin, T. Y., Liao, B. K., Horng, J. L., Yan, J. J., Hsiao, C. D. and Hwang, P. P. (2008). Carbonic anhydrase 2-like a and 15a are involved in acid-base regulation and Na^+ uptake in zebrafish H^+-ATPase-rich cells. *Am J Physiol Cell Physiol* **294**, C1250-60.

Liu, Z., Peng, J., Mo, R., Hui, C. and Huang, C. H. (2001). Rh type B glycoprotein is a new member of the Rh superfamily and a putative ammonia transporter in mammals. *J Biol Chem* **276**, 1424-33.

Marini, A. M., Soussi-Boudekou, S., Vissers, S. and Andre, B. (1997). A family of ammonium transporters in *Saccharomyces cerevisiae*. *Mol Cell Biol* **17**, 4282-93.

Marini, A. M., Vissers, S., Urrestarazu, A. and Andre, B. (1994). Cloning and

expression of the MEP1 gene encoding an ammonium transporter in *Saccharomyces cerevisiae*. *EMBO J* **13**, 3456-63.

McDonald, D. G. and Millsgan, C. L. (1988). Sodium transporter in the brook trout, *Salvelinus fontinalis*: effects of prolonged low pH exposure in the presence and absence of aluminum. *Can J Fish Aauat Sci* **45**, 1606-1613.

Missner, A., Kugler, P., Antonenko, Y. N. and Pohl, P. (2008a). Passive transport across bilayer lipid membranes: Overton continues to rule. *Proc Natl Acad Sci U S A* **105**, E123; author reply E124.

Missner, A., Kugler, P., Saparov, S. M., Sommer, K., Mathai, J. C., Zeidel, M. L. and Pohl, P. (2008b). Carbon dioxide transport through membranes. *J Biol Chem* **283**, 25340-7.

Musa-Aziz, R., Chen, L. M. and Boron, W. F. (2007). The CO_2/NH_3 selectivity of AQP1, AQP4, and AQP5 and now it is affected by DIDS. *J Am Soc Nephrol* **18**.

Musa-Aziz, R., Chen, L. M., Pelletier, M. F. and Boron, W. F. (2009a). Relative CO_2/NH_3 selectivities of AQP1, AQP4, AQP5, AmtB, and RhAG. *Proc Natl Acad Sci U S A* **106**, 5406-11.

Musa-Aziz, R., Jiang, L., Chen, L. M., Behar, K. L. and Boron, W. F. (2009b). Concentration-dependent effects on intracellular and surface pH of exposing Xenopus oocytes to solutions containing NH_3/NH_4^+. *J Membr Biol* **228**, 15-31.

Nagami, G. T. (1988). Luminal secretion of ammonia in the mouse proximal tubule perfused in vitro. *J Clin Invest* **81**, 159-64.

Nakada, T., Hoshijima, K., Esaki, M., Nagayoshi, S., Kawakami, K. and Hirose, S. (2007a). Localization of ammonia transporter Rhcg1 in mitochondrion-rich cells of yolk sac, gill, and kidney of zebrafish and its ionic strength-dependent expression. *Am J Physiol Regul Integr Comp Physiol* **293**, R1743-53.

Nakada, T., Westhoff, C. M., Kato, A. and Hirose, S. (2007b). Ammonia secretion from fish gill depends on a set of Rh glycoproteins. *FASEB J* **21**, 1067-74.

Nakada, T., Westhoff, C. M., Yamaguchi, Y., Hyodo, S., Li, X., Muro, T., Kato, A., Nakamura, N. and Hirose, S. (2010). Rhesus glycoprotein p2 (Rhp2) is a novel member of the Rh family of ammonia transporters highly expressed in shark kidney. *J Biol Chem* **285**, 2653-64.

Nakhoul, N. L., Davis, B. A., Romero, M. F. and Boron, W. F. (1998). Effect of expressing the water channel aquaporin-1 on the CO_2 permeability of *Xenopus* oocytes. *Am J Physiol* **274**, C543-8.

Nakhoul, N. L. and Hamm, L. L. (2004). Non-erythroid Rh glycoproteins: a putative new family of mammalian ammonium transporters. *Pflugers Arch* **447**, 807-12.

Nawata, C. M., Hirose, S., Nakada, T., Wood, C. M. and Kato, A. (2010). Rh glycoprotein expression is modulated in pufferfish (*Takifugu rubripes*) during high

environmental ammonia exposure. *J Exp Biol* **213**, 3150-60.

Nawata, C. M., Hung, C. C., Tsui, T. K., Wilson, J. M., Wright, P. A. and Wood, C. M. (2007). Ammonia excretion in rainbow trout (*Oncorhynchus mykiss*): evidence for Rh glycoprotein and H^+-ATPase involvement. *Physiol Genomics* **31**, 463-74.

Parks, S. K., Tresguerres, M. and Goss, G. G. (2008). Theoretical considerations underlying Na^+ uptake mechanisms in freshwater fishes. *Comp Biochem Physiol C Toxicol Pharmacol* **148**, 411-8.

Payan, P. (1978). A study of the Na^+/NH_4^+ exchange across the gill of perfused head of the trout (*Salmo gairdneri*). *J Comp Physiol* **124**, 181-188.

Prasad, G. V., Coury, L. A., Finn, F. and Zeidel, M. L. (1998). Reconstituted aquaporin 1 water channels transport CO_2 across membranes. *J Biol Chem* **273**, 33123-6.

Purkerson, J. M. and Schwartz, G. J. (2007). The role of carbonic anhydrases in renal physiology. *Kidney Int* **71**, 103-15.

Quentin, F., Eladari, D., Cheval, L., Lopez, C., Goossens, D., Colin, Y., Cartron, J. P., Paillard, M. and Chambrey, R. (2003). RhBG and RhCG, the putative ammonia transporters, are expressed in the same cells in the distal nephron. *J Am Soc Nephrol* **14**, 545-54.

Randall, D. J. and Ip, Y. K. (2006). Ammonia as a respiratory gas in water and air-breathing fishes. *Respir Physiol Neurobiol* **154**, 216-25.

Randall, D. J. and Tsui, T. K. (2006). Tribute to R. G. Boutilier: acid-base transfer across fish gills. *J Exp Biol* **209**, 1179-84.

Randall, D. J., Wilson, J. M., Peng, K. W., Kok, T. W., Kuah, S. S., Chew, S. F., Lam, T. J. and Ip, Y. K. (1999). The mudskipper, Periophthalmodon schlosseri, actively transports NH_4^+ against a concentration gradient. *Am J Physiol* **277**, R1562-7.

Ripoche, P., Bertrand, O., Gane, P., Birkenmeier, C., Colin, Y. and Cartron, J. P. (2004). Human Rhesus-associated glycoprotein mediates facilitated transport of NH_3 into red blood cells. *Proc Natl Acad Sci U S A* **101**, 17222-7.

Salama, A., Morgan, I. J. and Wood, C. M. (1999). The linkage between Na^+ uptake and ammonia excretion in rainbow trout: kinetic analysis, the effects of $(NH_4)_2SO_4$ and NH_4HCO_3 infusion and the influence of gill boundary layer pH. *J Exp Biol* **202 (Pt 6)**, 697-709.

Seshadri, R. M., Klein, J. D., Kozlowski, S., Sands, J. M., Kim, Y. H., Han, K. H., Handlogten, M. E., Verlander, J. W. and Weiner, I. D. (2006). Renal expression of the ammonia transporters, Rhbg and Rhcg, in response to chronic metabolic acidosis. *Am J Physiol Renal Physiol* **290**, F397-408.

Shen, W. P., Horng, J. L. and Lin, L. Y. (2011). Functional plasticity of

mitochondrion-rich cells in the skin of euryhaline medaka larvae (*Oryzias latipes*) subjected to salinity changes. *Am J Physiol Regul Integr Comp Physiol* **300**, R858-68.

Shih, T. H., Horng, J. L., Hwang, P. P. and Lin, L. Y. (2008). Ammonia excretion by the skin of zebrafish (*Danio rerio*) larvae. *Am J Physiol Cell Physiol* **295**, C1625-32.

Shih, T. H., Horng, J. L., Liu, S. T., Hwang, P. P. and Lin, L. Y. (2012). Rhcg1 and NHE3b are involved in ammonium-dependent sodium uptake by zebrafish larvae acclimated to low-sodium water. *Am J Physiol Regul Integr Comp Physiol* **302**, R84-93.

Verlander, J. W., Miller, R. T., Frank, A. E., Royaux, I. E., Kim, Y. H. and Weiner, I. D. (2003). Localization of the ammonium transporter proteins RhBG and RhCG in mouse kidney. *Am J Physiol Renal Physiol* **284**, F323-37.

Waisbren, S. J., Geibel, J. P., Modlin, I. M. and Boron, W. F. (1994). Unusual permeability properties of gastric gland cells. *Nature* **368**, 332-5.

Wang, Y. F., Tseng, Y. C., Yan, J. J., Hiroi, J. and Hwang, P. P. (2009). Role of SLC12A10.2, a Na-Cl cotransporter-like protein, in a Cl uptake mechanism in zebrafish (*Danio rerio*). *Am J Physiol Regul Integr Comp Physiol* **296**, R1650-60.

Weihrauch, D., Chan, A. C., Meyer, H., Doring, C., Sourial, M. and O'Donnell, M. J. (2012a). Ammonia excretion in the freshwater planarian Schmidtea mediterranea. *J Exp Biol* **215**, 3242-53.

Weihrauch, D., Donini, A. and O'Donnell, M. J. (2012b). Ammonia transport by terrestrial and aquatic insects. *J Insect Physiol* **58**, 473-87.

Weihrauch, D., Wilkie, M. P. and Walsh, P. J. (2009). Ammonia and urea transporters in gills of fish and aquatic crustaceans. *J Exp Biol* **212**, 1716-30.

Weiner, I. D. and Hamm, L. L. (2007). Molecular mechanisms of renal ammonia transport. *Annu Rev Physiol* **69**, 317-40.

Weiner, I. D. and Verlander, J. W. (2011). Role of NH_3 and NH_4^+ transporters in renal acid-base transport. *Am J Physiol Renal Physiol* **300**, F11-23.

Wilkie, M. P. (2002). Ammonia excretion and urea handling by fish gills: present understanding and future research challenges. *J Exp Zool* **293**, 284-301.

Wilkie, M. P. and Wood, C. M. (1994). The effects of extremely alkaline water (pH 9.5) on rainbow trout gill function and morphology. *J Fish Biol* **45**, 87-98.

Wilson, J. M. and Laurent, P. (2002). Fish gill morphology: inside out. *J Exp Zool* **293**, 192-213.

Wilson, J. M., Randall, D. J., Donowitz, M., Vogl, A. W. and Ip, A. K. (2000). Immunolocalization of ion-transport proteins to branchial epithelium mitochondria-rich cells in the mudskipper (*Periophthalmodon schlosseri*). *J Exp Biol* **203**, 2297-310.

Wilson, R. W., Wright, P. M., Munger, S. and Wood, C. M. (1994). Ammonia excretion in freshwater rainbow trout (*Oncorhynchus mykiss*) and the importance of gill

boundary layer acidification : lack of evidence for Na^+/NH_4^+ exchange. *J Exp Biol* **191**, 37-58.

Wood, C. M. and Nawata, C. M. (2011). A nose-to-nose comparison of the physiological and molecular responses of rainbow trout to high environmental ammonia in seawater versus freshwater. *J Exp Biol* **214**, 3557-69.

Wright, P., Felskie, A. and Anderson, P. (1995). Induction of ornithine-urea cycle enzymes and nitrogen metabolism and excretion in rainbow trout (*Oncorhynchus mykiss*) during early life stages. *J Exp Biol* **198**, 127-35.

Wright, P. A., Randall, D. J. and Perry, S. F. (1989). Fish gill water boundary layer: a site of linkage between carbon dioxide and ammonia excretion. . *J Comp Physiol* **158**, 627-635.

Wright, P. A. and Wood, C. M. (1985). An analysis of branchial ammonia excretion in the freshwater rainbow trout: effects of environmental pH change and sodium uptake blockage. *J Exp Biol* **114**, 329-353.

Wright, P. A. and Wood, C. M. (2009). A new paradigm for ammonia excretion in aquatic animals: role of Rhesus (Rh) glycoproteins. *J Exp Biol* **212**, 2303-12.

Wu, S. C., Horng, J. L., Liu, S. T., Hwang, P. P., Wen, Z. H., Lin, C. S. and Lin, L. Y. (2010). Ammonium-dependent sodium uptake in mitochondrion-rich cells of medaka (*Oryzias latipes*) larvae. *Am J Physiol Cell Physiol* **298**, C237-50.

Yan, J. J., Chou, M. Y., Kaneko, T. and Hwang, P. P. (2007). Gene expression of Na^+/H^+ exchanger in zebrafish H^+-ATPase-rich cells during acclimation to low-Na^+ and acidic environments. *Am J Physiol Cell Physiol* **293**, C1814-23.

Tables and Figures

Table. 1. Morpholino (MO) sequence

Gene	Sequence
Rhbg	5’-CATGGCACTCTCCTTTGCTCACTCT-3’
Rhcg1	5’-CAGTTGCCCATGTCTACAGCTTGAG-3’
nhe3b	5’-AGTAGAAAACGCCATATCAGAACGC-3’
atp6v1a	5’-ATCCATCTTGTGTGTTAGAAAACTG-3’
foxi3a	5’- TCTTCCCGTTTCTCTTTGTTGAAGG -3’
foxi3b	5’- CTCGATCCTGAGGGTGCTCCAGTTG -3’
control	5’-CCTCTTACCTCAGTTACAATTTATA-3’

Table. 2. Primer sets for qPCR

Gene		Primer Sequence
Rhbg	F	5 -GCTCAAACAAAGGGTGGC- 3'
	R	5'-TGCGTGCTCACTTCGTTTAG-3'
Rhcg1	F	5’-TGCCAACTGTCCAGGGTG-3’
	R	5’-AGGATAAGACGGGAGGAATAAT-3’
NHE3b	F	5’-TGCAGACAGCGCCTCTAGC-3’
	R	5’-TGTGGCCTGTCTCTGTTTGC-3’
atp6v1a	F	5’-GAGGAACCACTGCCATTCCA-3’
	R	5’-CAACCCACATAAATGATGACATCG-3’
rpl13a	F	5’-CCTCGGTCGTCTTTCCGCTATTG-3’
	R	5’-CAGCCTGACCCCTCTTGGTTTTG-3’

Table. 3. Survival rate of Rh MO

	1 ng	2 ng	4 ng
Ctrl	83.5%	92.9%	89.5%
Rhbg MO	80.1%	76.9%	18.0%
Rhcg1 MO	90.2%	94.1%	81.0%

Chapter 1

Rhcg1 regulate ammonia excretion in the skin of zebrfish larvae: evidence of active ammonia excretion by HR cell

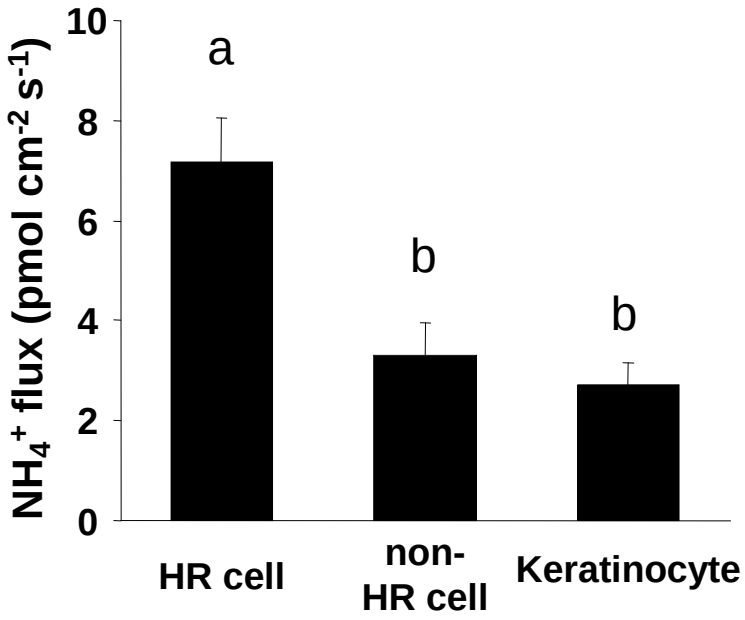

Fig. 1-1. NH_4^+ fluxes at H^+ pump-rich cells (HR cells), keratinocytes and other ionocytes (non-HR cell). NH_4^+ effluxes (means ± SE, *n*=11, 9, and 13, respectively) from different types of cells in the 4 days-post-fertilized(dpf) zebrafish larvae were compared. Different letters indicate a significant difference (one-way ANOVA, Tukey's comparison $p<0.05$).

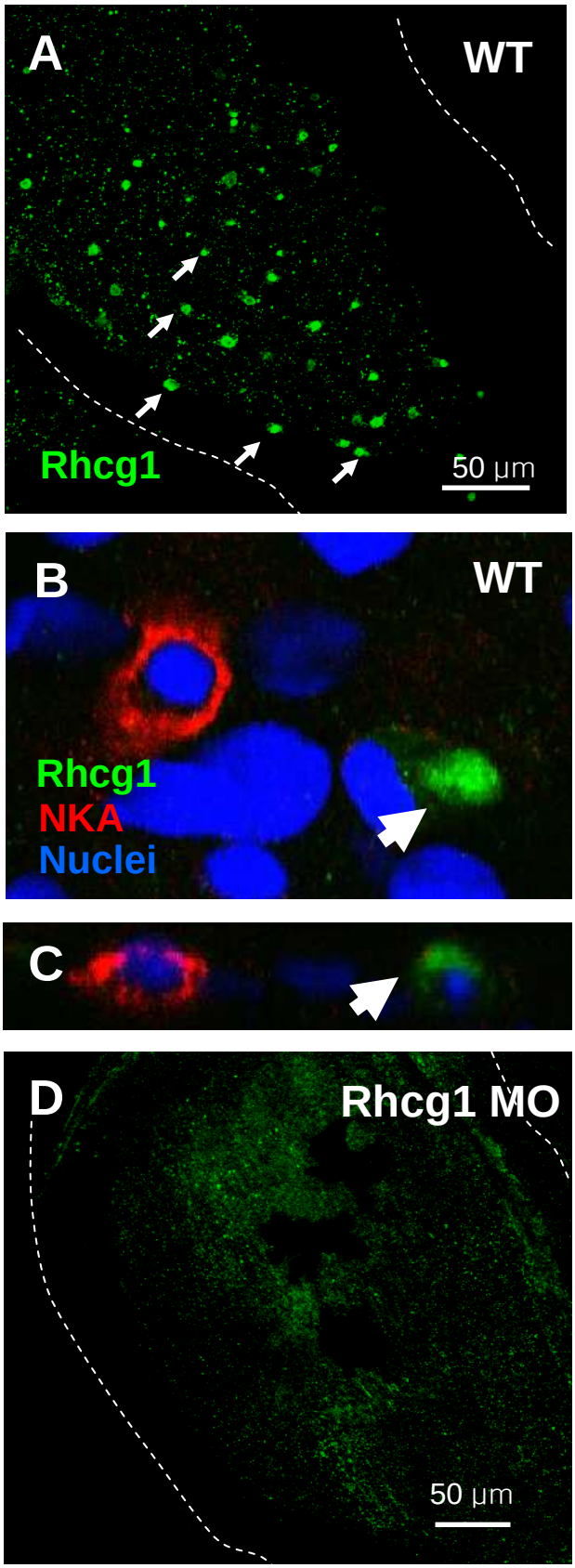

Fig. 1-2. Expression of Rhcg1 in the skin of zebrafish larvae. Immunohistochemistry analysis of Rhcg1 (arrow) in wildtype (WT) larvae (*A-C*) and *Rhcg1* morpholino (MO)-injected larvae (D). Na^+-K^+-ATPase (NKA) and DAPI were used to identify NaR cell and nucleus, respectively (*B,C*). All larvae were analyzed at 4dpf.

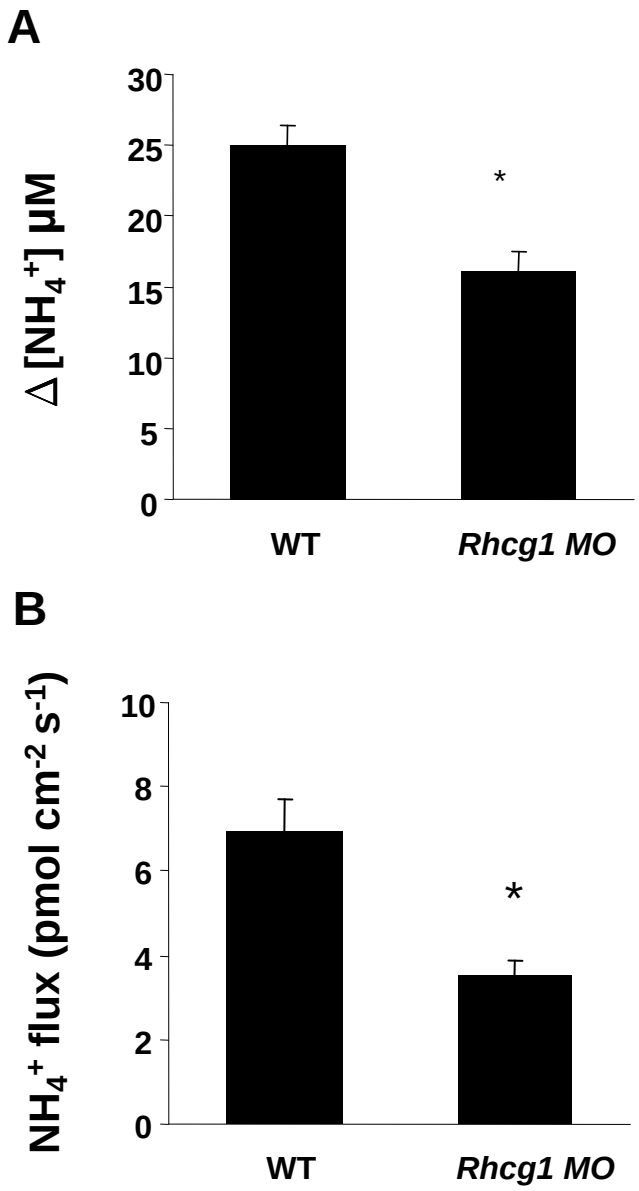

Fig. 1-3. Ammonia gradient ($\triangle NH_4^+$)(*A*) and HR cell NH_4^+ flux (*B*) of WT and *Rhcg1* MO larvae. Data are presented as the mean ± SE (*n* = 10 in (A); *n* = 13 for WT and 17 for *Rhcg1* MO in (*B*)). All larvae were analyzed at 4dpf *Significant difference between WT and *Rhcg1* MO-injected larvae (by Student's *t*-test, $p<0.05$).

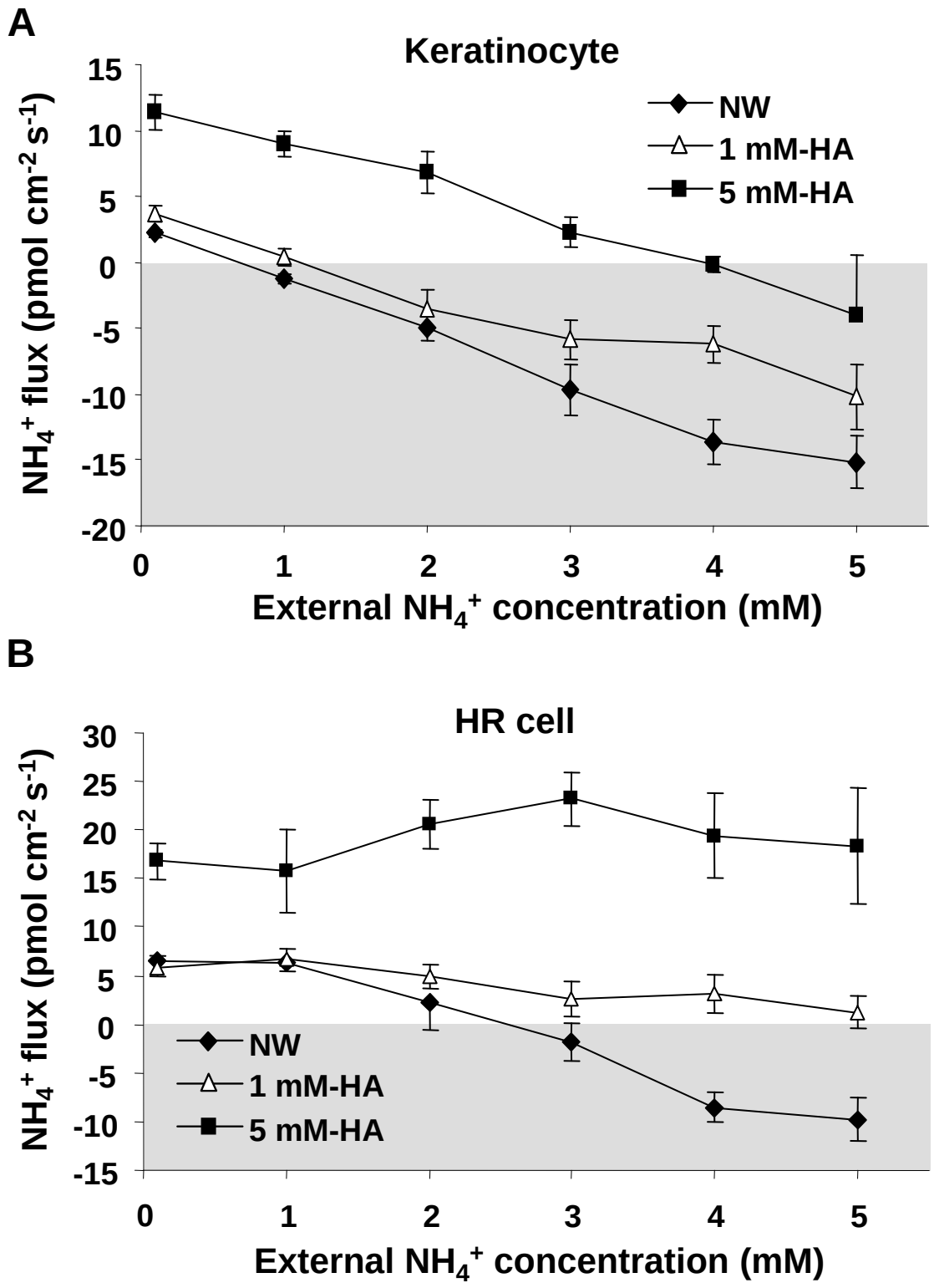

Fig. 1-4. The NH_4^+ flux of keratinocytes (*A*) and HR cells (*B*) in larvae immersed in various external NH_4^+ concentrations (0.1, 1, 2, 3, 4, and 5 mM). Three groups of larvae acclimated to normal water (NW), 1 mM NH_4^+ (1 mM-HA) or 5 mM NH_4^+ (5 mM-HA) for 4 days were compared. Data are presented as the mean ± SE (*n* = 8 cells).

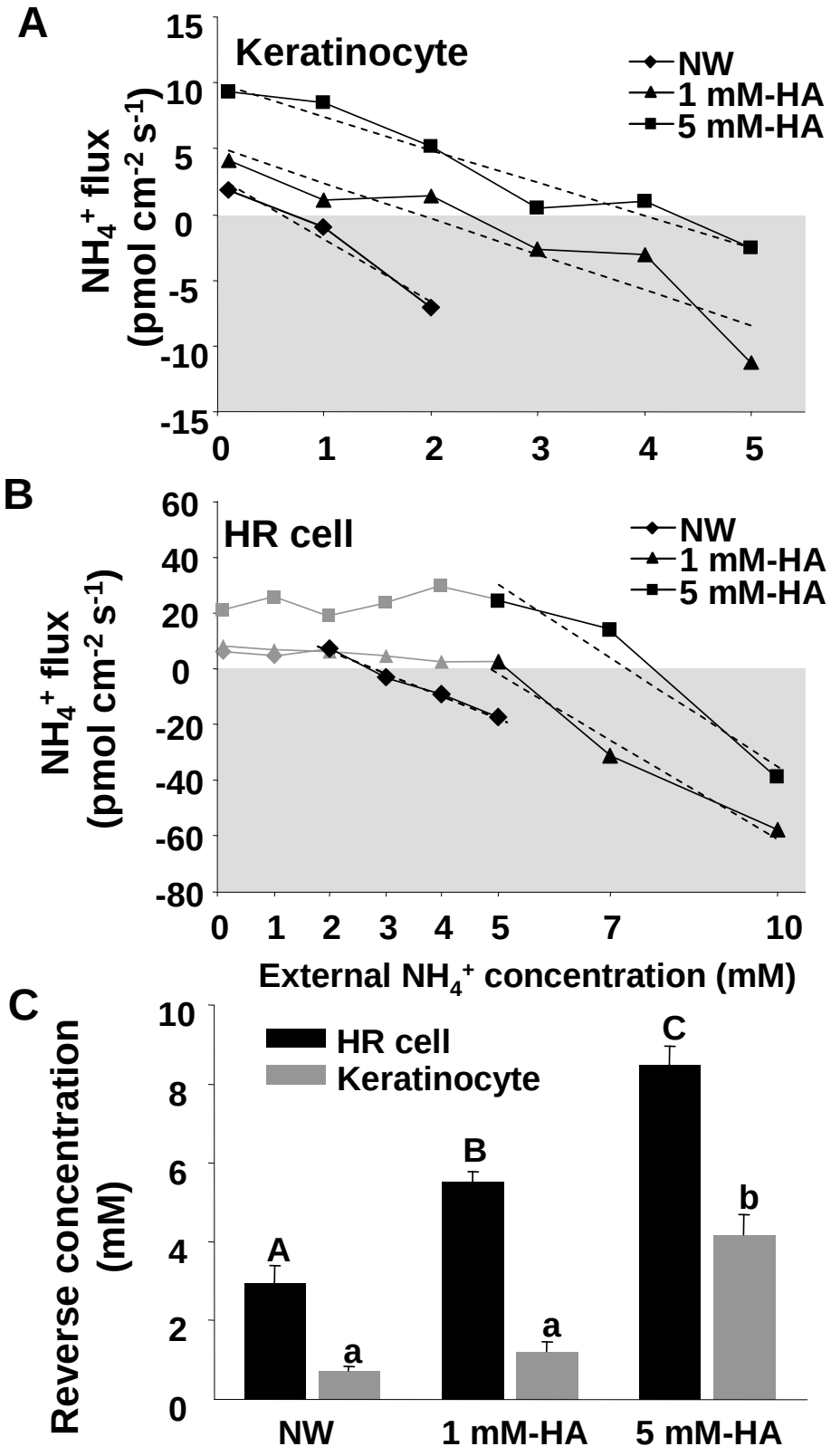

Fig. 1-5. The reverse concentration (RC) of keratinocytes (*A*) and HR cells (*B*) in larvae acclimated to normal water (NW), 1 mM NH_4^+ (1 mM-HA), and 5 mM-HA. The dashed line shows the regression of the measured curves. RCs were derived from the intercept of the regression line and x-axis. (*C*) RCs of keratinocytes and HR cells were compared (n = 8 cells in each group). All larvae were measured at 4 dpf. Data are presented as the mean ± SE. $^{A, B, C}$ or $^{a, b, c}$ Different letters indicate a significant difference among HR cells (capital letters) and keratinocytes (lowercase letters) (one-way ANOVA and Tukey's comparison, $p < 0.05$).

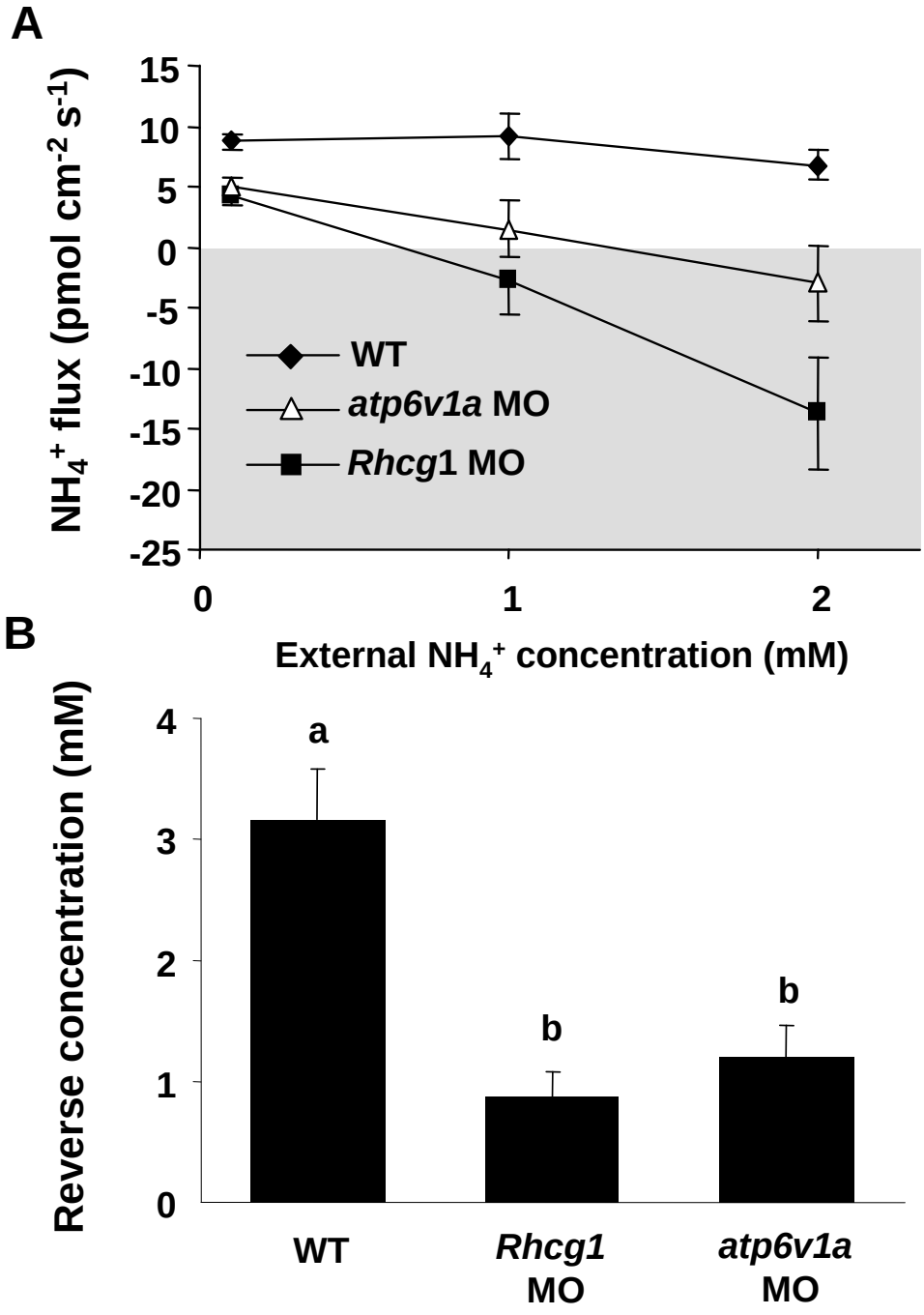

Fig. 1-6. The NH_4^+ flux (*A*) and reverse concentration (RC) (*B*) of HR cells in *Rhcg1* and *atp6v1a* morphants at 4 dpf. Data are presented as the mean ± SE. [a,b]Different letters indicate a significant difference (one-way ANOVA and Tukey's comparison, $p < 0.05$).

Chapter 2

Rhcg1 and NHE3b are involved in ammonium-dependent sodium uptake by zebrafish larvae acclimated to low-sodium water

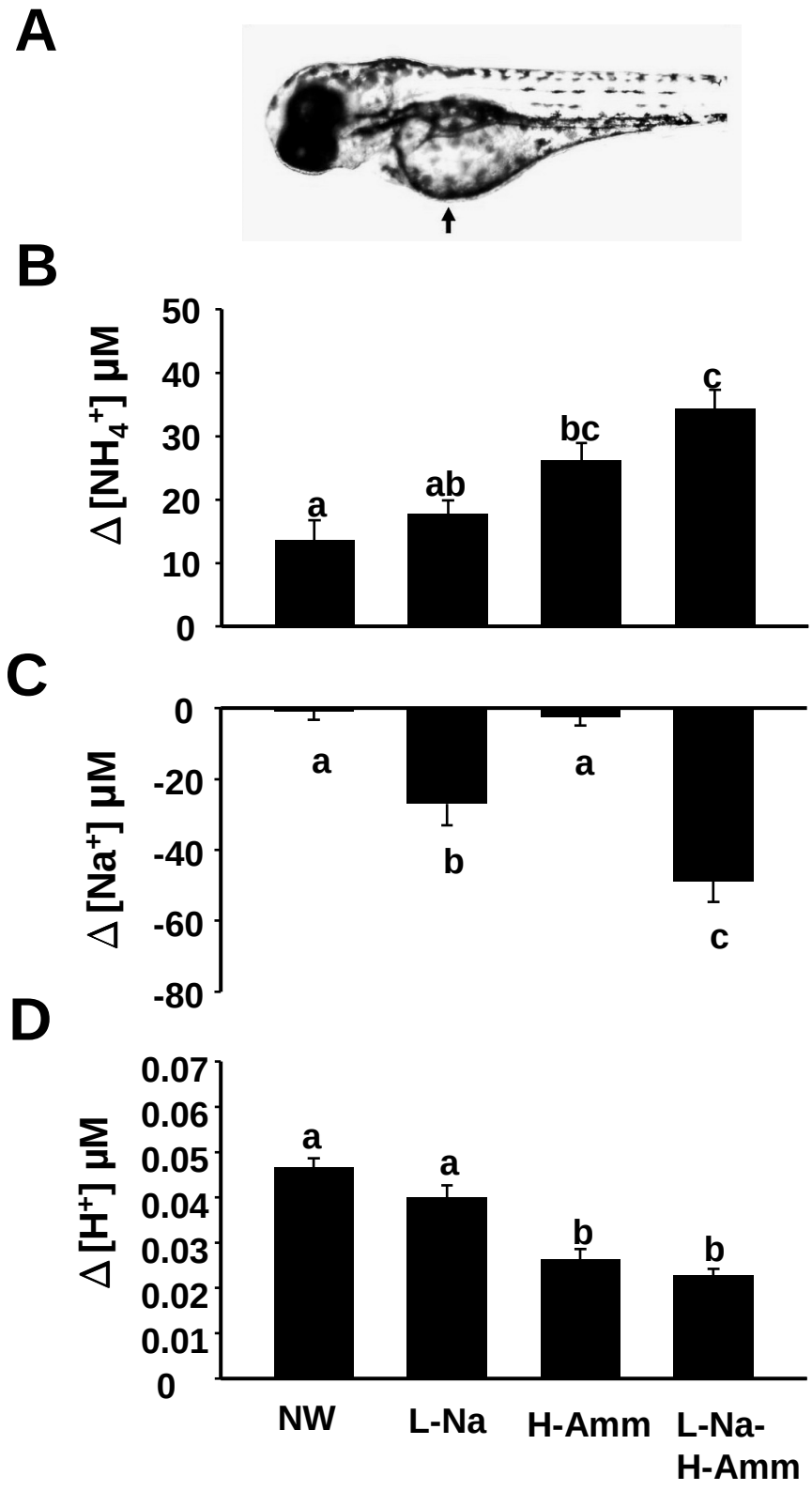

Fig. 2-1. *A*: Measurement of ionic gradients at yolksac surface of a 4 dpf zebrafish larva. The ion-selective probe was moved to location (arrow) to record the yolksac ionic concentrations. *B-D*: Ionic gradients ($\triangle[NH_4^+]$, $\triangle[Na^+]$, and $\triangle[H^+]$) at the yolk sac surface of larvae acclimated to normal water (NW), low-Na^+ water (L-Na), high ammonium water (H-Amm), or L-Na- H-Amm water. Data are presented as the mean ± SE (*n* = 10 larvae). Different letters indicate a significant difference (by one-way ANOVA and Tukey's comparison, $p < 0.05$).

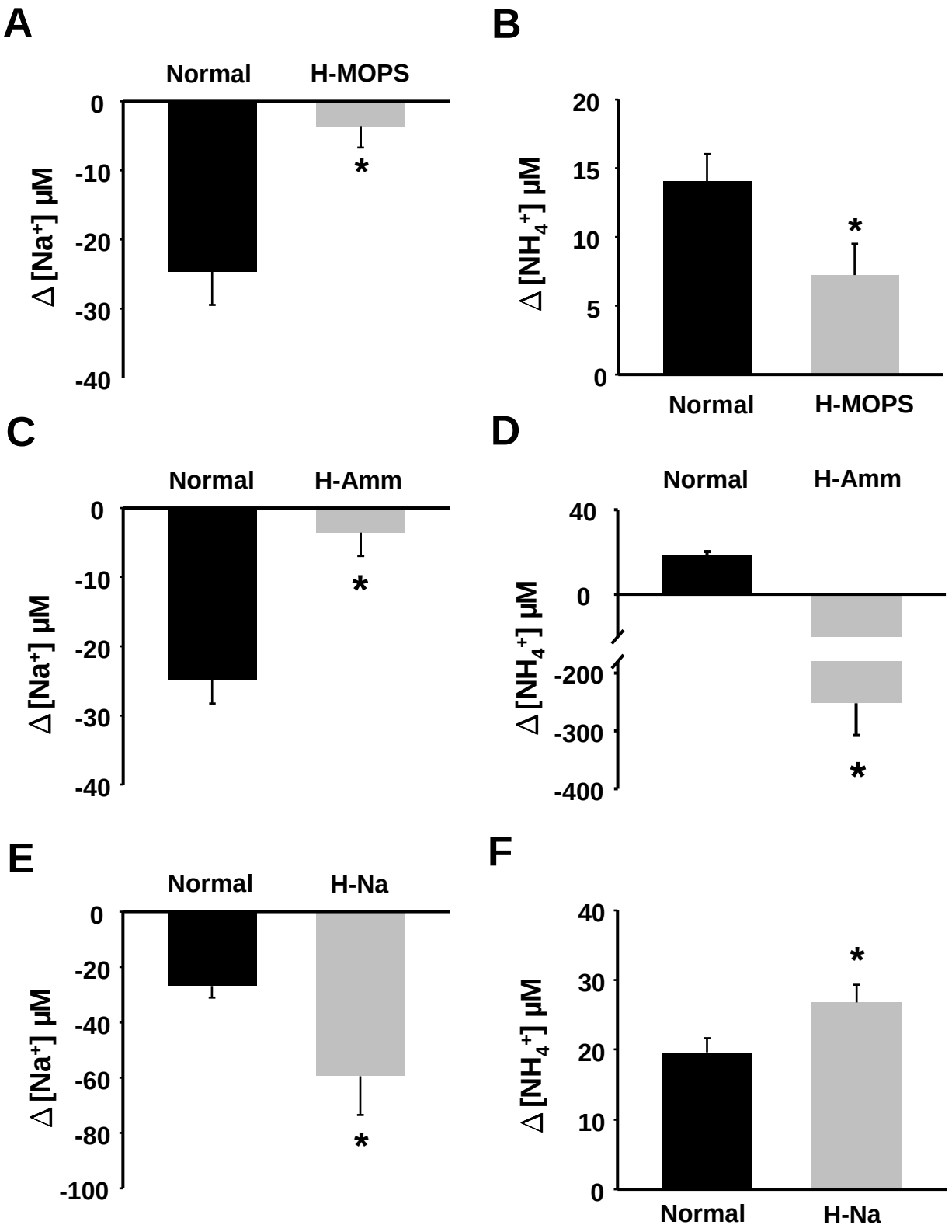

Fig. 2-2. Acute effects of external media on $\triangle[Na^+]$ (*A, C, E*) and $\triangle[NH_4^+]$ (*B, D, F*) at the yolk sac surface of low-Na^+ (L-Na) larvae (acclimated for 4 days). Larvae were measured in the following recording media: Normal (control), high-MOPS (H-MOPS, 5 mM), high-ammonium (H-Amm, 5 mM NH_4^+), and high Na^+ (H-Na, 10 mM Na^+). Data are presented as the mean ± SE (*n* = 10 larvae). All larvae were analyzed at 4dpf *Significant difference between the two groups (by Student's *t*-test, $p < 0.05$).

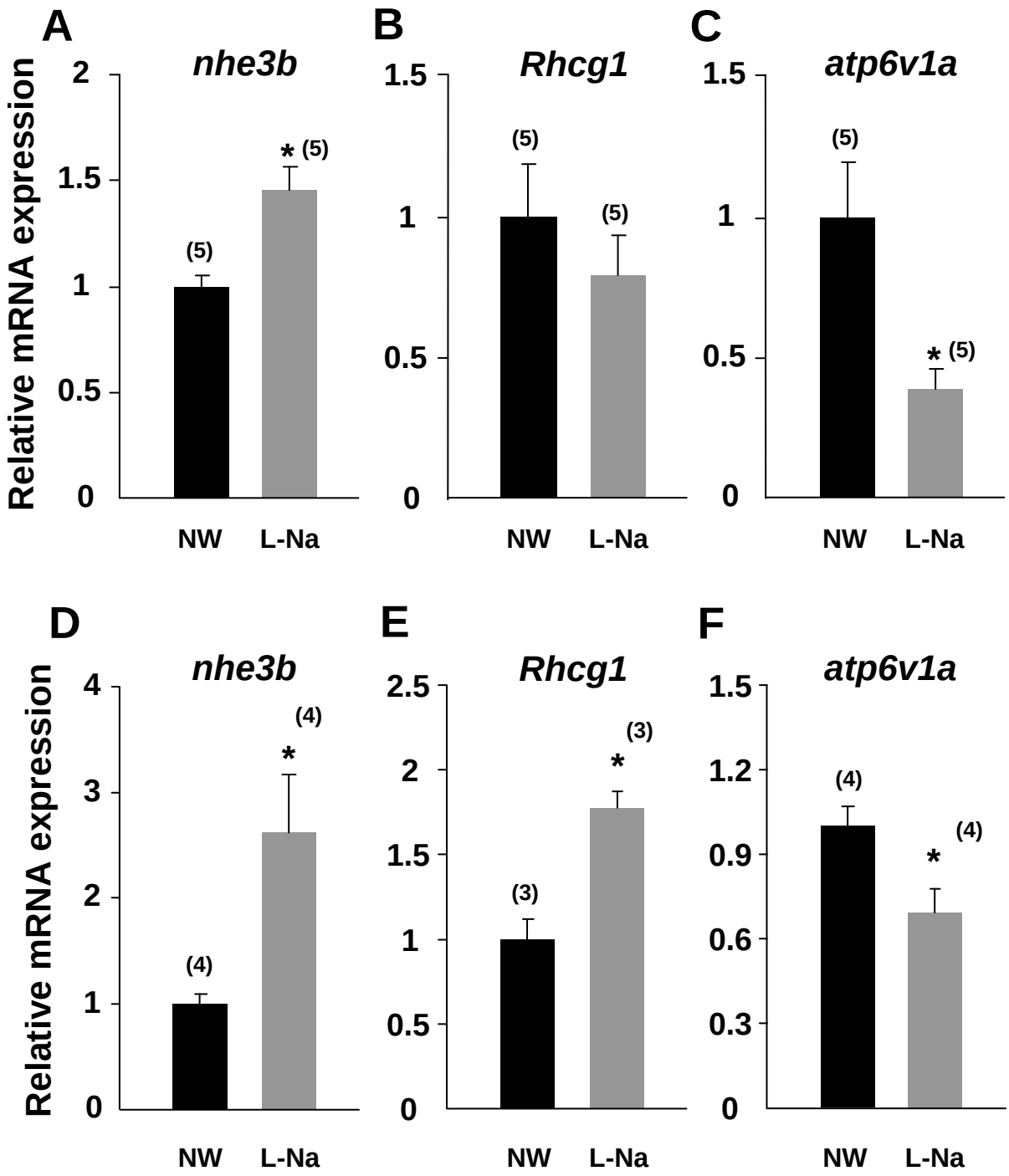

Fig. 2-3. Real-time PCR analysis of *nhe3b, Rhcg1,* and *atp6v1a* expressions in whole larvae (*A-C*; 4 dpf) and adult gills (*D-F*) of zebrafish acclimated to normal water (NW) and low-Na^+ (L-Na) water. Data are presented as the mean ± SE (the number of sample is shown in parentheses). *Significant difference between the NW and L-Na groups (by Student's *t*-test, $p < 0.05$).

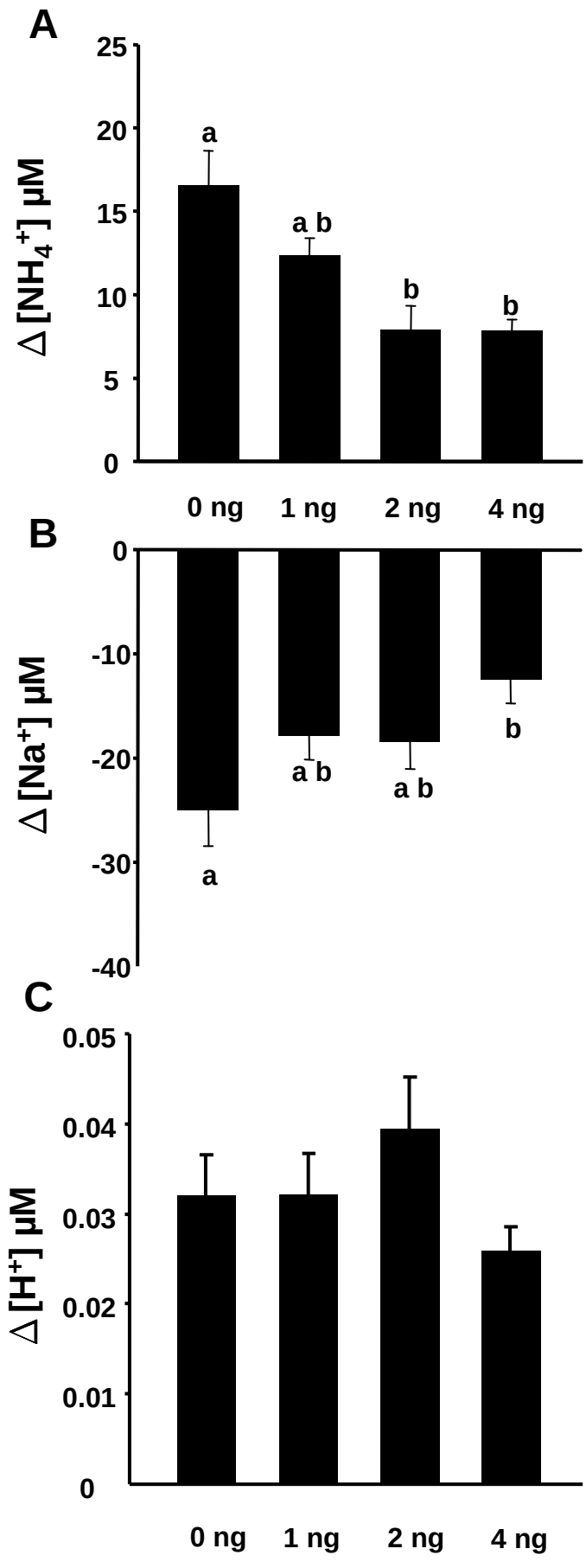

Fig. 2-4. Effects of *Rhcg1* knockdown on Na^+ uptake, NH_4^+ and H^+ excretion by zebrafish larvae. $\Delta[NH_4^+]$ (*A*), $\Delta[Na^+]$ (*B*) and $\Delta[H^+]$ (*C*) at the yolk sac surface of wild-type (WT; 0 ng) and 1~4 ng *Rhcg1* morpholino (MO)-injected larvae. The WT and MO-injected larvae were acclimated to low-Na^+ (L-Na) water and measured at 4 dpf. Data are presented as the mean ± SE (*n* = 10 larvae). Different letters indicate a significant difference (by one-way ANOVA and Tukey's comparison, $p < 0.05$).

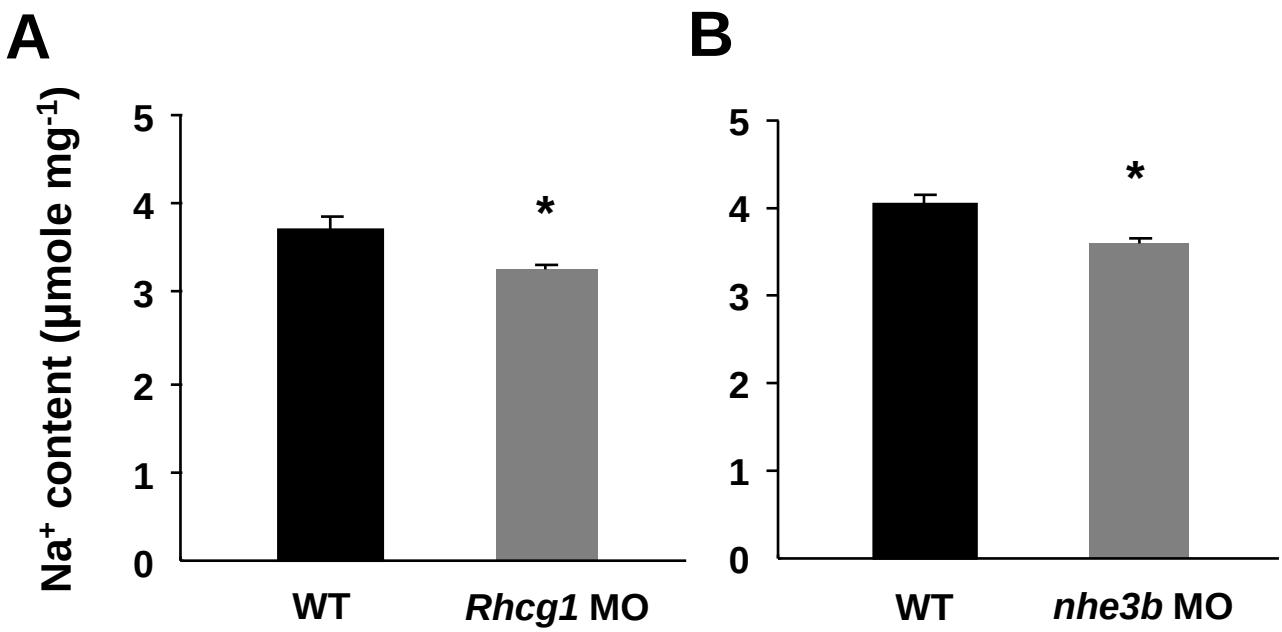

Fig. 2-5. Whole-body Na^+ content in zebrafish larvae acclimated to L-Na with *Rhcg1* (*A*) or *nhe3b* (*B*) knockdown. Data are presented as the mean ± SE (n = 6). All larvae were analyzed at 4 dpf. *Significant difference between the WT and MO (by Student's t-test, $p < 0.05$).

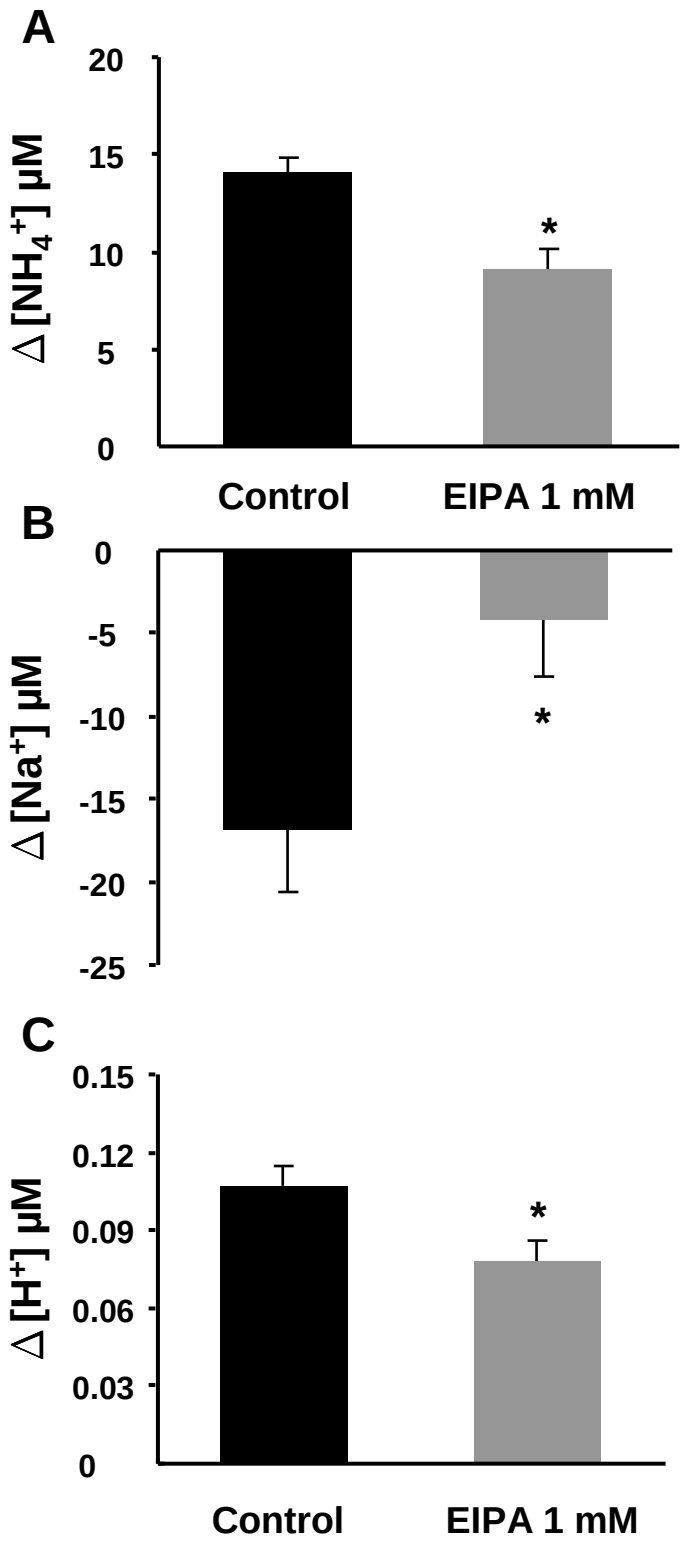

Fig. 2-6. Effects of EIPA (1 mM) on Na^+ uptake and NH_4^+ excretion by zebrafish larvae. $\triangle[NH_4^+]$ (*A*), $\triangle[Na^+]$ (*B*), and $\triangle[H^+]$ (*C*) at the yolk sac surface of L-Na larvae. The same concentration of solvent (DMSO) was added to L-Na water as a control. Data are presented as the mean ± SE (*n* = 10 larvae). All larvae were analyzed at 4 dpf. * Significant difference between Control and EIPA groups (by Student's *t*-test, $p < 0.05$).

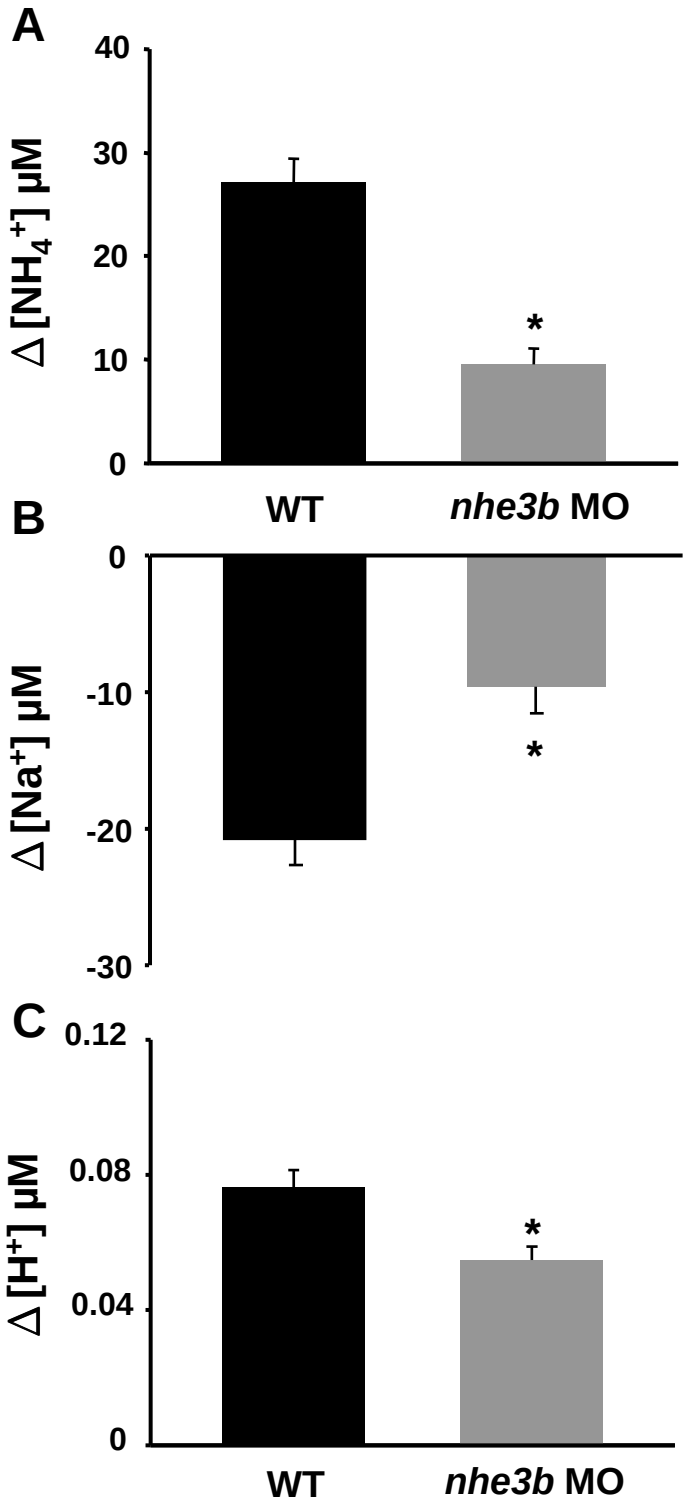

Fig. 2-7. Effects of *nhe3b* knockdown on Na^+ uptake and NH_4^+ excretion by zebrafish larvae. $\triangle[NH_4^+]$ (*A*), $\triangle[Na^+]$ (*B*), and $\triangle[H^+]$ (*C*) at the yolk sac surface of wild-type (WT) and 4 ng *NHE3b* morpholino (MO)-injected larvae. The WT and MO-injected larvae were acclimated to low-Na^+ (L-Na) water and measured at 4 dpf. Data are presented as the mean ± SE (n = 10 larvae). *Significant difference between WT and MO (by Student's t-test, $p < 0.05$).

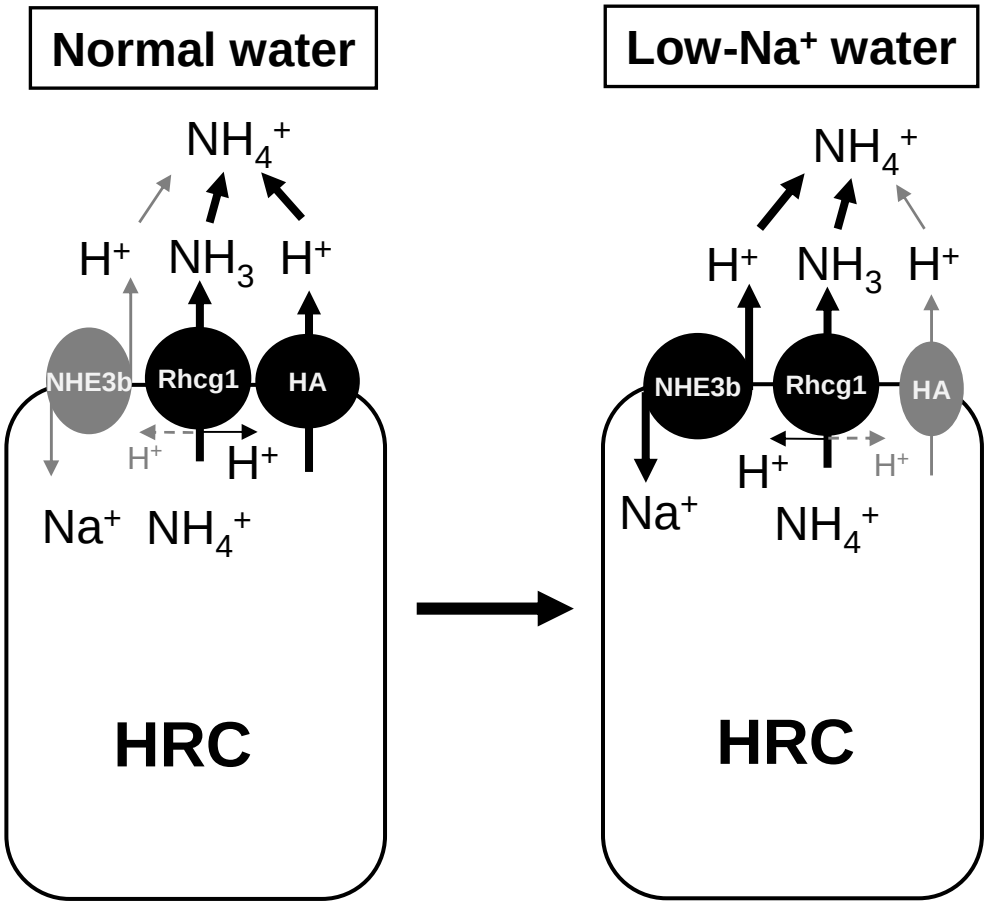

Fig. 2-8. Proposed model of NH_4^+-dependent Na^+ uptake in H^+-pump-rich (HR) cells of zebrafish larvae. H+-ATPase (HA), NHE3b, and Rhcg1 are located in apical membranes of HR cells. Both H^+-ATPase and NHE3b contribute to H^+ secretion and facilitate non-ionic NH_3 diffusion across Rhcg1. Rhcg1 promotes the dissociation of H+ from NH_4^+, and the accumulated H^+ gradient drives the Na^+/H^+ exchange via NHE3b. In water with a low-Na^+ level, H+-ATPase is downregulated, and NHE3b is upregulated to achieve NH_4^+-dependent Na^+ uptake.

Chapter 3

Rhbg mediate ammonia excretion by keratinocyte in the skin of zebrafish larvae

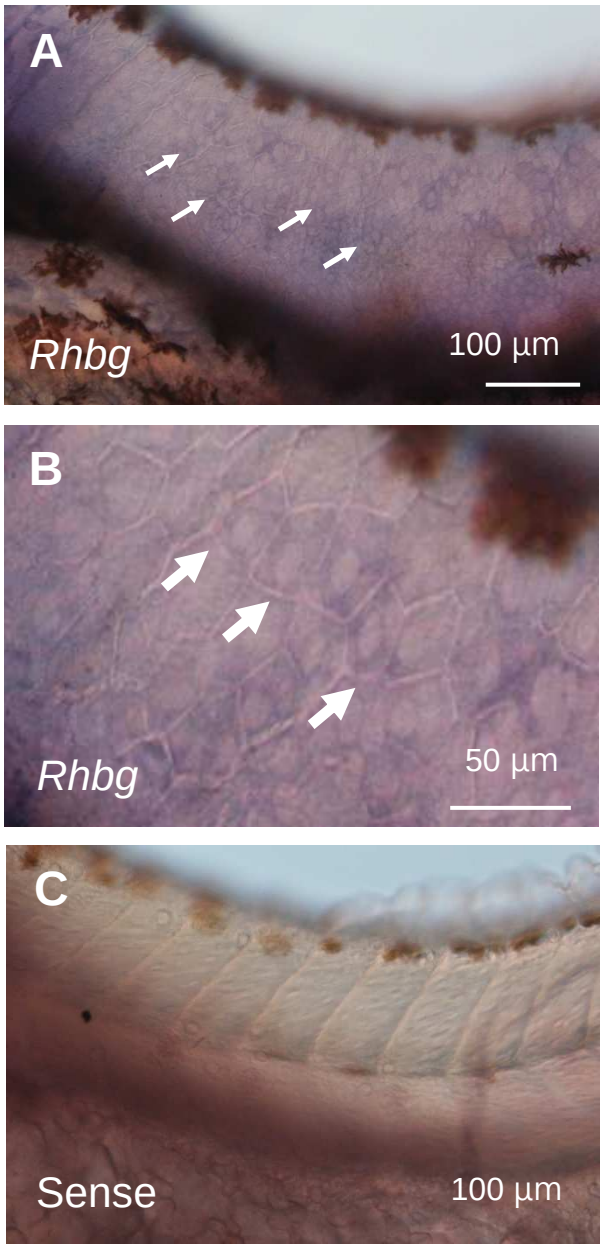

Fig. 3-1. Whole-mount *in situ* hybridization of Rhbg in 3 dpf larvae. The *Rhbg* antisense probe is labeled on polygonal keratinocytes (arrows, purple signal) covering the larval surface (*A*, *B*). The *Rhbg* sense probe was used as a negative control (*C*).

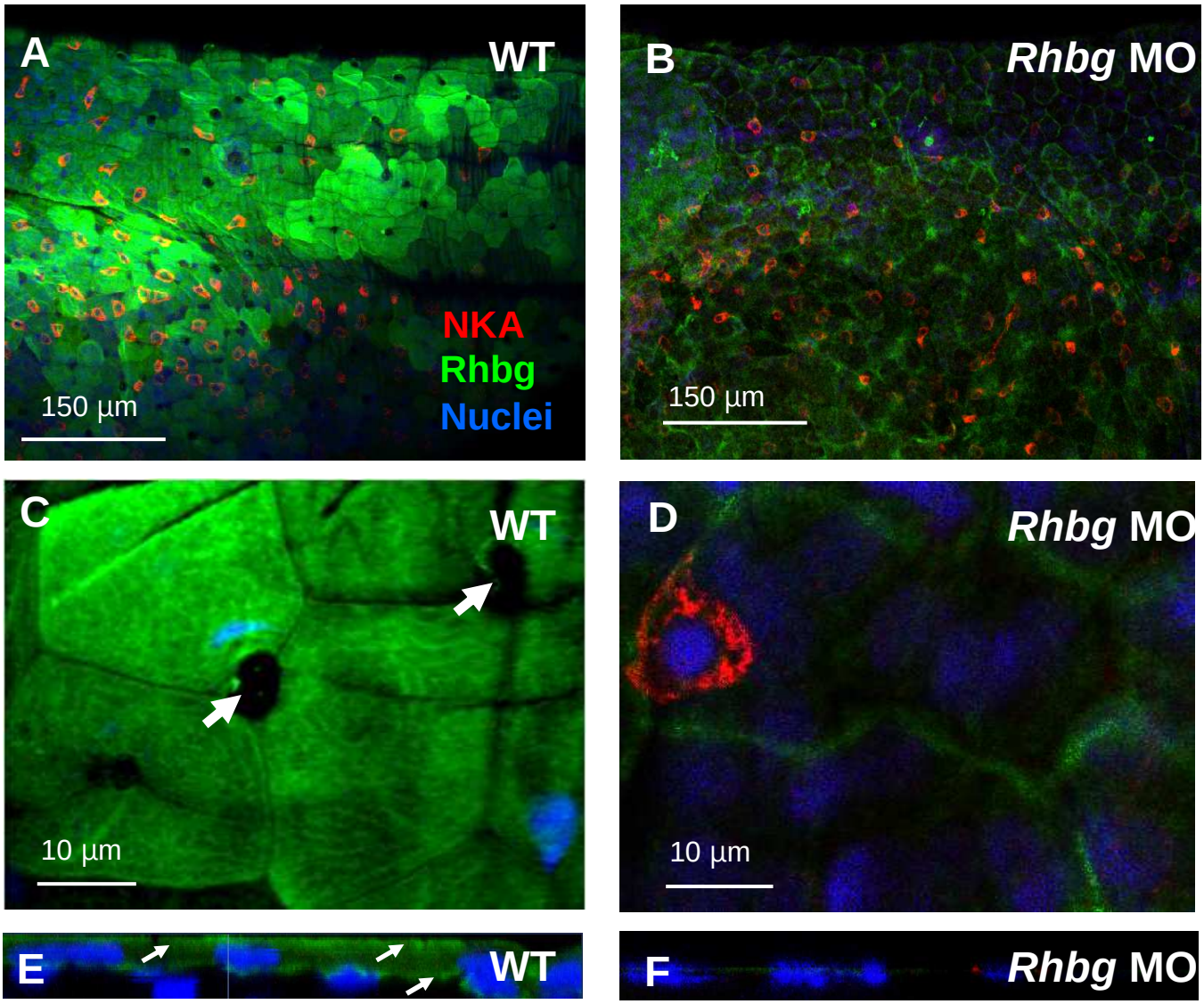

Fig. 3-2. Confocal microscopic images of the immunohistochemistry in wild-type (WT; *A, C, E*) and *Rhbg* morphants (*Rhbg* MO; *B, D, F*). Green signals showed that Rhbg is located in keratinocytes but not in ionocytes (*A*, *C*). Red signals revealed NaR cells. Other subtypes of ionocyte were not labeled by Rhbg or NKA and thus are shown as black holes surrounded by keratinocytes (arrows in *C*). The z-plane scanning image (*E*) shows that Rhbg was located in both apical and basolateral membranes (arrows) of keratinocytes. The green signals were decreased in *Rhbg* mophants (*B*, *D*, *F*). All larvae were analyzed at 4 dpf.

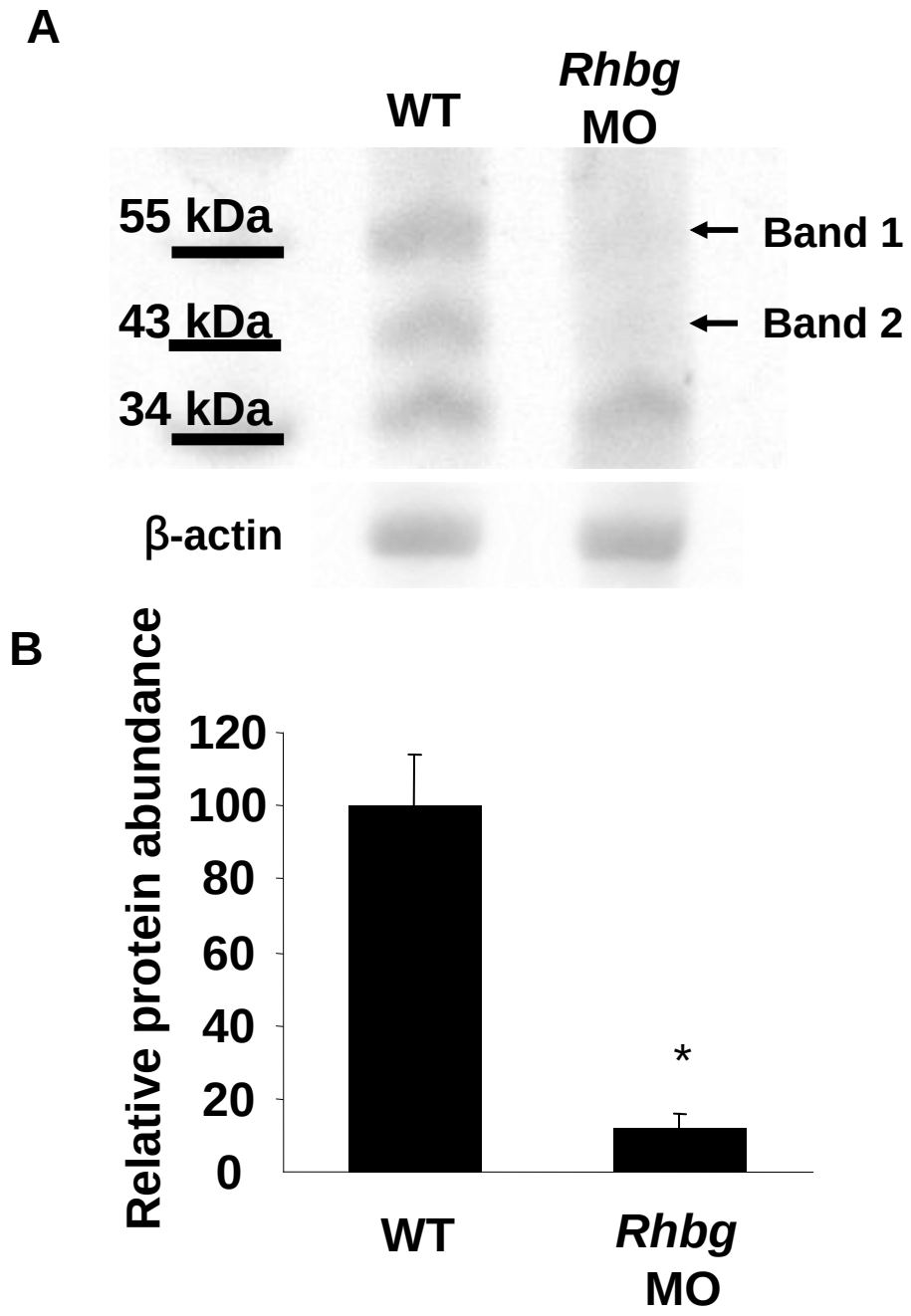

Fig. 3-3. Rhbg protein abundance in *Rhbg* morphants. (*A*) Western blotting of Rhbg in wild-type (WT) and *Rhbg* MO. (*B*) Relative protein abundances of WT and *Rhbg* MO. Data are presented as the mean ± SE (n = 3). All sample were obtained from 4 dpf larvae. *Significant difference (Student's t-test, $p < 0.05$).

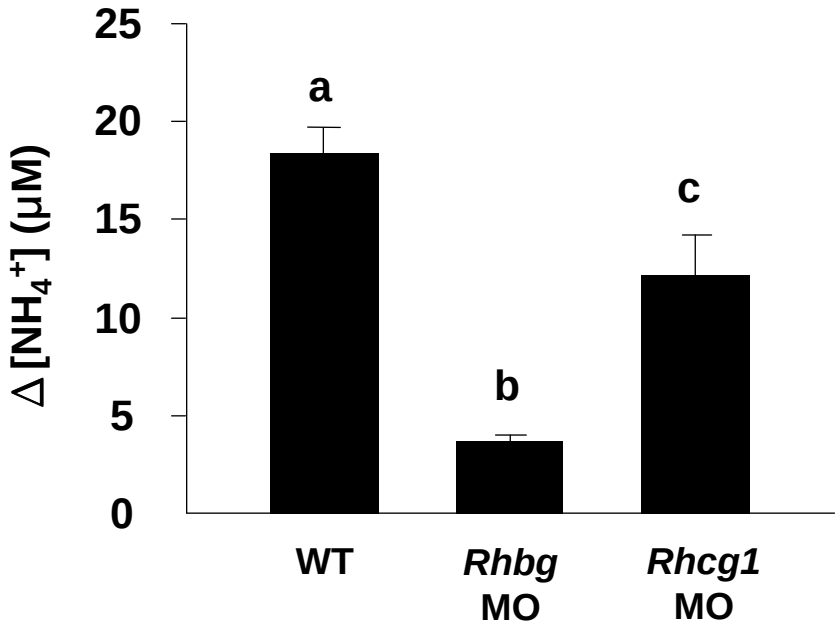

Fig. 3-4. The NH_4^+ gradient ($\triangle[NH_4^+]$) at the yolk-sac surface of *Rhbg* and *Rhcg1* morphants. SIET was used to measure the NH_4^+ gradient of 4 dpf larvae. *Rhbg* morphants were injected with 2 ng of the morpholino oligonucleotide (MO), *Rhcg1* morphants were injected with 4 ng MO. Data are presented as the mean ± SE (n = 10). ^{a,b,c} Different letters indicate a significant difference. (one-way ANOVA and Tukey's comparison, $p < 0.05$).

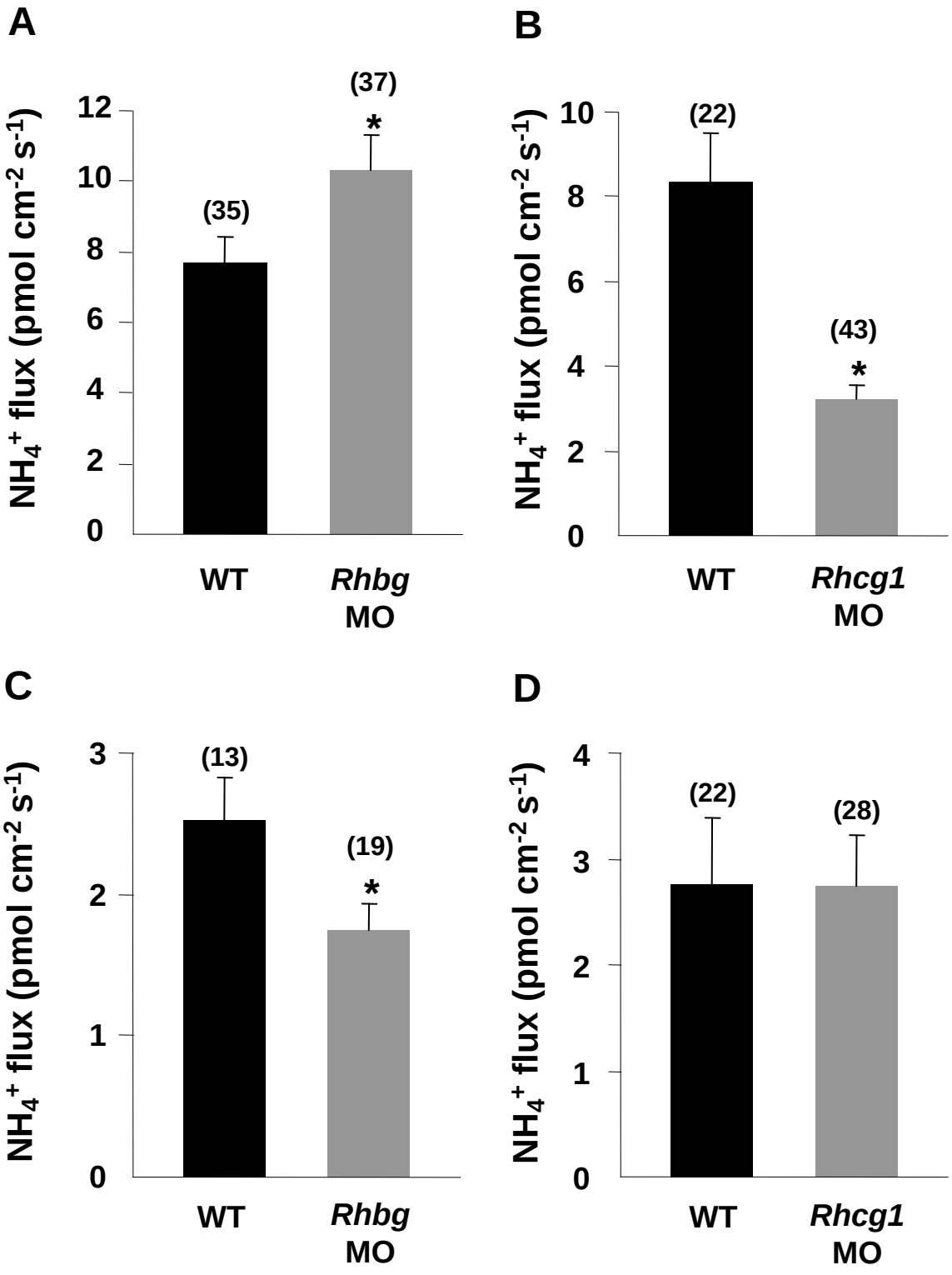

Fig. 3-5. The NH_4^+ flux of HR cells (*A*, *B*) and keratinocytes (*C*, *D*) in *Rhbg* and *Rhcg1* morphants. SIET was used to measure the NH_4^+ flux of cells in *Rhbg* morphants (2 ng morpholino oligonucleotide; MO) and *Rhcg1* morphants (4 ng MO) at 4 dpf. Data are presented as the mean ± SE (the number of samples is shown in parentheses). *Significant difference (Student's *t*-test, $p < 0.05$).

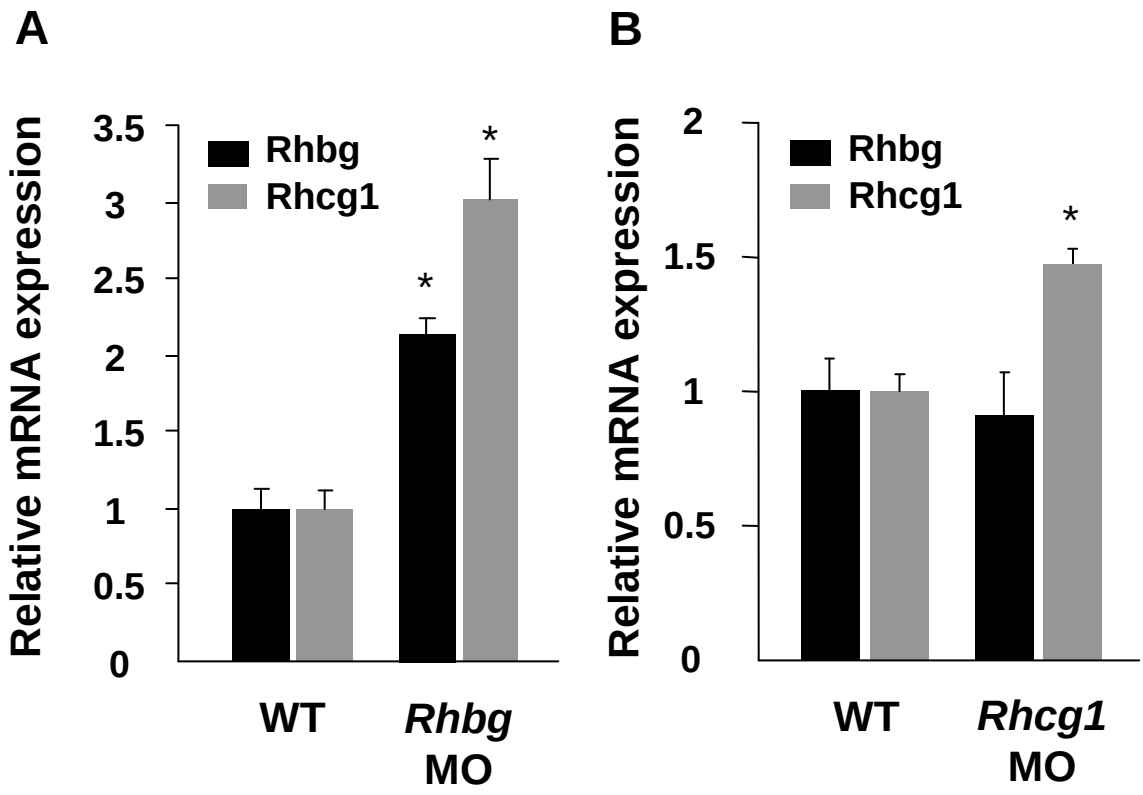

Fig. 3-6. Relative expressions of *Rhbg* (*A*) and *Rhcg1* (*B*) mRNA in *Rhbg* and *Rhcg1* morphants. A real-time PCR was used to determine the expressions of *Rhbg* and *Rhcg1* in 4 dpf larvae injected with 2 ng *Rhbg* morpholino oligonucleotides (MOs) or 4 ng *Rhcg1* MOs. Values are given relative to the amount of the wild-type (WT). Data are presented as the mean ± SE (n = 5). *Significant difference (Student's t-test, $p < 0.05$).

Chapter 4

Rhbg transports CO_2 in the keratinocytes of zebrafish larvae

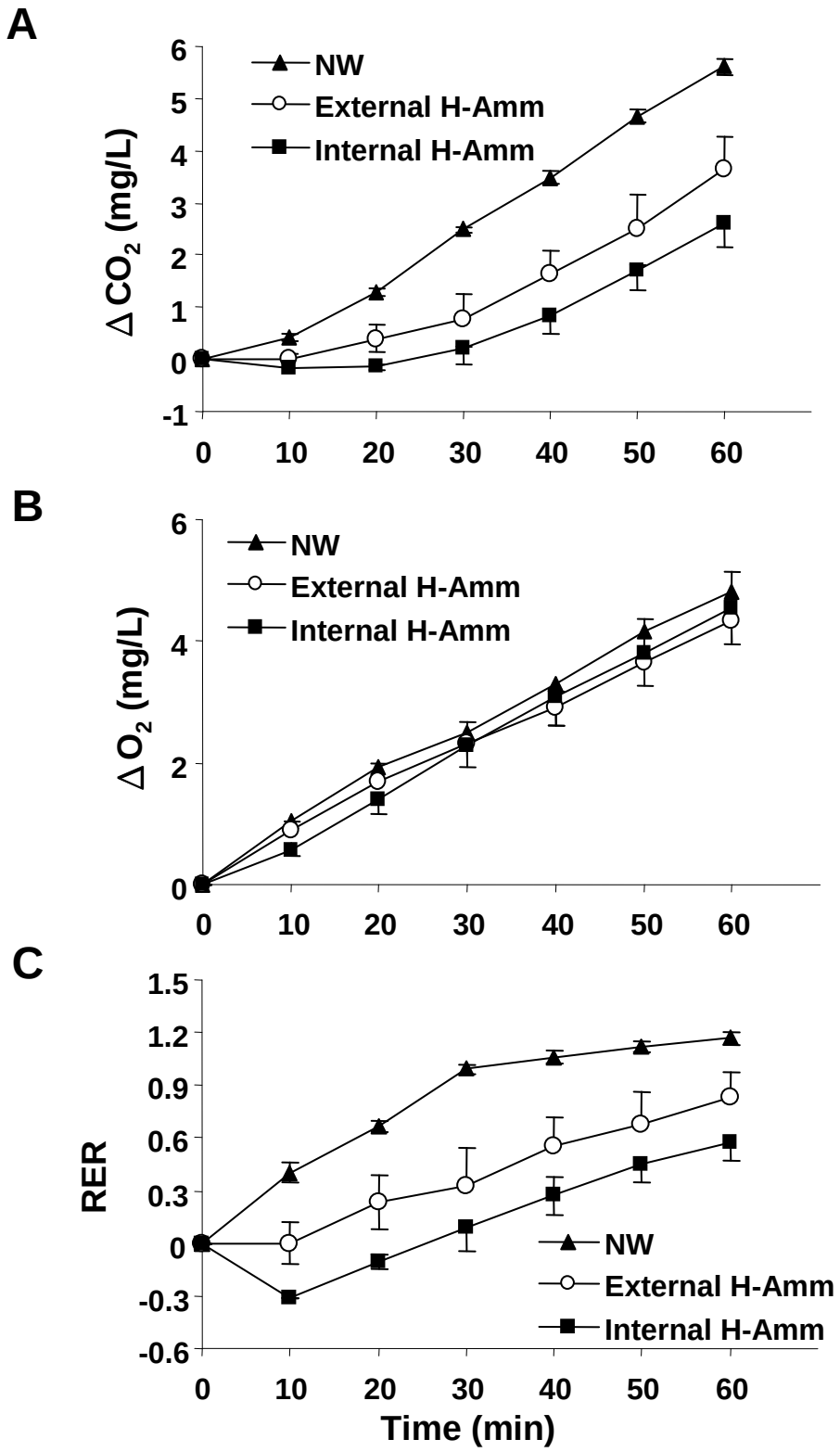

Fig. 4-1. Effect of external and internal high ammonia (H-Amm) on CO_2 excretion (*A*), O_2 uptake (*B*) and respiratory exchange ratio (RER)(*C*). The H-Amm medium contained 5 mM NH_4^+. Internal H-Amm larvae were pre-incubated in H-Amm for 1 hour. Data are presented as the mean ± SE (n = 3 in each group). All larvae were analyzed at 4 dpf.

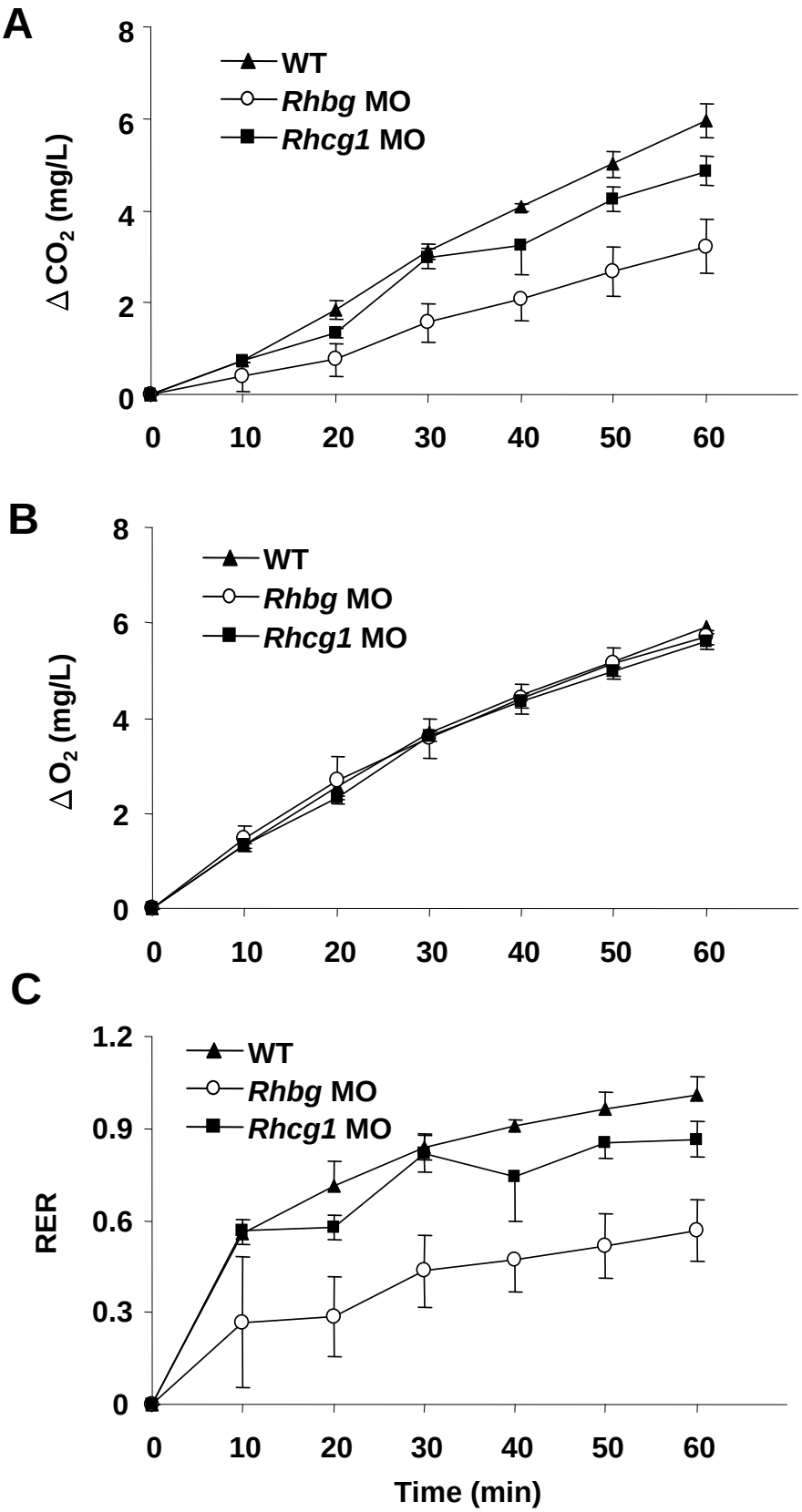

Fig. 4-2. Effect of *Rhbg* and *Rhcg1* translational knockdown (MO) on the CO_2 excretion (*A*), O_2 uptake (*B*) and respiratory exchange ratio (RER)(*C*) in zebrafish larvae. Data are presented as the mean ± SE (*n* = 3 in each group). All larvae were analyzed at 4 dpf.

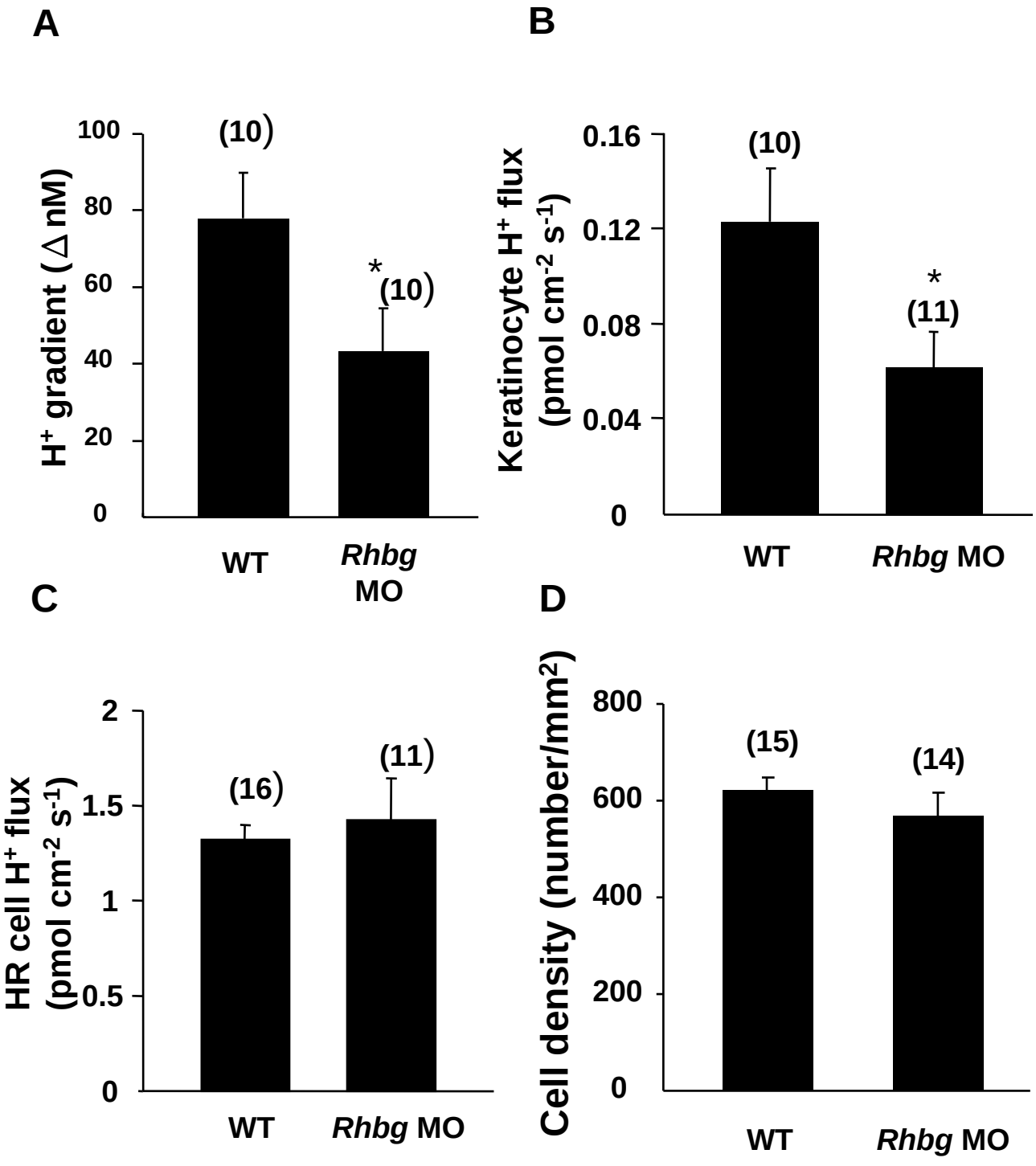

Fig. 4-3. H^+ gradient (*A*), keratinocyte H^+ efflux (*B*) and HR cell efflux (*C*) in the WT and *Rhbg* MO larvae. *D*: HR cell density in the WT and *Rhbg* MO larvae. Data are presented as the mean ± SE (the number of sample is shown in parentheses). All larvae were analyzed at 4 dpf. *Significant difference (Student's *t*-test, $p < 0.05$).

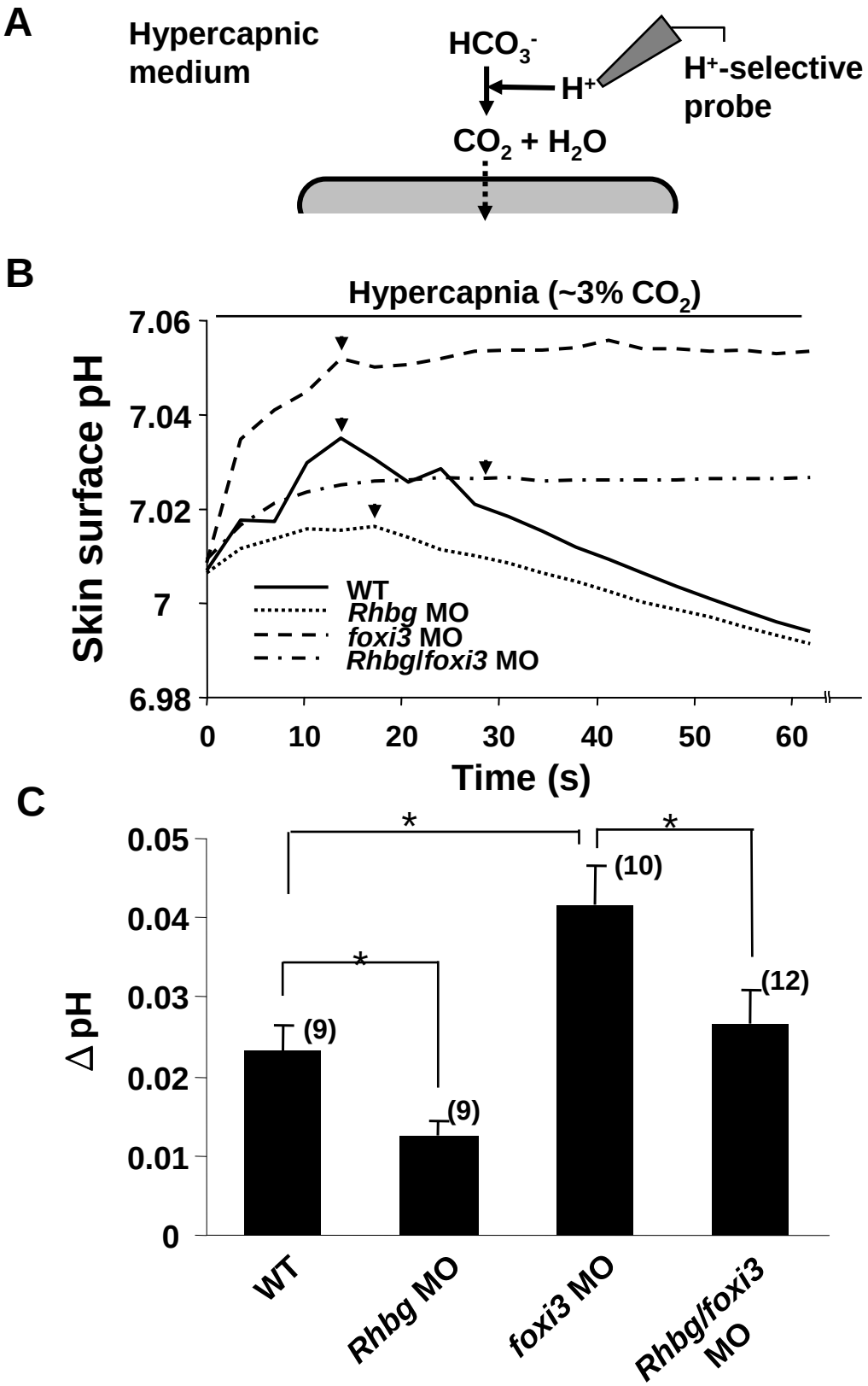

Fig. 4-4. *A*: Basis of H^+ change at the membrane surface under hypercapnia. Surface H^+ is consumed for producing CO_2. *B*: Skin surface pH of WT, *Rhbg* MO, *foxi3* MO and *Rhbg*/*foxi3* MO larvae exposed to hypercapnia (~3% CO_2). Each curve indicated an individual larva. *C*: The average of maximum pH change (△pH) in WT and MO larvae (the value for determining maximum △pH in each cell were showed in the arrows in *B*). Data are presented as the mean ± SE (the number of sample is shown in parentheses). All larvae were analyzed at 4 dpf. *Significant difference (one-way ANOVA and Tukey's comparison, $p < 0.05$).

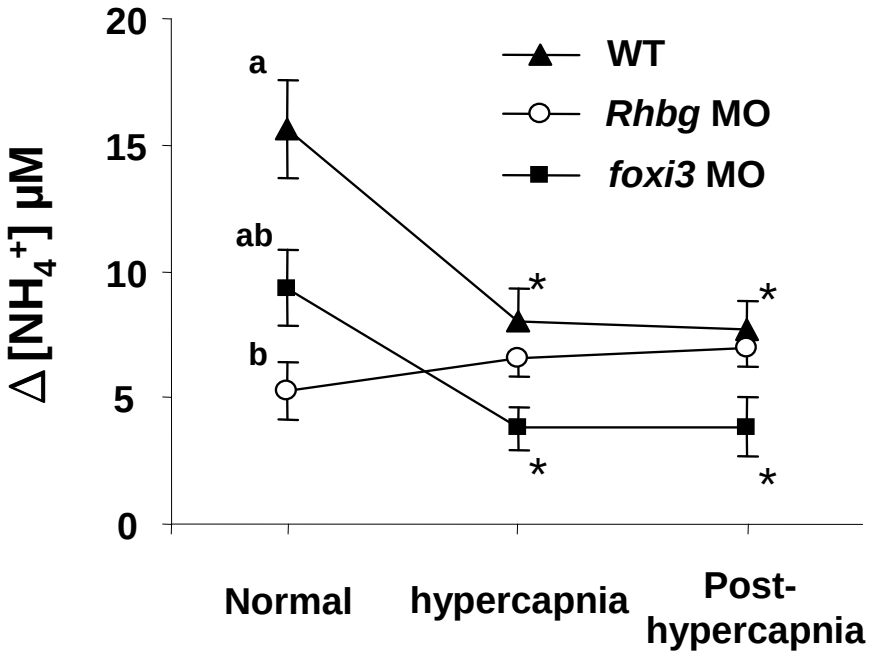

Fig. 4-5. The effect of hypercapnia on NH_4^+ gradient ($\triangle[NH_4^+]$) of WT, *Rhbg* MO, and *foxi3* MO. Larvae were sequentially incubated in Normal, hypercapnia, and back to normal (Post-hypercapnia) medium. Data are presented as the mean ± SE (n = 10 larvae). All larvae were analyzed at 4 dpf. *Significant difference from the Normal group; ^{a,b}Different letters indicate a significant difference among WT and MO larvae in Normal (one-way ANOVA and Tukey's comparison, $p < 0.05$).